

POLITECNICO DI TORINO

Master's Degree in Mechanical Engineering

Master's Degree Thesis

Experimental testing and numerical modelling of an electric
scooter



Supervisors

VIGLIANI ALESSANDRO
VELLA ANGELO DOMENICO

Candidates

JOEL GUARDIET VEGA

December 2021

Abstract

The growth of e-scooter users on the urban micromobility over the past years has been such that the study of this vehicle is gaining more and more importance thus opening many branches of study.

This paper intends to present a detailed study of the user comfort while riding an electric scooter through an exhaustive experimentation and the consequent creation of a mathematical model that simulates the e-scooter dynamics.

The thesis is organized as follows.

First, a thorough overview of the electric scooter will be presented. This contains a definition of the vehicle with an enumeration of its advantages and disadvantages, a brief story of its evolution, a comparison with other powered micromobility devices, a depiction of the different elements that form an e-scooter and a description of the specific model used throughout the study.

Second, an explanation of the experiments carried out and the aim of every and each of them is detailed. While one of the experiments allowed to study the influence of the vibration on human comfort, another one permitted to study the vehicle's braking response. On the other hand, a couple of other tests helped to create the mathematical model.

Next, an explanation of the data acquisition system can be found. The data acquirement was done thanks to the proper configuration of a SCADA-XS device and the appropriate disposition of the sensors: a GPS and four accelerometers.

Afterwards, a preliminary study followed by an in-depth analysis are deeply exposed. Meanwhile the first one verified the rightfulness of the data acquired by the sensors to later process it, the second one post-processed the data by varying the survey according to the final aim of the corresponding experiment.

Last but not least, the mathematical model created thanks to the data extracted from the study is showcased.

Finally, conclusions from this research are drawn.

Table of Contents

Abstract.....	3
Table of Contents	5
List of figures	7
List of tables	11
1. Overview on e-Scooter	12
1.1 Definition:.....	12
1.2 Advantages and disadvantages:	12
1.3 History of the scooter:	13
1.4 Comparison with other powered micromobility devices:	14
1.5 Parts of the e-scooter:	18
1.6 Technical drawings of the e-scooter	18
2. Experiments of study	21
2.1 Comfort study	22
2.1.1 Vibration impact on human body	22
2.1.2 Known surfaces with measurable bumps	26
2.1.3 Irregular surfaces with unknown and not measurable obstacles: Cobblestoned Road.....	30
2.2 Braking distance	31
3. Data acquisition system	35
3.1 Sensors and scooter set-up.....	35
3.2 Data acquisition with SCADA SC-XS	39
3.2.1 Description of the SCADA system.....	39
3.2.2. SCADA system set up	41
3.2.3. Testlab SCOPE: creating a template	42
3.2.4 Data export from Testlab SCOPE to MATLAB	44
4. Preliminary data post processing	45
4.1 Initalization of the variables	45
4.2 Preliminar analysis: validity of the experiments	46
5. Data post processing.....	53
5.1 Bike path bumps	53
5.1.1 Comparison of Back wheel accelerometer and Back floor accelerometer	60
5.1.2 Repeatability of the experiments	62
5.1.3 Bumps crossing at 19 km/h	64
5.1.4 Bumps crossing at 14 km/h	71
5.1.5 Bumps crossing at 9 km/h	73
5.2 Road bump.....	75
5.2.1 Repeatability	80
5.2.2 Bump crossing at 20 km/h.....	81
5.2.3 Bump crossing at 14 km/h.....	84
5.2.4 Bump crossing at 9 km/h.....	85
5.3 Cobblestoned Road.....	88
5.4 Braking test.....	92
6. Numerical model of the e-scooter	102

6.1 Mathematical equations	104
6.2 Calculations of the parameters	104
6.2.1 Mass and centre of gravity.....	105
6.2.2 Moment of inertia	106
6.3 Simulink Model	106
6.4 Results and parameter optimization	110
6.4.1 Estimator parameter.....	111
Conclusions	116
Reference	117

List of figures

Figure 1.4.1: Electric bike	15
Figure 1.4.2: Segway	15
Figure 1.4.3: Electric skateboard.....	16
Figure 1.4.4: Self-balancing unicycle.....	16
Figure 1.4.5: Hoverboard	17
Figure 1.4.6: Onewheel	17
Figure 1.5.1: Parts of the e-scooter.....	18
Figure 1.7.1: Front view of the scooter	19
Figure 1.7.2: Top view of the scooter.....	19
Figure 1.7.3: Top view of the steering.....	20
Figure 1.7.4 Front view of the scooter and the driver	20
Figure 2.1.1.1: Case of study, position of the user [6]	23
Figure 2.1.1.2: Table of the frequency weightings factors. ISO 2631-1:1997[6]	25
Figure 2.1.1.3: Guidelines values for the comfort of the human. ISO 2631-1:1997[6]	25
Figure 2.1.2.1: Location of the bike path bumps.....	27
Figure 2.1.2.2: Bike path bumps	27
Figure 2.1.2.3: Measurement of the bike bumps	27
Figure 2.1.2.4: Technical drawing of the bike path bumps	28
Figure 2.1.2.5: Location of the Road Bump	29
Figure 2.1.2.6: Road Bump	29
Figure 2.1.2.7: Measurement of the bump.....	29
Figure 2.1.2.8 Technical drawing of the Road Bump	30
Figure 2.1.3.1: Location of the Road Bump	31
Figure 2.1.3.2 Different views of the cobblestoned road	31
Figure 2.2.1: Set up for the measurement with a laser meter	33
Figure 2.2.2: Final set up for the measurement with a meter	34
Figure 3.1.1: GPS model	35
Figure 3.1.2: Accelerometer 356A24 (left) and accelerometer 356A15 (right).....	36
Figure 3.1.3. GPS and Front Floor Accelerometer.....	37
Figure 3.1.4 Back Floor and Back Wheel Accelerometers	37
Figure 3.1.5. Technical drawing with the positions of the accelerometers on the scooter.....	38
Figure 3.2.1.1 - SCADA SC-XS [10]ref	40

Figure 3.2.1.2 - Front connections of SCADA system [10].....	41
Figure 3.2.2.1 Set up of the SCADA support.....	42
Figure 3.2.3.1 - Main screen on Testlab SCOPE , “Templates tab”	43
Figure 3.2.3.2 - Creation of a template, tabs.	43
Figure 4.2.1 Triaxial accelerations of the Front floor accelerometer	47
Figure 4.2.2: Front floor acceleration during the crossing of the bumps	48
Figure 4.2.3: Hypothetical peaks corresponding to the bumps crossing.....	49
Figure 4.2.4: Vertical lines showing the instant when the wheels cross the bike bumps.....	50
Figure 4.2.5.: Signals measured by the GPS	51
Figure 5.1.1: Route followed by the driver for the bike path bumps experiment	54
Figure 5.1.2.: Acceleration in Z axis of the Steering, for an experiment at 19 km/h	55
Figure 5.1.3: Isolation of the interval of interest	56
Figure 5.1.4. Time isolation for the 9 km/h experiment.....	57
Figure 5.1.5: Time isolation for the 14 km/h experiment.....	57
Figure 5.1.6: Time isolation for the 19 km/h experiment.....	58
Figure 5.1.7 Comparison of filtered and original accelerations for X and Z axes for the 4 accelerometers	59
Figure 5.1.8: Comparison of filtered and original Acceleration, Steering Z axis	59
Figure 5.1.9: 3 Axial accelerations of the Steering accelerometer at 19 km/h.....	60
Figure 5.1.1.1: Back Floor accelerometer vs Back Wheel accelerometer.....	61
Figure 5.1.2.1: Time isolation for the 3 experiments	63
Figure 5.1.2.2: X and Z axes accelerations for three experiments at 19 km/h	64
Figure 5.1.3.1: Z axis acceleration for the Front Floor. Three zones of study with peaks of interest.....	65
Figure 5.1.3.2: Zone of study, Front Floor Accelerometer, X and Z axes accelerations	68
Figure 5.1.3.3 Zone of study, Back Floor Accelerometer, Z axis acceleration.....	69
Figure 5.1.3.4: Zone of study, Back Floor Accelerometer, X and Z axes accelerations	71
Figure 5.1.4.1: Zone of study, Front Floor Accelerometer, X and Z axes accelerations	72
Figure 5.1.4.2: Zone of study, Back Floor Accelerometer, X and Z axes accelerations.....	73
Figure 5.1.5.1: Zone of study, Front Floor Accelerometer, X and Z axes accelerations	74
Figure 5.1.5.2: Zone of study, Back Floor Accelerometer, X and Z axes accelerations.....	75
Figure 5.2.1: Route followed by the driver for the road bump experiment.....	76
Figure 5.2.2: Isolation of the interval of interest	77
Figure 5.2.3: Time isolation for 19 km/h.....	78

Figure 5.2.4: Comparison of filtered and original Acceleration, Steering Z axis	79
Figure 5.2.5: 3 axial accelerations of the Steering at 19 km/h	80
Figure 5.2.1.1: Front floor accelerometer, X and Z axes acceleration for three experiments.....	81
Figure 5.2.2.1: Front Floor Accelerometer, X and Z axes accelerations.....	82
Figure 5.2.2.2: Back Floor Accelerometer, X and Z axes accelerations	83
Figure 5.2.3.1: Front Floor Accelerometer, X and Z axes accelerations.....	84
Figure 5.2.3.2: Back Floor Accelerometer, X and Z axes accelerations	85
Figure 5.2.4.1: Front Floor Accelerometer, X and Z axes accelerations.....	86
Figure 5.2.4.2: Back Floor Accelerometer, X and Z axes accelerations	87
Figure 5.3.1: Route followed by the driver for the cobblestoned road experiment.....	88
Figure 5.3.2: Time Isolation of the interval at constant speed	89
Figure 5.3.3: Isolation of the interval of interest applied to the Steering acceleration.....	90
Figure 5.3.4: Comparison of filtered and original Acceleration, Steering Z axis	91
Figure 5.4.1: Route followed by the driver for the braking test experiment	92
Figure 5.4.2: GPS signals of the speed during all the experiment.....	94
Figure 5.4.3: GPS signals of the speed during the braking	95
Figure 5.4.4: Accumulated distance over time.	96
Figure 5.4.5: GPS vs By hand measurements of braking distance.....	97
Figure 5.4.6: Braking distance over speed of the measurements by hand...:	98
Figure 5.4.7: Calculation of the coefficient a with the Curve Fitting Tool.....	99
Figure 5.4.8: Braking distance as a function of velocity	100
Figure 6.1.1: Mass-spring-damper model for 2-wheeled vehicle [21]	102
Figure 6.1.2: Mass-spring-damper model for the e-scooter	103
Figure 6.3.1 Numerical model of the scooter with SIMULINK	106
Figure 6.3.2: Left side of the SIMULINK model.....	107
Figure 6.3.3: Right side of the SIMULINK model.....	108
Figure 6.3.4: Input signal, front wheel	109
Figure 6.3.5: Geometry of the wheel and a bike bump	109
Figure 6.3.6: Modification of the input signal.....	110
Figure 6.4.1.1: Modified experimental acceleration.....	112
Figure 6.4.1.2.: Parameter optimization for the experiment of 9 km/h.....	113
Figure 6.4.1.3 Experimental vs. Simulated. 9 km/h	114
Figure 6.4.1.4: Experimental vs. Simulated. 14 km/h	115

Figure 6.4.1.5: Experimental vs. Simulated. 19 km/h 115

List of tables

Table 3.1.1 Relation between Global Axis of the scooter and Local Axis of the accelerometers	38
Table 3.1.2 Sensitivities of the accelerometers in the Local Axis.....	39
Table 5.1.3.1: Acceleration and time instant of the Peaks	66
Table 5.1.3.2: Acceleration values for the equivalent peaks	66
Table 5.1.3.3: Relative errors between equivalent peaks	67
Table 5.1.3.4: Acceleration and time instant of the Peaks	69
Table 5.3.1: weighted frequencies r.m.s accelerations	92
Table 5.4.1: Measures taken by hand	93
Table 5.4.2: Friction coefficient of different vehicles	101
Table 6.2.1.1: Centre of gravity and mass of the different elements.....	105
Table 6.4.1: Simulations changing parameters manually	111
Table 6.4.1.1: Parameter's values for the three speeds	113

1. Overview on e-Scooter

1.1 Definition:

A scooter is a vehicle ridden while standing that consists of a narrow footboard mounted between or atop two wheels tandem that has an upright steering handle attached to the front wheel, and that is moved by pushing with one foot. On the other hand, an electric scooter is a similar vehicle but propelled by an electric motor.

1.2 Advantages and disadvantages:

Scooters are very popular for personal transportation in urban areas due to their advantages in comparison with larger means of transport. Such advantages include their low purchasing and maintenance costs, ease of operation, driving license nonnecessity, driveability in heavy traffic, low noise pollution and parking in small spaces. The recently developed electric scooters add faster speed rate, no need of user effort and energy saving to the above-mentioned benefits, without this affecting much the environment as other larger non-electric vehicles would do. Therefore, it can be said that electric scooters are relatively eco-friendly. Furthermore, e-scooter sharing is possible in big cities and its appearance on them can decongest public transport saturation. [1]

While there are many advantages to the introduction of electric scooters in our cities, 'every rose has its thorn' and we should not be blind to its arising disadvantages. Although there is a willingness of people to acquiring e-scooters, some issues can be found hindering the market expansion. Such barriers include danger without sufficient scooter lanes, only suitable for short distances due to low range, shortage of charging facilities, problems with overcharging or other battery-related issues and few governmental measures supporting the industry and promoting regulations to encourage its use. Furthermore, many models are imported from Asia and they have poor quality according to the European or American standards. In the other hand, some models are built using imported parts and then assembled by distributors who are attracted to an emerging business but lack the knowledge and experience needed to do so in a proper way. Economically speaking, we should not ignore the fact that e-scooters entail a high purchase price for individuals followed by high depreciation once acquired. If in addition, the obvious insurance problems related to possible accidents are considered, the truth is its advantages might not seem that appealing for users. If we take the user usage of it into account, new problems appear. The lack of driving knowledge and the poor civic responsibility of certain users has caused not just an increase on the number of accidents, but also other concerns specially when related with scooter-sharing

system. Like the fact that they are sometimes stolen or often left behind everywhere, causing new disruption on the urban order, to mention a few examples. Other disadvantages we should not overlook are the fact that they have little to no storage space; they sometimes present technical issues with scooter sharing apps; and, why no to say it, people may become lazy after getting use to them. [1]

1.3 History of the scooter:

So, where did electric scooters come from? Many people tend to think that scooters, rideshares and e-bikes did not exist in our vocabulary a decade ago. They may seem new, but in fact, powered bikes and scooters have been around for at least as long as the car.

The wooden kick scooter with skate wheels dates back to sometime in the late 19th century, when motorized bikes were also developed. The first motorized scooter for adults, the Autoped, was developed in 1913 and patented in 1916 by inventor Arthur Hugo Cecil Gibson. Built from 1915 to 1922, the scooter promised to revolutionize short trips, work commutes and the lives of doctors, students, grocers, merchants, collectors, repairmen, messengers and anybody else who wants to save money, time and energy in going about. [2]

The gas-powered, two-wheeled, folding scooter marketed itself as the “motor vehicle of the millions at a price so low that almost everybody can afford one.” That wasn’t exactly true. The Autoped was well designed. It generated speeds up to 50 km/h. The Autoped’s steering rod was collapsible for easy storage. At over 45kg, however, the scooter was hardly portable, just as it was not particularly affordable. But like the electric scooter, it surpassed initial expectations, and it did appeal to a wide range of users.

ABC Motorcycles produced the Skootamota, which had a top speed of 24 km/h, and The Gloster Aircraft Company introduced the Reynolds Runabout in 1919, followed by the Unibus in 1920. The Unibus was promoted as the "car on two wheels". Some of these early scooter designs were unstable, uncomfortable to ride and difficult to handle. The decades leading up to World War II saw the gradual introduction of a range of refinements, including efficient lights and brakes, gears, suspension, enclosed bodies and leg shields. Subsequent decades would witness ups and downs in the popularity of both standing and seated kick and motorized scooters.

Meanwhile, the non-motorized kick scooter underwent a revolution when Wim Ouboter invented a lightweight, portable model in 1990. Although his first creation became an afterthought, Ouboter kept tinkering, and created a three-wheeled version, the Kickboard. The success of the Kickboard precipitated the launch of Ouboter’s Micro Mobility Systems in 1999, which manufactured his original two-wheeled concept.

Demand for the scooter was so high, that in 2003, the brand added an electric motor. The story of the modern electric scooter begins after 2009, as Lithium-ion battery technology becomes refined enough to integrate into small vehicles like scooters that can be charged at home.

The mid-2000s the very expensive and popular two-wheeled device called Segway was developed by Dean Kamen. The electric vehicles faded for some time, until American businessman Shan Chen launched a Kickstarter campaign to raise funds for his self-balancing Hoverboard.

In 2018, Segway made a comeback to become the world's primary source for the scooter-revolution that continues to the present day. Rather than appearing out of nowhere, the modern electric scooter is instead the product of over 100 years of research, development, and real-world testing by inventors, engineers and commuters.

According to a Pike Research study, the number of electric scooters increased from 12 million to 103 million in 2018. Most of these vehicles will be used in China (approximately 91 million) due to rising urbanization (and thus increase of population density and income levels) and the creation of new government policies that demand lightweight highly mobile electric scooters. [3] According to the Municipal Transport Company of Madrid the amount of sales of powered micromobility devices done by European manufacturers has increased 700% between 2016 and 2019. [4]

1.4 Comparison with other powered micromobility devices:

However, as mentioned previously, the electric kick scooter was not the only powered micromobility device that appeared on the market. On the meantime, other types of electric rideable were developed. Those, commonly called personal transporters or electrical-powered mobility vehicles (e-PMV), are motorized micromobility vehicles for transporting an individual at speeds that do not normally exceed 25 km/h. In this category are included the following vehicles (in order of appearance on the market): the **electric bicycles**, the **Segway**, the **electric skateboard**, the **self-balancing unicycle**, the **hoverboard**, the **onewheel** and the recently developed **electric skates**.

In the United States, one of the first patents of an **electric bike** (fig. 1.4.1) was awarded in 1895 for a battery-powered bicycle that had its hub motor mounted inside the rear wheel and a battery sitting inside the main triangle of the frame, which is not too different in concept to some modern electric bikes. As time began to pass, more designs and bikes entered the world, some of which represent the foundational ideas behind many of our present-day machines. Through the middle of the 20th century, electric bikes began to experience their earliest occurrences of mass production. Europe was one of the first places to see these early adoptions with higher production levels and greater usage. In 1989, one of the most important innovations was created in the form of the first 'Pedelec' or Pedal Electric Cycle (now known as pedal-assist) in which the motor

power is triggered as assistance when any pedaling action is registered by the bike. Rather than using a throttle mechanism to control the motor, as all previous models had, this allowed riders to utilize an electric bike not so dissimilar to how one would ride a regular bike.



Figure 1.4.1: Electric bike

The **Segway** (fig. 1.4.2) had its first patent filed in 1994 but was not brought to market until 2001. It is a computer-controlled, self-balancing, two-sided bi-wheeled electric gyroscopic vehicle, invented as stated previously by Dean Kamen and produced by Segway Inc. The computer and motors located in the base keep the Segway base horizontal at all times. The user must lean towards the direction he wants to take (forward, backward, right or left). The motor is electric and silent, reaching 20 km/h.



Figure 1.4.2: Segway

As for the **electric skateboard** (fig. 1.4.3), it had a patent filled in 1999 but it was not effectively powered until the 2004–2006 due to unavailability of electric motors and batteries with sufficient torque and efficiency. It consists of a deck, which is usually made of a specially designed 7-8 ply maple plywood, and four polyurethane wheels attached to the underside by a pair of skateboarding trucks. The speed is either controlled by a wireless hand-held throttle remote or the rider body weight-shifting between front of the board for forward motion and rear for braking. As for the direction of travel to the right or left, it is adjusted by tilting the board to one side or the other.



Figure 1.4.3: Electric skateboard

Through the years, the **self-balancing unicycle** (fig. 1.4.4) had seated as well as standing versions. These transporters consist of a unique wheel on top of which the person seats or stands placing the feet on two pads located at the sides of it. Probably, the first balancing unicycle of two axes rideable by people was the Encycle, created in 2006. Nowadays, most commercial units are self-balancing in a single axis direction with lateral stability being provided by the rider; more complex fully self-balancing dual-axis devices also need to self-balance from side to side. Although some models are able to exceed 40 km/h, many companies have established a 25km/h limit in order to accomplish the speed limit settled by many countries' legislation.



Figure 1.4.4: Self-balancing unicycle

The **hoverboard** (1.4.5), also known as self-balancing scooter, was patented in 2013 and distributed since 2015. It is a self-balancing personal transporter consisting of two parallel motorized wheels connected to a pair of articulated pads on which the rider places their feet. By tilting the pads, the rider can control the speed and direction of travel achieving speeds from 9.7 to 24 km/h.



Figure 1.4.5: Hoverboard

In 2014, the **onewheel** (fig. 1.4.6) was brought to Kickstarter and it was then released in 2015. It is a self-balancing single wheel electric board-sport, recreational personal transporter. Unlike the electric unicycle, the rider's feet (and body) are typically pointed at a perpendicular angle to the wheel and direction of travel. The original model had a range of 6,5-9,5 km. As of 2021, two models are in production, one of which reaches a speed of 30km/h.



Figure 1.4.6: Onewheel

The classification of these personal transporters (e.g. whether they qualify as a 'vehicle') and legality of their use on roads or pavements varies between countries. For instance, in United Kingdom powered transporters are prohibited from using pavements and other pedestrian-only areas, bicycle tracks, cycle lanes on roads or other spaces dedicated to pedal cycle use only. For motor vehicles to use public roads lawfully, they must meet a number of different requirements. These include insurance; conformity with technical standards and standards of use; payment of vehicle tax, licensing, and registration; driver testing and licensing; and the use of relevant safety equipment. On the other hand, in the United States, there have to be considered both city and state regulations, but also differences between true electric scooter regulations and that of other form factors (i.e. mopeds) applied to scooters in absence of specific regulation. Those regulations differ among states. Meanwhile some states allow speed limits up to 48 km/h, others forbid to exceed 36km/h. In some states is not legal to ride them on the street, but in others is not legal to do so on the sidewalks. In some of them just a helmet is required, but others ask for a 16-year minimum age or a driving license.

1.5 Parts of the e-scooter:

To understand better the e-scooter working, a detailed representation of its parts is depicted in the following figure (1.5.1). Some of these terms will be used repeatedly throughout the following pages.

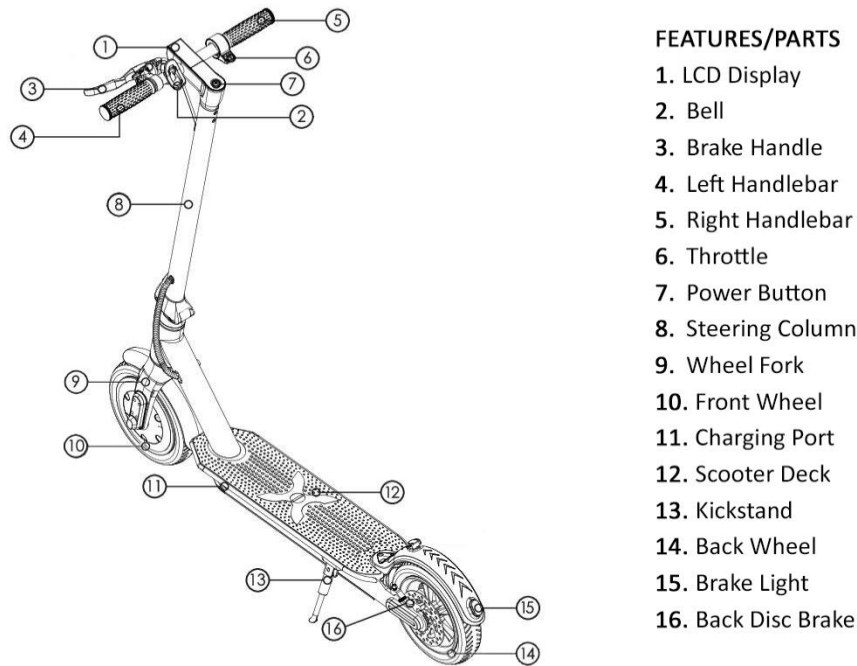


Figure 1.5.1: Parts of the e-scooter

1.6 Technical drawings of the e-scooter

For the work of this thesis, it is important to have some important measures of the e-scooter. These dimensions are important for different reasons as to have information to calculate the centre of mass or ubicate the sensors. For this reason different drawings has been made in order to avoid the later calculations. These dimensions are represented in four drawings. The front view of the scooter (fig. 1.7.1), the top view of the scooter (fig 1.7.2), the top view of the steering (fig 1.7.3) and finally the front view with the inclusion of the driver (fig. 1.7.4)

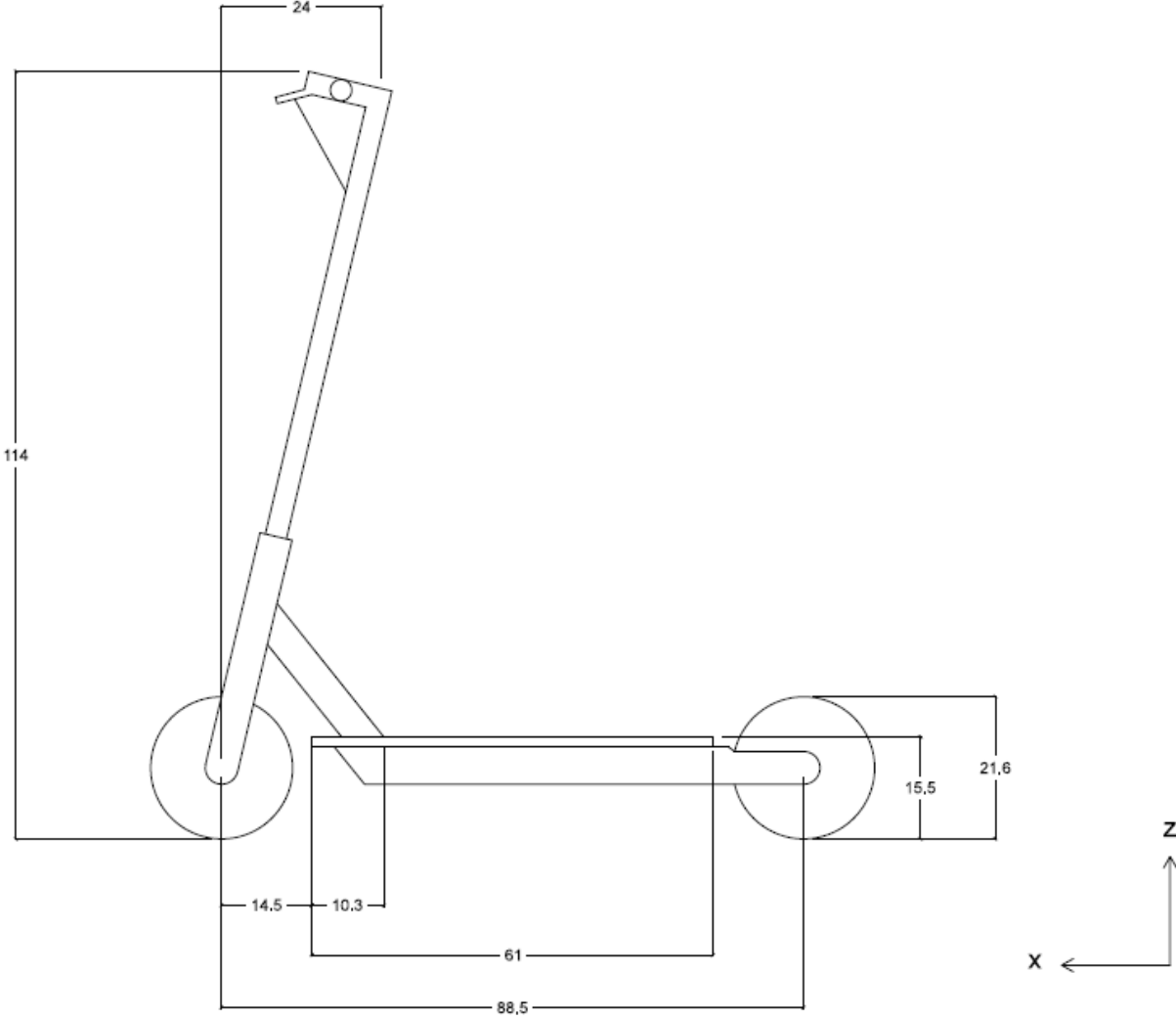


Figure 1.7.1: Front view of the scooter

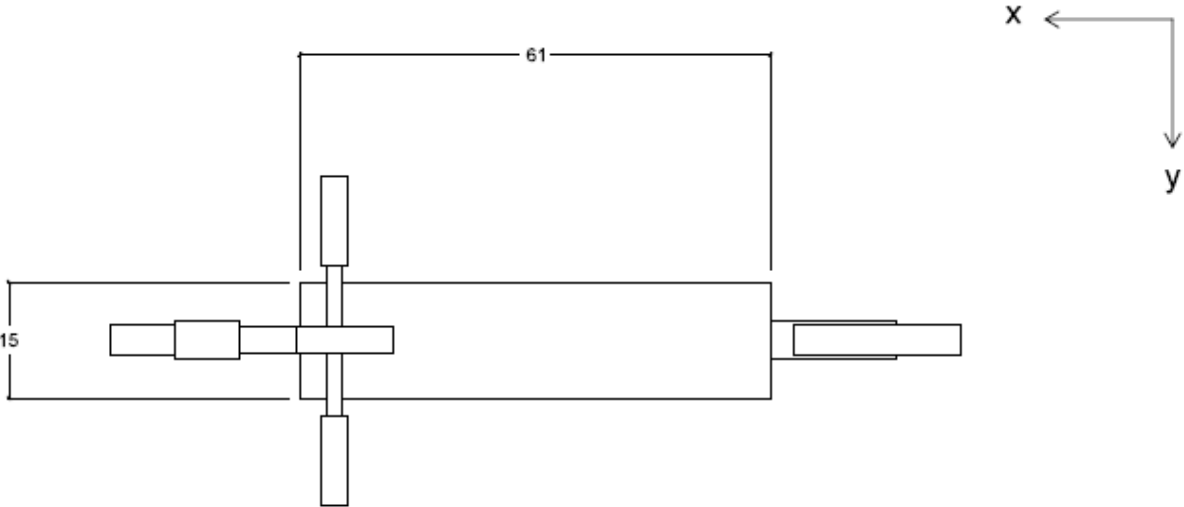


Figure 1.7.2: Top view of the scooter

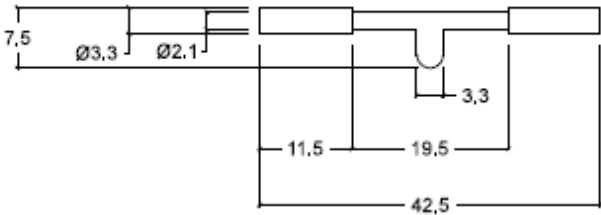


Figure 1.7.3: Top view of the steering

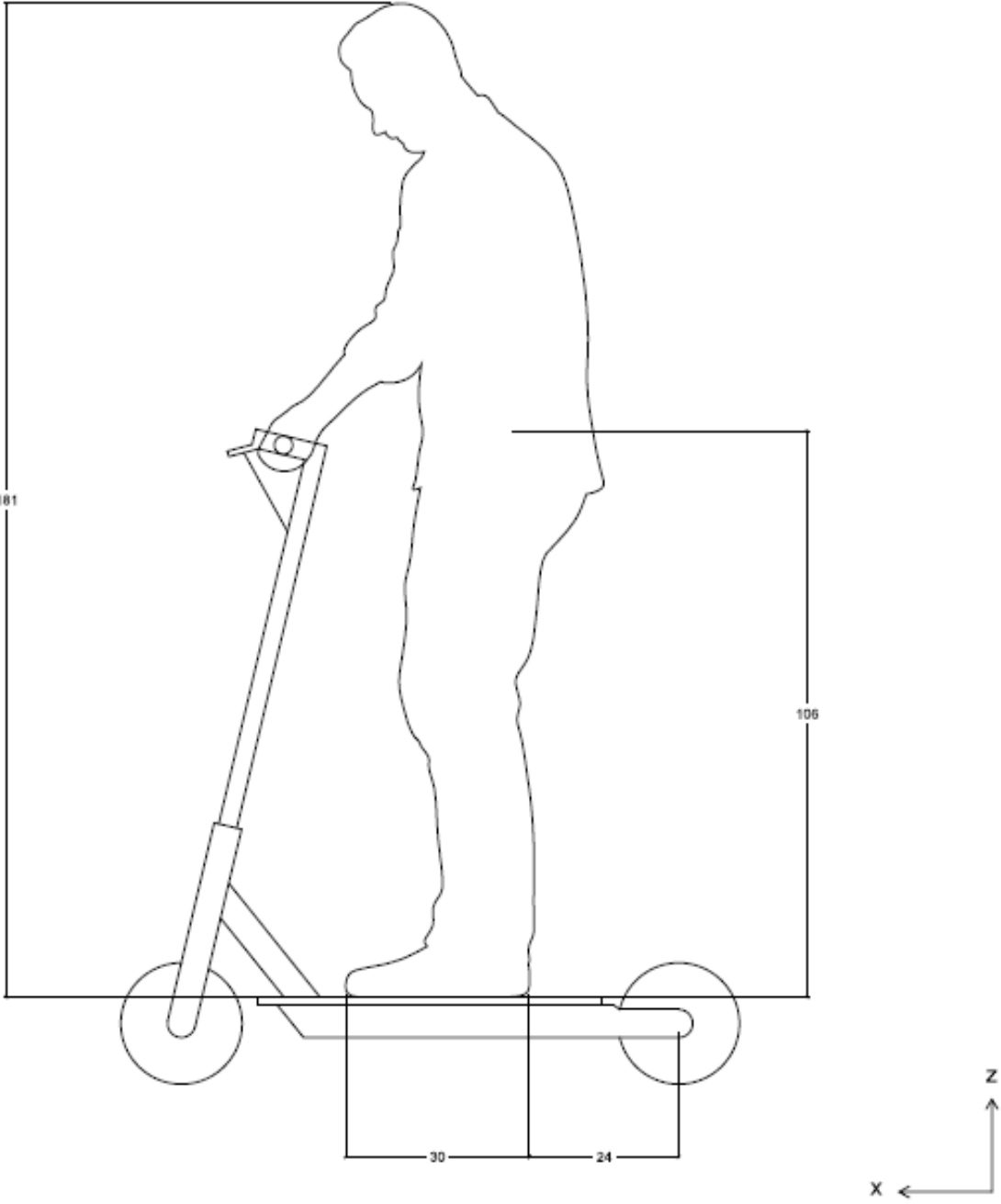


Figure 1.7.4 Front view of the scooter and the driver

2. Experiments of study

In this thesis different experiments will be carried out in order to study the behaviour of the e-scooter.

The main objective with these experiments will be to study the comfort of the user when he is driving the vehicle, that is related to the vibrations transmitted by the vehicle to the user.

To perform these experiments and find an interesting situation to study, it is required to find different places with different surfaces and obstacles. However, it is not the only type of experiment that will be performed, and a breaking test was found interesting to add to the experimentation.

Each kind of experiment will have their own specific aspects to take into account when the experiment is carried out.

However, some aspects will be common for all. An important requirement when the measurements are done, it is to try to carry out in the most repeatable way. This means that some aspects have to be taken into account when performing these measurements.

One aspect is to maintain a constant speed on each experiment. As it will be explained in the next sections, on each type of experiment, the measurements will be divided in different velocities. To achieve these velocities and maintain them constant during the crossing of the obstacles is quite difficult if it is controlled by hand. Then to minimize the variability of the speed, the experiments will be done with the control cruise active. In this way the velocity will be controlled electronically by the e-scooter.

With the control cruise option active, the user will be capable of maintaining a constant speed when the speed is being maintained constant by hand during 5 seconds, then a sound will alert the user, then if the user stops to accelerate the e-scooter will maintain the speed constant until the user decides to accelerate or brake the vehicle.

However, the only way that the user has to achieve a specific velocity is trying to maintain the desired speed for 5 seconds, but to check the velocity that the user wants to maintain, he will look the screen on the e-scooter. And this speed is shown in km/h without decimals. This means that, if for instance two measures have been taken when the screen shows 12 km/h, they can have up to 1km/h of difference. This means that in the analysis of the data it will be important to check the speed with the GPS. When comparing the different values from a specific velocity it will be required to take into account these differences of speed.

To achieve the control cruise option, the user has to first achieve the desired speed and then maintain that speed 5 seconds, so for each measurement it will be necessary to start from a point far enough to achieve it before reach the obstacles.

2.1 Comfort study

For this study it will be necessary first of all to understand the impact of the vibrations to the human body. To analyse and make some conclusions after comparing with the data measured with the experiments

For what concerns to the experimentation, it has been separated in two types. The first one it will be in a regular surface where the objective will be to study a specific obstacle that is known and measurable. The second it will be an irregular surface where the obstacles will be not measurable.

2.1.1 Vibration impact on human body

To study the vibration on the user, it has been used the ISO 2631-1:1997 [6]. Following its guidelines, it makes possible to evaluate the human exposure to the whole-body vibration. This evaluation is based on frequency weighting of the r.m.s acceleration. And different frequency weightings are given for the evaluation of different effects.

This ISO has as main purpose to define methods of quantifying whole-body vibration in relation of different aspects. For this thesis purpose, the aspect that will be studied is the human health and comfort. The frequency range considered for the human health and comfort is from 0,5 Hz to 80Hz.

Depending on the position of the human body and how the vibration is transmitted to the body, the procedure to evaluate it is different. In the case of study, its will be followed the guidelines for a standing person (fig. 2.1.1.1), maintaining its axes, that already have the same directions than the reference system chosen.

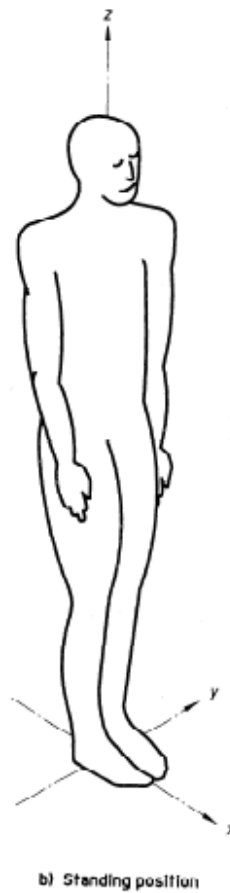


Figure 2.1.1.1: Case of study, position of the user [6]

To analyse the comfort is necessary to calculate the weighted r.m.s acceleration. This weighing is necessary as the frequencies do not have the same impact, it depends on the position of the person, the aspect of study and the axis studied. That in the case of study, as said before it will be a standing person and the comfort aspect.

The weightings used in this configuration are:

W_k for Z axis

W_d for X and Y axis

Each of these weightings are curves that depends on the frequency.

To calculate the value which will serve to study the comfort it has to be followed the next procedure:

The final value is the weighted frequency r.m.s acceleration, and is calculated as:

$$a_v = (k_x^2 a_{wx}^2 + k_y^2 a_{wy}^2 + k_z^2 a_{wz}^2)^{\frac{1}{2}} \quad (2.1.1.1)$$

Where:

$k_x = k_y = k_z = 1$. For this configuration

a_{wj} = weighed frequency r.m.s. acceleration for axis j

The frequency-weighted r.m.s acceleration has to be calculated by weighing the appropriate one-third octave band data. For the conversion, the weightings factors are given in the figure 2.1.1.1 The overall weighed acceleration has to be calculated with the following equation:

$$a_w = \left[\sum_i (w_i a_i)^2 \right]^{\frac{1}{2}} \quad (2.1.1.2)$$

Where:

a_w = weighed frequency r.m.s. acceleration for one axis

w_i = the weighing factor for the i-th one-third octave band given in the figure 2.1.1.2.

a_i = the r.m.s acceleration for the i-th one-third octave band given in the figure 2.1.1.2.

The center frequency of the one-third octave band that have to be used and the correspondant weightings are shown in the figure 2.1.1.2.

Frequency band number ¹⁾ <i>x</i>	Frequency <i>f</i> Hz	<i>W_c</i>		<i>W_e</i>		<i>W_j</i>	
		factor x 1 000	dB	factor x 1 000	dB	factor x 1 000	dB
-10	0,1	62,4	-24,11	62,5	-24,08	31,0	-30,18
-9	0,125	97,2	-20,25	97,5	-20,22	48,3	-26,32
-8	0,16	158	-16,03	159	-15,98	78,5	-22,11
-7	0,2	243	-12,30	245	-12,23	120	-18,38
-6	0,25	364	-8,78	368	-8,67	181	-14,86
-5	0,315	527	-5,56	536	-5,41	262	-11,65
-4	0,4	708	-3,01	723	-2,81	351	-9,10
-3	0,5	843	-1,48	862	-1,29	417	-7,60
-2	0,63	929	-0,64	939	-0,55	458	-6,78
-1	0,8	972	-0,24	941	-0,53	478	-6,42
0	1	991	-0,08	880	-1,11	484	-6,30
1	1,25	1 000	0,00	772	-2,25	485	-6,28
2	1,6	1 007	0,06	632	-3,99	483	-6,32
3	2	1 012	0,10	512	-5,82	482	-6,34
4	2,5	1 017	0,15	409	-7,77	489	-6,22
5	3,15	1 022	0,19	323	-9,81	524	-5,62
6	4	1 024	0,20	253	-11,93	628	-4,04
7	5	1 013	0,11	202	-13,91	793	-2,01
8	6,3	974	-0,23	160	-15,94	946	-0,48
9	8	891	-1,00	125	-18,03	1 017	0,15
10	10	776	-2,20	100	-19,98	1 030	0,26
11	12,5	647	-3,79	80,1	-21,93	1 026	0,22
12	16	512	-5,82	62,5	-24,08	1 018	0,18
13	20	409	-7,77	50,0	-26,02	1 012	0,10
14	25	325	-9,76	39,9	-27,97	1 007	0,06
15	31,5	256	-11,84	31,6	-30,01	1 001	0,00
16	40	199	-14,02	24,7	-32,15	991	-0,08
17	50	156	-16,13	19,4	-34,24	972	-0,24
18	63	118	-18,53	14,8	-36,62	931	-0,62
19	80	84,4	-21,47	10,5	-39,55	843	-1,48
20	100	56,7	-24,94	7,07	-43,01	708	-3,01
21	125	34,5	-29,24	4,31	-47,31	536	-5,36
22	160	18,2	-34,80	2,27	-52,86	364	-8,78
23	200	9,71	-40,26	1,21	-58,33	243	-12,30
24	250	5,06	-45,92	0,63	-63,99	158	-16,03
25	315	2,55	-51,88	0,32	-69,94	100	-19,98
26	400	1,25	-58,08	0,16	-76,14	62,4	-24,10

Figure 2.1.1.2: Table of the frequency weightings factors. ISO 2631-1:1997[6]

Once the total weighted frequency r.m.s acceleration has been calculated for an experiment, it has to be compared to the values provided by the ISO 2631-1:1997, that serve as a guidelines for the comfort of the human (fig. 2.1.1.3).

Less than 0,315 m/s ² :	not uncomfortable
0,315 m/s ² to 0,63 m/s ² :	a little uncomfortable
0,63 m/s ² to 1 m/s ² :	fairly uncomfortable
1 m/s ² to 1,6 m/s ² :	uncomfortable
1,6 m/s ² to 2,5 m/s ² :	very uncomfortable
Greater than 2,5 m/s ² :	extremely uncomfortable

Figure 2.1.1.3: Guidelines values for the comfort of the human. ISO 2631-1:1997[6]

2.1.2 Known surfaces with measurable bumps

For this type of experiment, the measurements have been divided in two and done in two different places. Both obstacles are known and measurable, but will differ in their shape. In one hand there will be a series of a smaller bumps located in a bike path and in the other hand a big bump located in the road.

As explained on previous points, one important aspect is to maintain the speed as much constant as possible but another aspect to take into account at least for the two experiments where the obstacles are known is to try to cross the obstacle in the most similar way on all the experiments.

In the figures 2.1.2.2. and 2.1.2.6 it can be appreciated the obstacles. These obstacles are perpendicular to the direction of the path/road,

- **Bike path bumps**

This series of bumps are located behind the main building of the Politecnico di Torino, on the Corso Castelfidardo. in which there is a bike path.

In this bike path there is some series of 7 or 14 bumps. These series can be found near the entrances to the Politecnico, with the objective to force the drivers of the bikes or e-scooter to reduce the speed.

The figure 2.1.2.1 shows the location of these bumps thanks to the google maps application, and to be more precise the obstacles are indicated with a red ellipse, the figure 2.1.2.2 shows the view of these bumps from a closer distance.

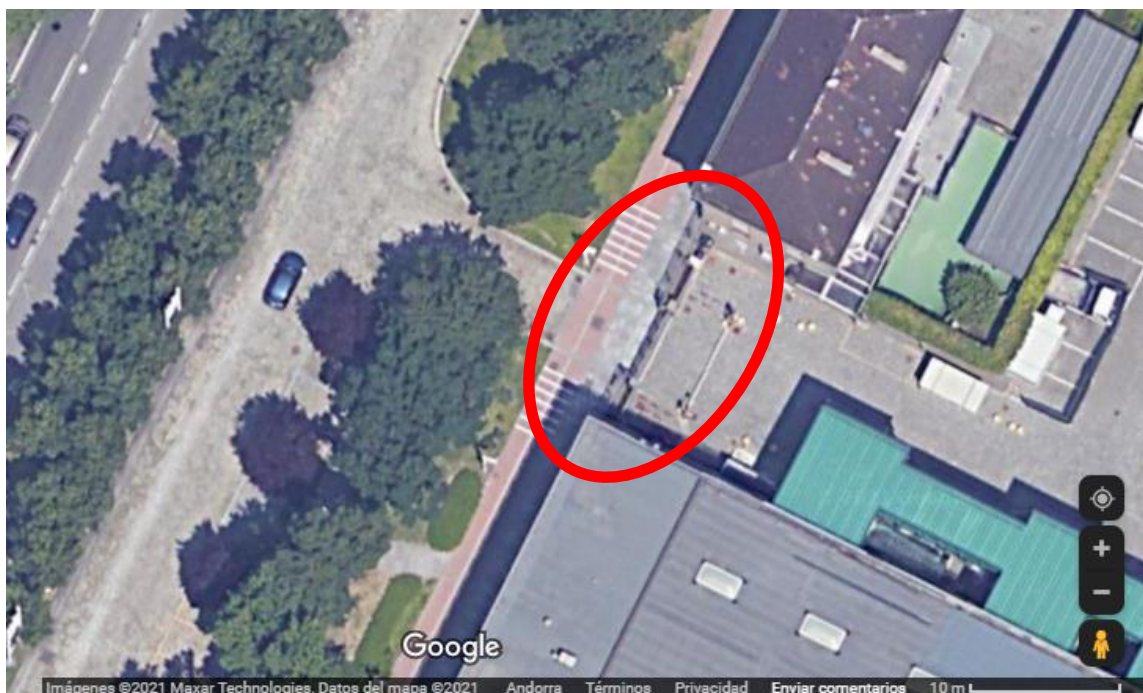


Figure 2.1.2.1: Location of the bike path bumps



Figure 2.1.2.2: Bike path bumps

For this experiment, the obstacles are known and measurable. For this reason, the measures of the bumps have been taken. The figure 2.1.2.3 shows an example of how the measures have been taken, using a calliper for short distances and a meter for the larger ones. The figure 2.1.2.4 shows the technical drawing made after the measurements with the shape and the size of these bumps, made with AutoCAD.



Figure 2.1.2.3: Measurement of the bike bumps

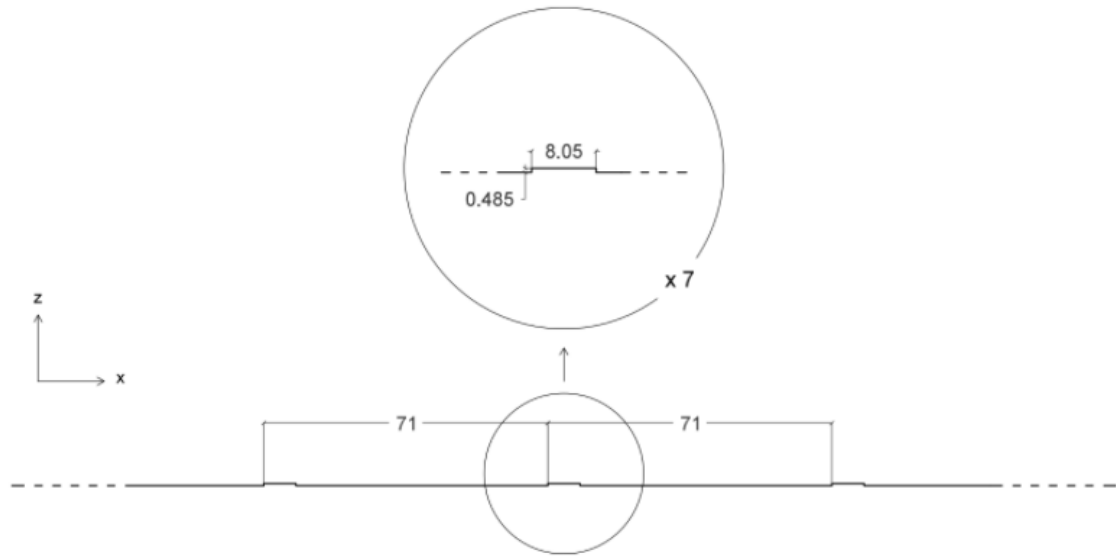


Figure 2.1.2.4: Technical drawing of the bike path bumps

- **Road bump**

This obstacle is located in the road on via Paolo Braccini. The main difference with the bike path bumps is that this one is bigger and there is only one.

The objective however, is similar as it wants to force the drivers of vehicles to reduce the speed because there is a crossing.

The figure 2.1.2.5. shows the location of this bump thanks to the google maps application, and to be more precise the obstacles are indicated with a red ellipse, and the figure 2.1.2.6. shows the view of the bump from a closer distance.



Figure 2.1.2.5: Location of the Road Bump

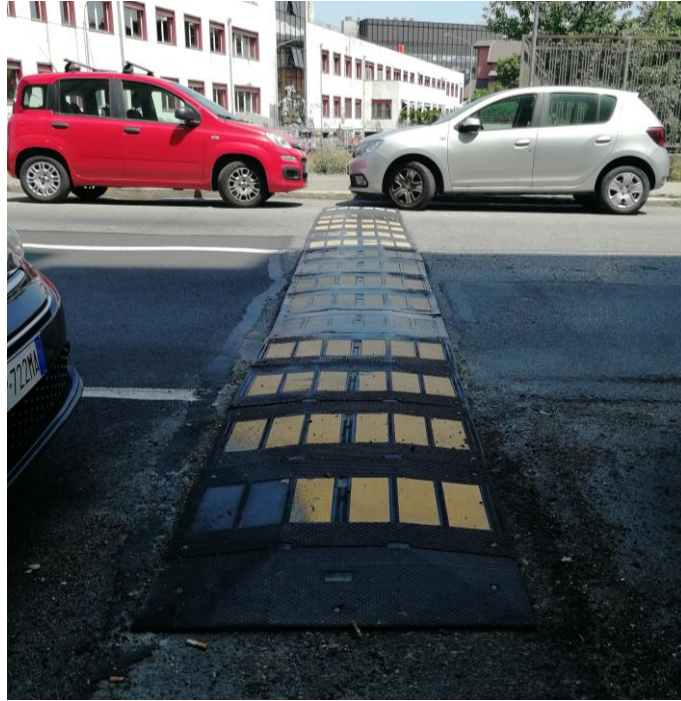


Figure 2.1.2.6: Road Bump

For this experiment, the obstacles are known and measurable. For this reason, the measures of the bumps have been taken. The figure 2.1.2.7 shows an example of how the measures have been taken, the figure 2.1.2.8 shows the technical drawing made after the measurements with the shape and the size of these bumps, made with AutoCAD.

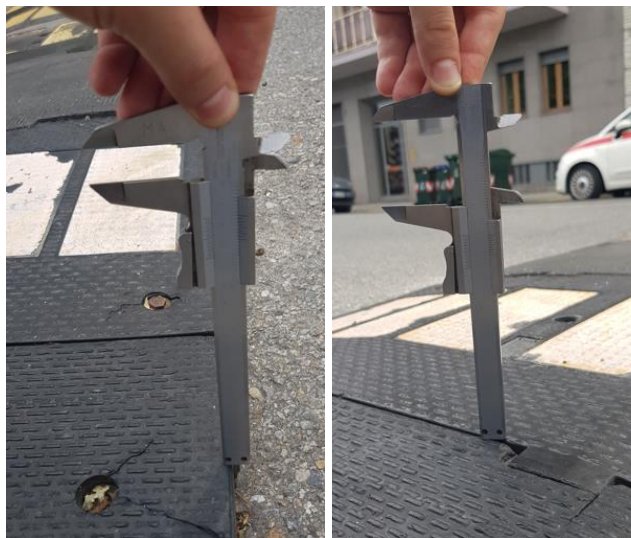


Figure 2.1.2.7: Measurement of the bump

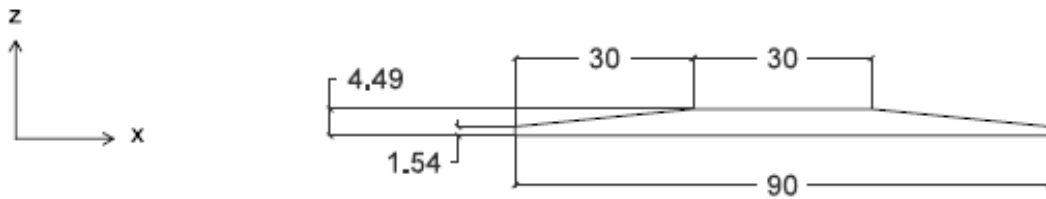


Figure 2.1.2.8 Technical drawing of the Road Bump

2.1.3 Irregular surfaces with unknown and not measurable obstacles: Cobblestoned Road

This experiment will be made on a road that is full of small obstacles, this is because the road is made by small rocks put it in a random and not uniformed way. This road is located in Corso Stati Uniti.

In this experiment it will be impossible to relate the outputs with the inputs. As it will be analysed later, with the known obstacles it will be possible to relate the outputs from the sensor to the moment when the e-scooter cross the bumps.

However, in this irregular surface this will not be possible to realize this relation, but it will give different information as a larger time of exposure at a high level of vibration.

The figure 2.1.3.1. shows the location of the road with the google maps application and the figure 2.1.3.2 shows three photographs of the road, the first one in the direction of the road, and the other two the unevenness of the road in two different places along the road, taken from the upside.



Figure 2.1.3.1: Location of the Road Bump

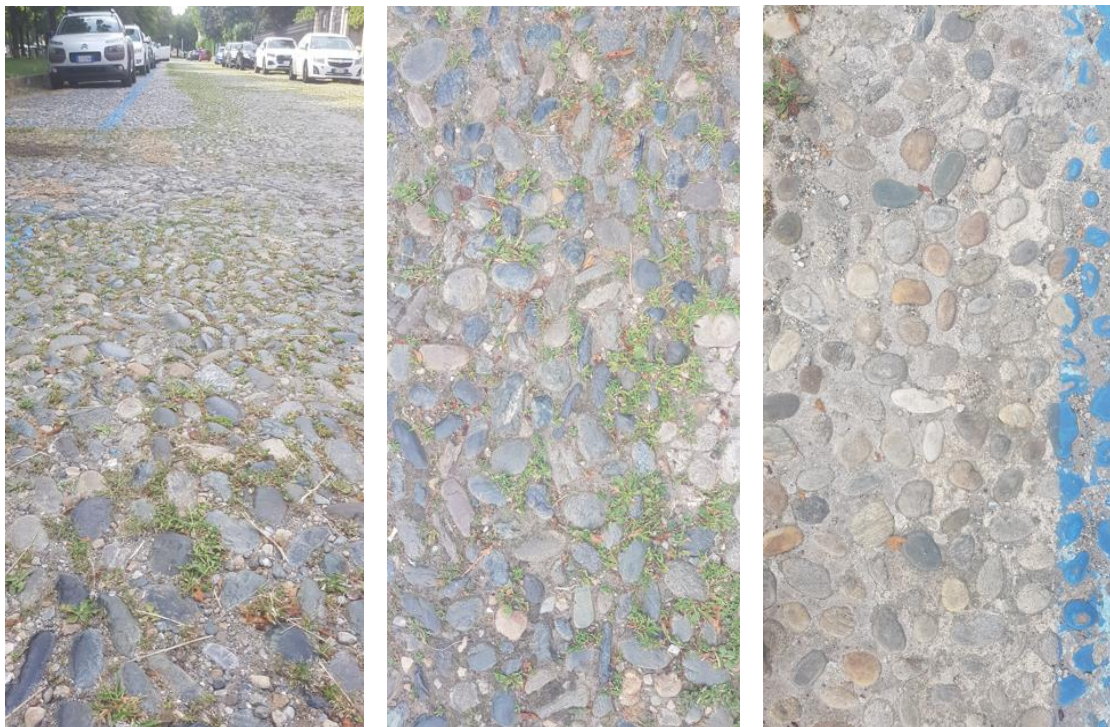


Figure 2.1.3.2 Different views of the cobblestoned road

2.2 Braking distance

Another type of experiment that will be carried out is to study the braking distance. These experiments will not give more information about the main topic of this thesis that is related to the vibrations and the comfort for the user. But it will contribute in a different way, allowing to study another performance of the e-scooter.

- The first objective will be to study the braking distance in function of the velocity. Thanks to this it will be possible to understand the performance and anticipate the braking distance depending on the velocity.
- Then it will be also studied if there is a difference between activating the regeneration mode when an emergency braking is done. With the application on the phone, it is possible to activate the regeneration mode or to deactivate it and then study if there are differences in the braking distance. The regenerative brakes couple the DC motor into a charging circuit, creating a drag force to the motor, this provides a brake and energy saving [7]. Allowing to not dissipate all the energy when it brakes and transforming some part of the kinetic energy to electric energy again to store it on the battery. Theoretically it is a really good solution to brake the vehicle, but at practice it has some problems. First of all, there is not much kinetic energy that can be captured. Secondly, the batteries cannot be recharged very fast, and this method is not constant on time, it has peaks that depends on the moments that the user brakes. Thirdly it is only effective when the velocity is quite high. Finally, the regenerative braking has not a good performance when it is needed of and emergency braking. The regenerative braking system will be effective when the user needs to reduce the speed from a high one to a lower one. In the case of study an emergency braking will be done, this means that it will be possible to study the difference between the regenerative mode activated and deactivated if there is such. Or see if the regenerative mode participates to the emergency brake or it does not.
- And finally, it will be carried out a study of the friction coefficient. The friction coefficient it is important because from this one it depends the braking distance. The higher it is this coefficient the lower it will be the braking distance. Then it will be compared with other two-wheeled electrical vehicles.

The experiments were performed at the parking located on Corso Castelfidardo 36, 10129 Torino.

To perform these measurements, it is been tried to measure in different ways to find to most suitable one.

Firstly, it was tried to measure the braking distance with a laser meter. For each experiment made, the braking distance was measured more than one time, and these measurements had a high variability. This fact it was probably due to the lack of a stable surface of the measuring device. Although a structure was made specifically to perform the measurements with this device, the measurements still had a great variability. Then the measurements were performed with a meter. The figure 2.2.1. shows the set up for

the braking distance experiment that was been carried with the laser meter, showing the two cones that marked the starting braking point and the structures that were used to measure with the laser meter.



Figure 2.2.1: Set up for the measurement with a laser meter

These experiments were not considered when performing the data analysis as the variability for each experiment was really high. However, it allowed to see some problems on the experimentation. First of all, as it can be saw it on the figure 2.2.1 the cones were marking the place where the user had to activate the braking system. This was a problem due to the variability of the starting point of brake. This problem was improved on the next days of measurement. As it can be observed in the figure 2.2.1. there is also a line that marks the starting point uniting the two cones, made by tape.

Another problem that was noticed during the laser meter measurements was that the direction of the braking was not always perpendicular to the line that created the cones. Then the experiments were not parallel. As the directions were in diagonal, the starting location of the braking along the line between the cones, was also important. Making more difficult the measurements.

And the last problem was that the distances were in some cases quite high, enough to need two measurements with the meter that would be used on the next experiments. As the maximum length of the meter was 3 meters and some braking distances were up to 2 times this length, these measurements would have a big error and would be more difficult to take.

The last two problems were improved by putting parallel lines to the starting line on the following six meters after the brake, and with a distance of 0.5 meters (fig. 2.2.2). On one hand this allowed the user to have a better idea of the direction that he had to maintain during the brake. And on the other hand it allowed to measure the distance as the sum of all the lines that the scooter crossed (0,5 m each one) plus the distance from the last line to the point where the scooter completely stopped, that was less than 0,5 m. This allowed to make the measurements that were bigger than 3 meters with much more precision, and in general to perform these measurements much faster.



Figure 2.2.2: Final set up for the measurement with a meter

3. Data acquisition system

The aim of the Data Acquisition System is to collect data, process it in the desired way, then record this data and store it to be able to perform a post-processing. The DAS is composed by a group of components that measure one or more electrical quantities and record their values in a digital form

The DAS can be defined by

- The number of quantities that it can acquire
- Sampling rate (Samples/s)
- Resolution and accuracy (N bits)
- Dimension
- Internal DAS Layout

For the study of this thesis the system that has been used is composed by four accelerometers, a GPS and the Simcenter SCADA SC-XS.

3.1 Sensors and scooter set-up

To acquire the desired data, it will be necessary to use the correspondent sensors. In this thesis two types of sensors were used, a GPS and accelerometers.

The GPS (fig. 3.1.1) will allow to measure the following data:

3 variables of a Geographical Coordinate System: Latitude, Longitude and Altitude

3 variables that correspond to the projections of the velocity: East, North and Up velocity.

The number of satellites

The GPS total speed



Figure 3.1.1: GPS model

For the GPS data it will be important to check signal of the number of satellites. The number of satellites has to be minimum 4 to ensure the veracity of the other GPS signals [7].

The accelerometers used are a triaxial ICP sensors allowing to measure the acceleration of each axis but with a problem that has to be taken into account. The values of acceleration that these accelerometers can measure are fluctuant and with a quite high frequency. For instance as it will be explained on the correspondent point, in the braking test these measurements will not be correct in all the time history.

Two models of accelerometers were used for these experiments. For the steering and the front floor, it has been used the model 356A24, ICP®, TRIAXIAL with a sensitivity of 10mV/g(±15%) a measurement range of ±500 g and the frequency rate up to 9 kHz, (fig. 3.1.2.) [8]. For the steering and the front floor, it has been used the model 356A15, ICP®, TRIAXIAL with a sensitivity of 100mV/g(±10%) a measurement range of ±50 g and the frequency rate up to 5 kHz (fig. 3.1.2) [9].

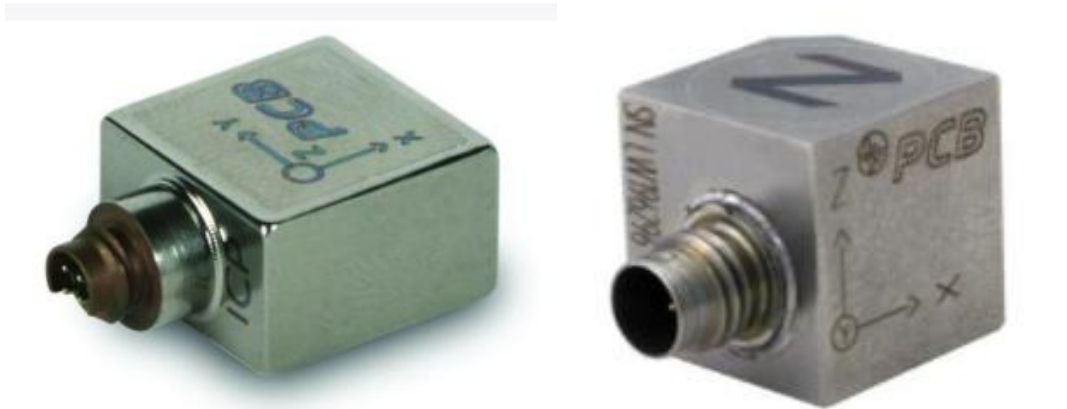


Figure 3.1.2: Accelerometer 356A24 (left) and accelerometer 356A15 (right)

Not all the experiments have been taken with the four accelerometers, but the position of each one it will be always the same. There have been chose 4 positions named as: Steering, Front Floor, Back Floor, and Back Wheel in the figures 3.1.3 and 3.1.4 are shown the position where the accelerometers were located in the scooter, then in the figure 3.1.5 there is the technical drawing of the scooter with the locations of the accelerometers. Not all the experiments have been made with the same configuration of the accelerometers, in each case it will be explained which ones have been used.



Figure 3.1.3. GPS and Front Floor Accelerometer (left) Steering Accelerometer (right)

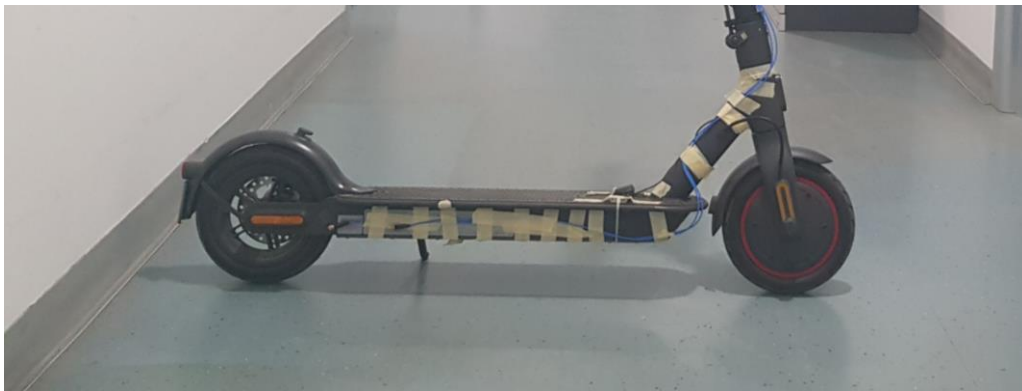


Figure 3.1.4 Back Floor and Back Wheel Accelerometers

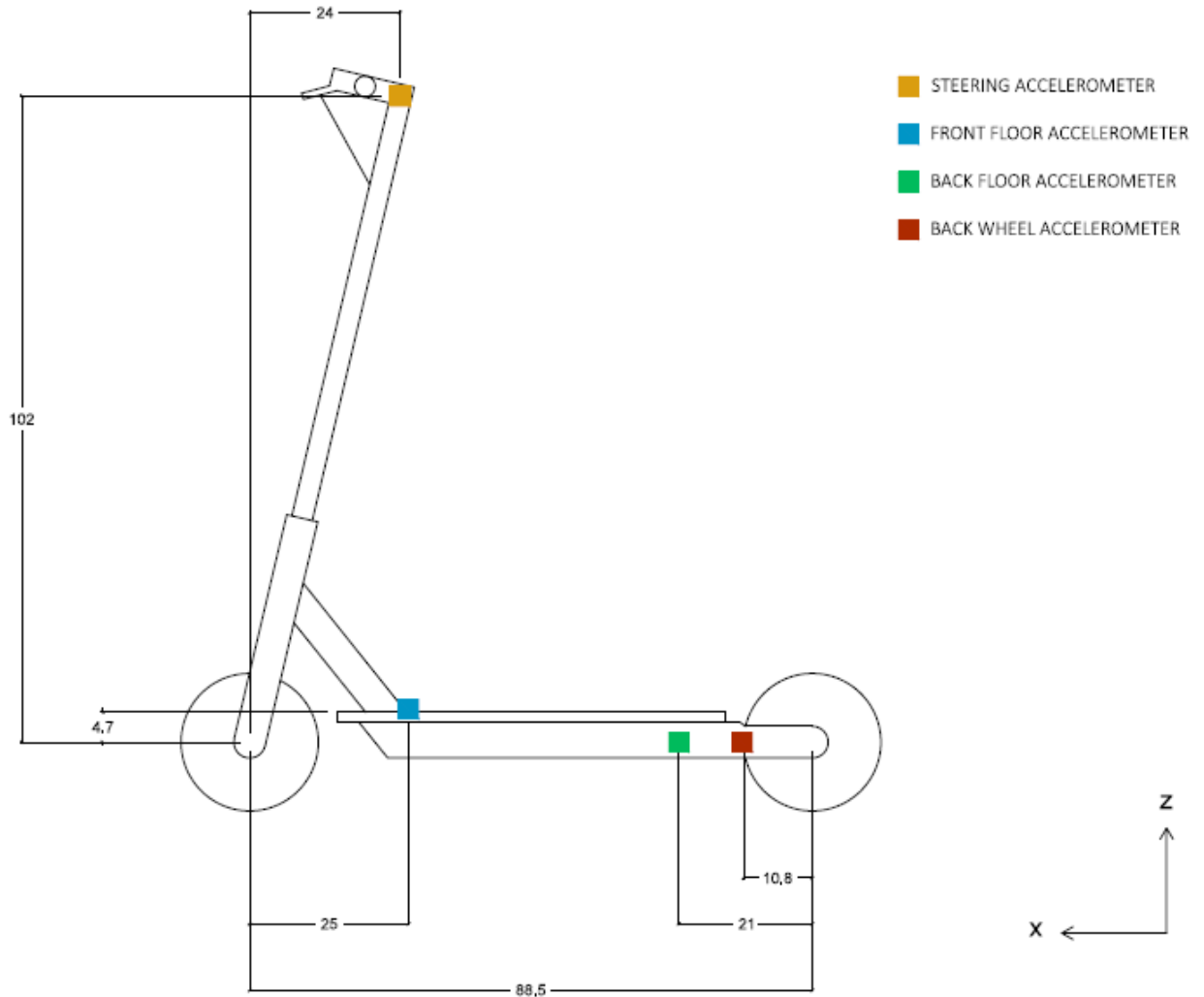


Figure 3.1.5. Technical drawing with the positions of the accelerometers on the scooter

These accelerometers have their own Local axis so it will be necessary to transform this local axis into the global axis of the scooter that has been explained before, if necessary. The easiest way to make this set up would be that the Local axis were the same than the Global, but physically it was difficult due to the cables. With the need to put them in a different way, it has been chosen to put them always with the same directions. In this way when the accelerations measured in local axis are converted in a global axis, it will be not necessary to make a sum of vectors. It will only be needed to change the orientation. In the table 3.1.1. it can be seen the local axis of each accelerometer transformed in the global axis.

Table 3.1.1 Relation between Global Axis of the scooter and Local Axis of the accelerometers

Global Axis	Local Axis			
	Steering	Front Floor	Back Floor	Back Wheel
X	Y	-X	-X	-X
Y	Z	-Y	-Z	Y
Z	X	Z	-Y	-Z

Another aspect to take into account is the sensitivity. For these accelerometers the supplier gives their sensitivity for each axis. These sensitivities will be important to introduce them into the SCADA template that will be explained on the next section. In the table 3.1.2 there is the sensitivity for each accelerometer for their Local Axis

Table 3.1.2 Sensitivities of the accelerometers in the Local Axis

Local Axis	Sensitivity [mV/g]			
	Steering	Front Floor	Back Floor	Back Wheel
X	10,38	10,07	102	102,5
Y	10,57	9,48	102,1	97,5
Z	10,31	10,31	102,3	98,6

3.2 Data acquisition with SCADA SC-XS

To record the data that will generate the sensors, it will be used the Simcenter SCADA XS. This device is a handheld recorder and it will record (by template) predefined measurement data on a micro-SD card. To record with this device, it can be used connected to a PC or the tablet that comes in with the device, and control it with the program Simcenter Testlab. And also controlled directly with the SCADA. In the first case it will be possible to measure with different templates but the second it will be recorded with the last template.

In the next points an explanation of how works the device and how it has been used will be carried out.

3.2.1 Description of the SCADA system

The figure 3.2.1.1 shows the three important sides of the SCADA system. From the top to the bottom there are [10]:

- Front connections: where the cables have to be connected to the correspondent sensors for the acquisition.
- Control Panel: from which it is possible to control the system such as power on/off, start/stop recording if it intended to use it without a PC.
- Power – communication – data: in this side it will be possible to charge the device, connect it by cable to the computer and insert the micro-SD card where data will be stored.



Figure 3.2.1.1 - SCADA SC-XS [10]ref

On the figure 3.2.1.2. there is an overview of the front connections of the Simcenter SCADA XS, for the study of this thesis it has been used the type SC-XS12-A/N.

	Type: SC-XS12-A/N
	Type: SC-XS06-E
n ABC ('n' stands for 1, 2, 3, 4) 9-pin LEMO connector.	To be used as: input for one tri-axial sensor, or 3 V/ICP®/TEDS single-ended inputs.
TACHO 4-pin LEMO connector.	For dual tacho input.
CAN 4-pin LEMO connector.	For CAN 2.0B compliant message recording.
SPDIF	Supports HMS functionality.
	Supports Global Navigation Satellite System (GNSS)
HS 9-pin LEMO connector.	To be used as binaural headset interface.

Figure 3.2.1.2 - Front connections of SCADA system [10]

In the case of study, the connections that will be used will be: the *nABC* connectors for the accelerometers, they can work as an ICP (fig 3.2.1.2) that is the type of accelerometer that has been used; and the connection that supports Global Navigation Satellite System to connect the GPS.

For the *nABC* connectors the sampling rate can be set to a maximum of 50kHz. For the GPS it is up to 4Khz

3.2.2. SCADA system set up

To perform the measurements with the SCADA, as it has to be connected to the accelerometers with cables, it is necessary to carry it in the scooter. To achieve it, it has been used a package that is attached to the steering, and inside there will be the SCADA system, and some part of the cables.

On the figure 3.2.2.1 it can be seen the set up.



Figure 3.2.2.1 Set up of the SCADA support

Then for a later calculation, the mass of the SCADA system and the cables have been measured. Each cable has a mass of the box, the SCADA system and the cables.

$$m = m_{SCADA} + m_{box} + m_{cable} = 540 + 1149 + 111 \cdot 4 = 2113 \text{ g} = 2,11 \text{ kg}$$

3.2.3. Testlab SCOPE: creating a template

The first step to start the data acquisition, is creating a template. It will be necessary to set the configuration of this template in order to have the desired specifications, such as the number of channels that will record some data, information about the sensors, triggers...

In the figure 3.2.3.1 there is an example of the main screen with the templates already created.

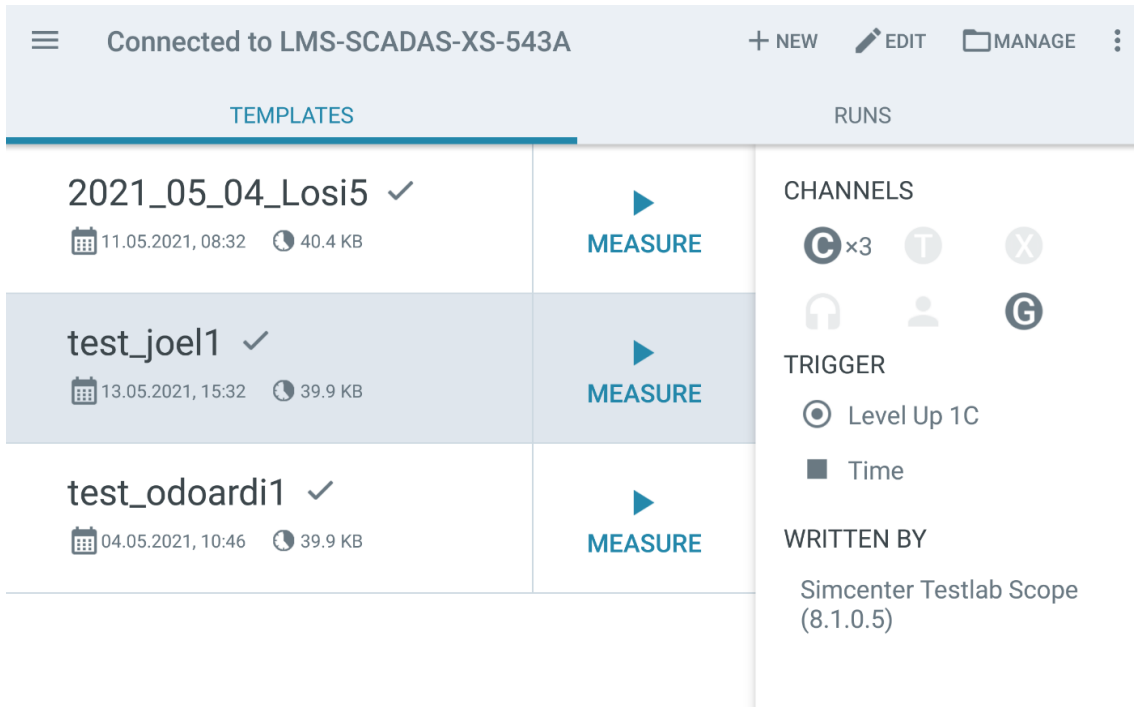


Figure 3.2.3.1 - Main screen on Testlab SCOPE , “Templates tab”

To create this template, it is necessary to set some information in order to make not only a correct acquisition but also in the desired way. The figure 3.2.3.2. shows how this information is divided in some tabs. In the case of study, the most important tabs are ADC, GPS and MEASUREMENT:

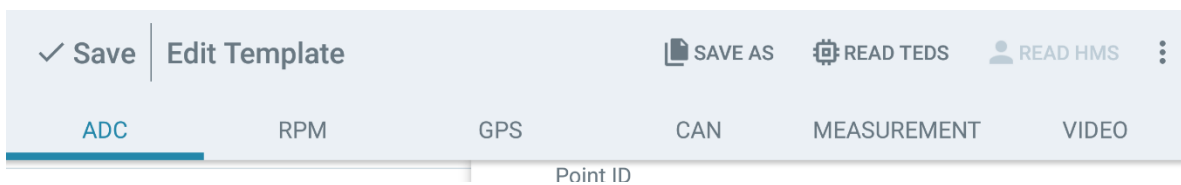


Figure 3.2.3.2 - Creation of a template, tabs.

The ADC tab gathers all the information about the $nABC$ connectors, that in this case will be the ones concerning the accelerometers. The first thing to do is to select or unselect depending on if it has to record or not. In the case of study, it will be selected the three channels (triaxial) for each accelerometer connected. For instance, when the experiments have been performed with 4 accelerometers, 12 channels have been activated.

Once all the desired channels have been selected, the next step is to configurate each one.

Each channel will represent one axis of one of the sensors, the next information have been applied:

1. the name to identify easily the channel;
2. the quantity that it measures and in which unit, in the case of study it is been chose “Acceleration” and “g”,
3. the sensitivity of the sensor, on that axis that is been provided by the manufacturer (see table 3.1.2.)
4. the channel group to identify the type of measurement, in this case it has been chose vibrational;
5. input range. it can be selected an amount, and after the measurements check if it is good otherwise, change the value, in the case of study it has been check that 40 dB is a good value;
6. the type of sensor, as explained before the accelerometers used are ICP.

For the GPS tab there is only the option to select the GPS module and the 9 possible measurements that can perform, because it cannot be modified.

In the measurement tab it can be selected some aspects about the way that the device will make or store the measurements. It can be selected the number of runs, the frequency sample rate, the storage sample rate and the triggers

For the frequency sample rate, it has been selected 51200 Hz and for the storage sample rate of the vibration 5120 Hz.

3.2.4 Data export from Testlab SCOPE to MATLAB

Once the data recorded is stored, it can be exported to a computer. For the treatment of this data, the software MATLAB has been used.

In the study case, as mentioned before, the data will be stored in a micro-SD and then exported to a computer that has the consequent port.

The files created by the SCADA system are on *.xtrp* format, to change to a type of file suitable for MATLAB, it has been used the Recorder data conversion program.

In the case of study, when the data has been exported, it has been selected an option to compress the information of the variables to a structure array, grouping the signals in fields, for example in one field there will be all the information about the accelerometers.

4. Preliminary data post processing

After obtaining the data, it has been made a preliminary post processing. This means that this first step is not focused on finding results and find conclusions. This first step has been done to understand the variable and how to treat them in order to see if they are coherent, and try to see if the measures are correct or there is a problem. This process allows to see if there is a problem to then solve it.

4.1 Initalization of the variables

Once the data measured with the SCADA has been transformed into a MATLAB file, it is necessary to understand how the information is organized. Each file correspond to one experiment, and will have 6 structure arrays, with the name *Signal_i*, with $i=[0,1,2,3,4,5]$. These structure arrays have the information about 1 or more signals.

These 6 *Signal_i* have the next information:

Signal_0: the triaxial acceleration of each accelerometer

Signal_1: the latitude and longitude measured with the GPS

Signal_2: the altitude measured with the GPS

Signal_3: East, North and Up velocity measured with the GPS

Signal_4: the number of satellites connected to the GPS

Signal_5: the total speed of the GPS

The ones that have more than one signal measured, store the information of these signals in the same matrix. For instance, the structure array called *Signal_1* has the information in matrix of 2 columns, the first one corresponding to Latitude and the second one to Longitude.

For each *Signal_i*, there will be three another three structures array inside.

X_values: it contains the information of the time vector.

Y_values: it contains the information about the corresponding signal values.

Funncion_record: stores general information about the signals measured, as their name.

The values that will be used to make the post processing are the *x_values*, and *y_values* but they cannot be used directly, they have to be treated first.

For the *y_values* it will be necessary to multiply the stored vectors concerning the variables, to a constant called *unit_transformation*. For the *x_values* it will be necessary to create the time vector. The information is given by different values: the time that it started to record that is bigger than 0, the time between two consecutives measures and the number of measures taken during the experiment, that as expected will be equal than the size of the *y_values* vectors. These three values are stored with the name of: *start_value*, *increment* and *num_values*. With these values it can be created a vector of

num_values elements, where the first value is *start_value* and then for each posterior element it will be needed to sum *increment*.

Then another step is required to initialize the variables. As explained before, for the signals corresponding the accelerometers, there is a matrix that stores the measures in columns. The number of columns will be 3 times the number of accelerometers, as they are tri-axial. The columns are sorted by accelerometers, meaning that the first three columns will correspond to the x, y and z axis of the first accelerometer, then the three axes of the second one and so on. However, these axes are the Local axes of the accelerometer, and it will be needed to match them to the Global axis of the scooter.

4.2 Preliminar analysis: validity of the experiments

The next step is to perform a first analysis of the experiments values in order to see if they are coherent. This first analysis determines if the sensors have acquired the measures correctly. There could be different scenarios where the measures are not correctly acquired, it could be due to the cables, the sensors or the SCADA system.

For the case of the accelerometers, some considerations have to be taken into account. They have to be glued to a surface so the vibration can be transmitted correctly from the surface of study to the sensor and the cables have to transmit the values correctly to the SCADA system.

To illustrate this first analysis, an example has been explained below, with one experiment of the bike path bumps at the velocity of 19 km/h

On the figure 4.2.1 it can be observed 4 graphs, the first three, corresponding to the accelerations from the three axes of the accelerometer on the front floor. And the last one a superposition of the 3 axes.

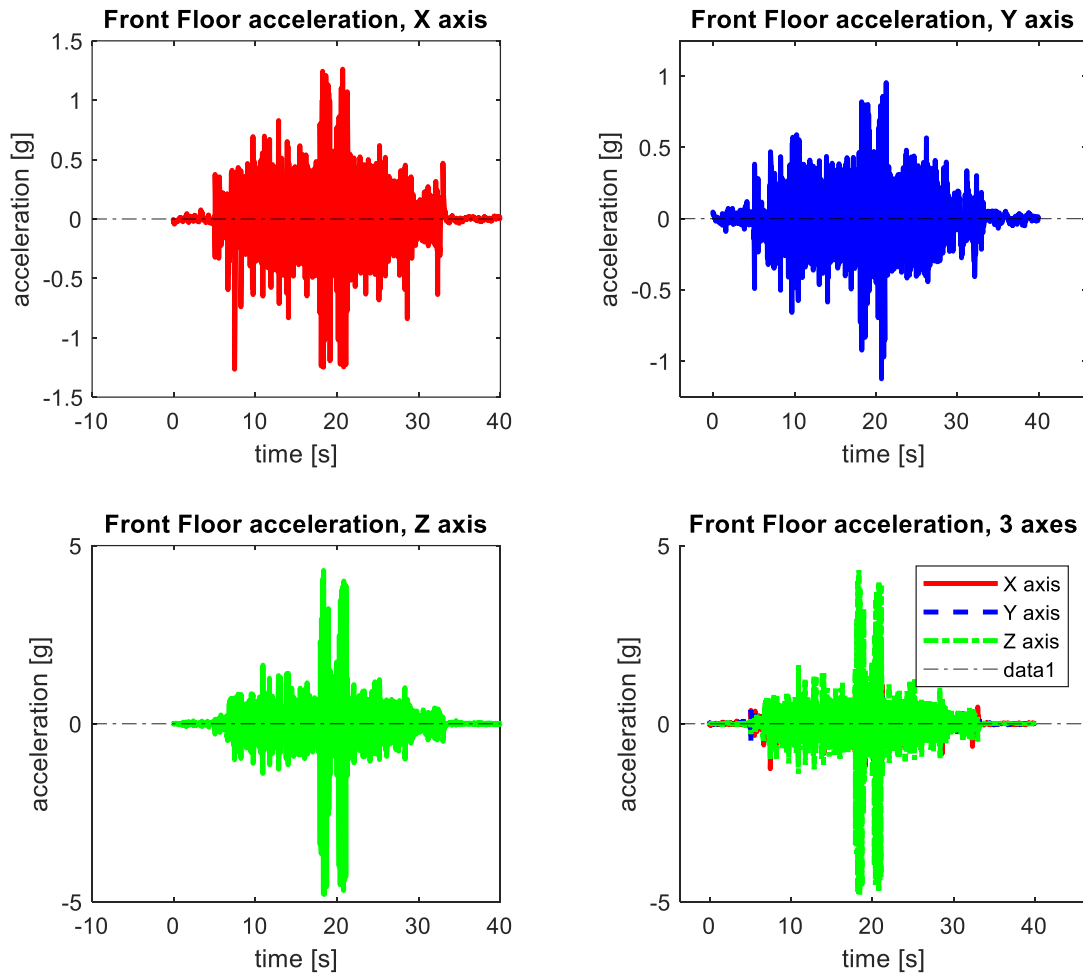


Figure 4.2.1 Triaxial accelerations of the Front floor accelerometer

As it can be seen, in the Z axis there are two intervals where the value of the acceleration is much higher than the rest of the time history. With this first look it seems coherent as the experiment composed by three differentiable sections. The first section is composed by the time that the scooter starts from a resting situation and then tries to reach control cruise mode, all this section will be on the bike path that do not have big obstacles. The second section corresponds to the bumps crossing, that are composed of two series of seven bumps that are quite close. And then another section where the user continues to drive until finding a resting zone where can stop the recording.

Then looking these graphs, it could be assumed that the results are coherent. However, to be surer about this, it can be take a closer view of the acceleration in the Z axis, and try to understand what is happening and relate the signal to the obstacles crossed. In the figure 4.2.2 it can be seen this acceleration over the interval of time that cross 7 bumps. The hypothesis that this part was a section of the 7 bumps will be validated in the next points. However, the hypothesis seemed quite probable after it has been seen that there

was 4 intervals (with almost the same duration in time) where the response of the X and Z acceleration was much bigger than the rest of the experiment, that concurs with the 4 series of 7 bumps that were crossed. Moreover, the response of the acceleration was very similar between these 4 intervals.

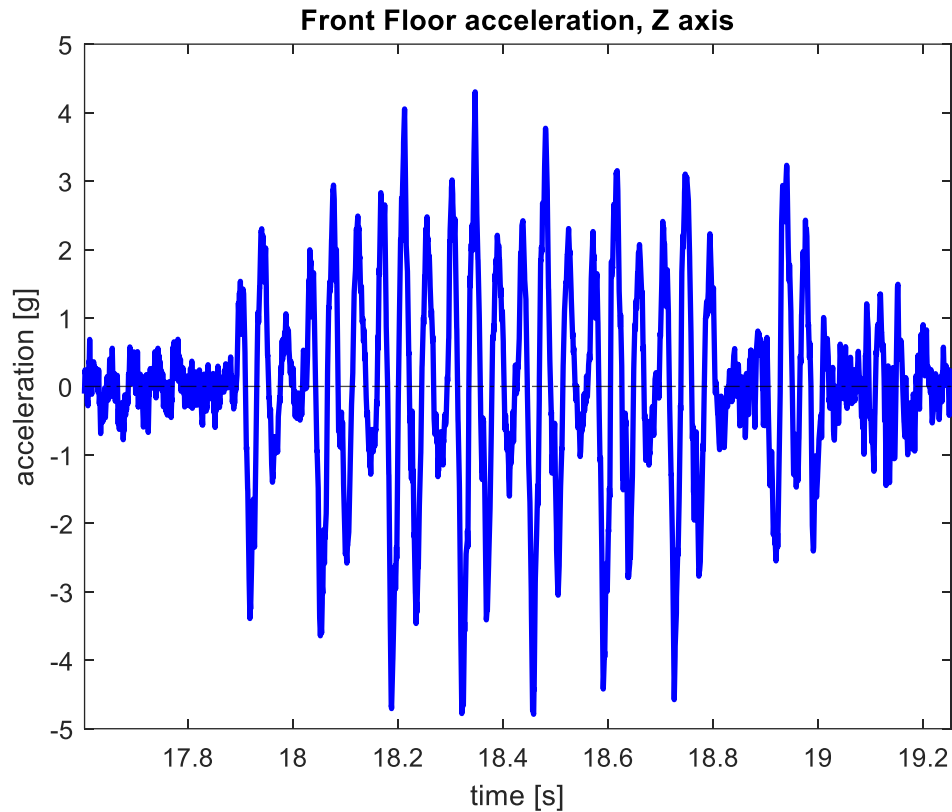


Figure 4.2.2: Front floor acceleration during the crossing of the bumps

As it can be seen, there are some peaks that stand out about the rest. As it has been explained, this first analysis it is focused on see if it has coherence. To check this coherence, it has been tried to analyse this response with the physical form of the bumps. Then a more exhaustive analysis will be carried out.

First of all, there is 7 bumps, and the two wheels pass through them, this makes a total of 14 times that a bump is being crossed.

Secondly there is also known comparing the distance between the wheels and the distance between bumps, that the back wheel crosses the first bump immediately after the front wheel crosses the second bump.

With this information, on the figure 4.2.3. it has been marked the points that would be suitable to match these conditions. This does not mean that are the instant of time that the wheel starts to cross it. These peaks seem to be a reaction of the bump. However, the values marked with dots have negative value of Z, this means that probably is not the first moment of impact between the wheel and the bump, because with the coordinate

system chosen, the first thought would be that at the moment of impact the value is positive. Then the dots marked are not related in a specific moment of the crossing of the bump. But it seems that they are connected, and equivalent between them. If this connection can be made, then the hypothesis that this interval correspond to the crossing of one series of 7 bumps will be validated.

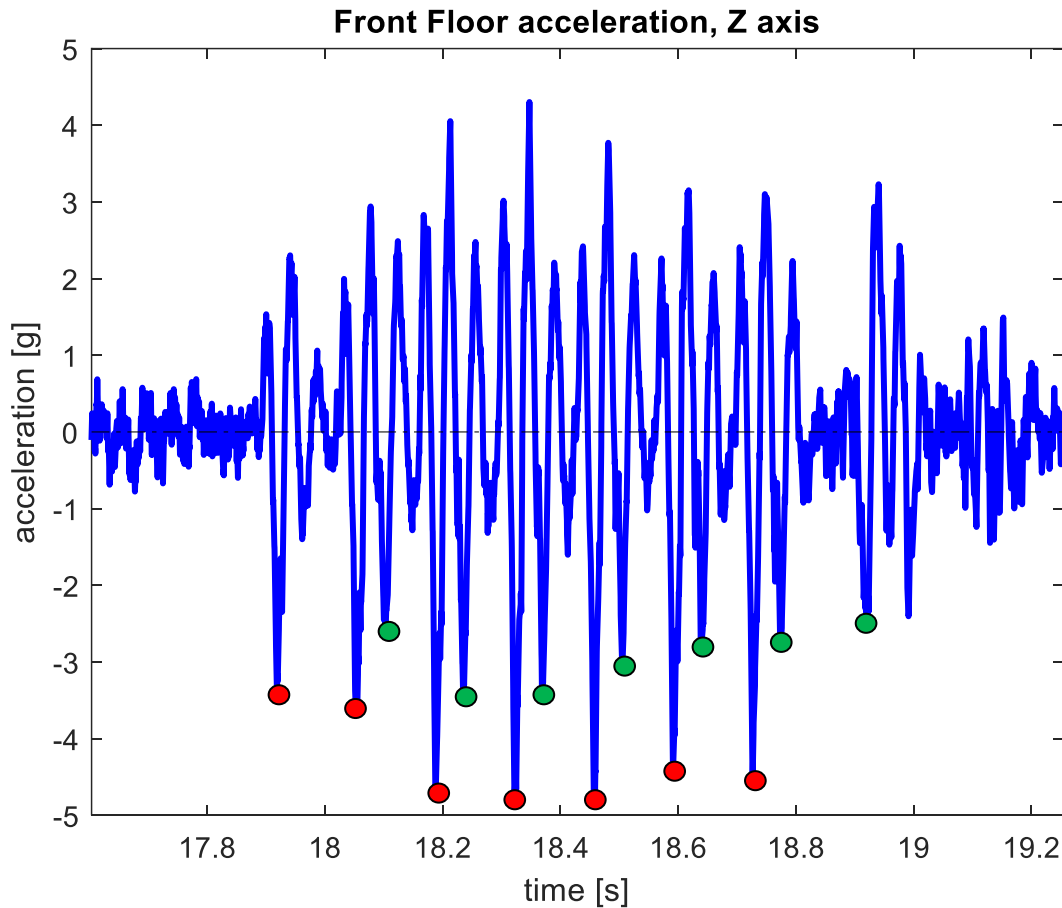


Figure 4.2.3: Hypothetical peaks corresponding to the bumps crossing

In the figure 4.2.3 it has been marked in red dots what would be the crossing of the bumps by the front wheel, and with green dots the crossing by the back wheel. Two aspects can be denoted looking at these, firstly that they are quite equidistant between the dots corresponding to a wheel. And that the peaks that marks the crossing of the front wheel are higher than the ones corresponding to the back wheel. This last one it has sense, as the accelerometer that is being analysed is placed closer to the front wheel. To ensure this hypothesis, it has been calculated the time between the crossing of two bumps from the same wheel. And then the time that the second wheel needs to cross the same bumps than the front floor.

Time between the crossing of two bumps for the same wheel:

$$t_{bumps} = \frac{D_{bumps}}{V} = \frac{71 \text{ cm}}{19 \text{ km/h}} = \frac{71}{19} \cdot \frac{1 \text{ km}}{10^5 \text{ cm}} \cdot \frac{3600 \text{ s}}{1 \text{ h}} = 0,1345 \text{ s}$$

And the time that the second wheel need to pass the same bump than the front wheel:

$$t_{back \text{ wheel}} = \frac{D_{bumps}}{V} = \frac{88,5 \text{ cm}}{19 \text{ km/h}} = \frac{88,5}{19} \cdot \frac{1 \text{ km}}{10^5 \text{ cm}} \cdot \frac{3600 \text{ s}}{1 \text{ h}} = 0,1677 \text{ s}$$

With these values it has been possible to plot verticals lines to see if the hypothesis made is correct. In the figure below it can be seen in red lines the moments where the front wheel should cross the bump, and the green lines that are the ones where the back wheel crosses the bumps.

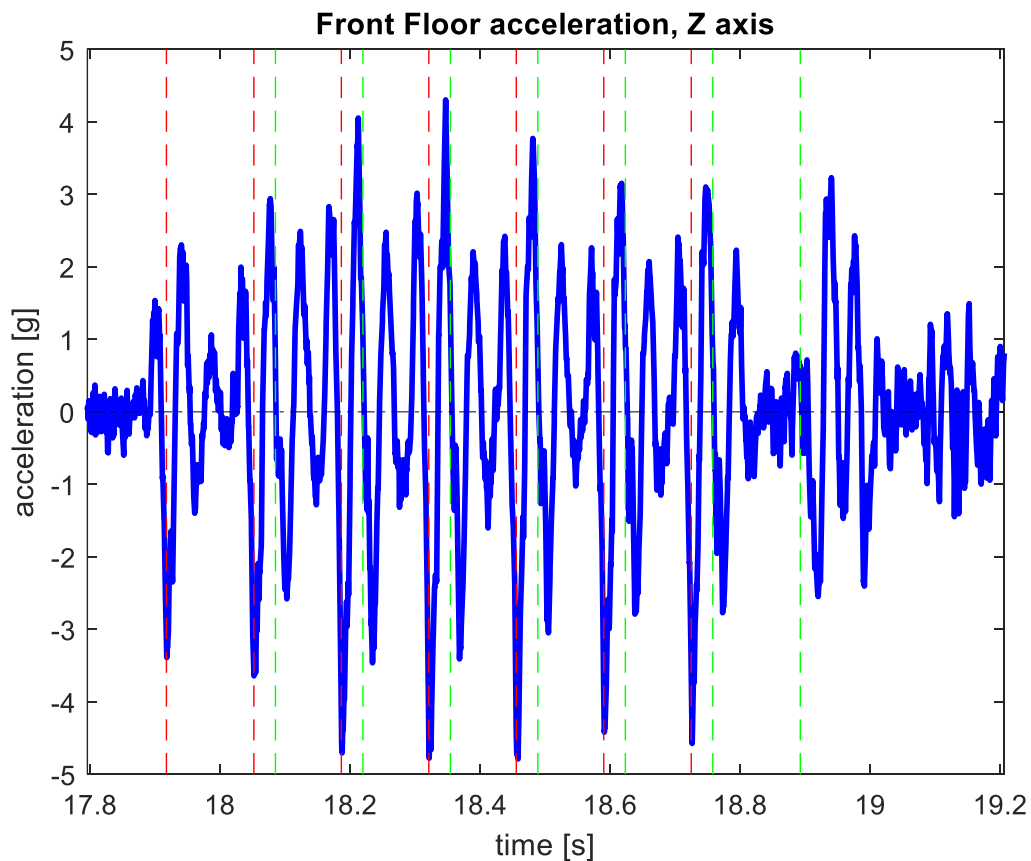


Figure 4.2.4: Vertical lines showing the instant when the wheels cross the bike bumps

As it can be seen, for the supposed bumps concerning the front wheel it matches perfectly. However, for the ones concerning the back wheel the green lines match with a series of peaks but not the ones that were thought on the first moment. This validates a

part of the hypothesis. Not all of the hypothesis is correct, but the main point was to see the coherence. For the red dots, it has been proved that they are related to the bumps crossed by the front wheel, then it can be supposed that the measure is coherent and has not any problem.

This procedure of looking the accelerometers must be done for all the accelerometers in order to ensure their validity, however a more superficial analysis has been made for the others, just checking by eye that the shape is similar.

After analysing the accelerometers, the GPS signal can be observed too. On the figure 4.2.5. it can be seen the main signals that the GPS records.

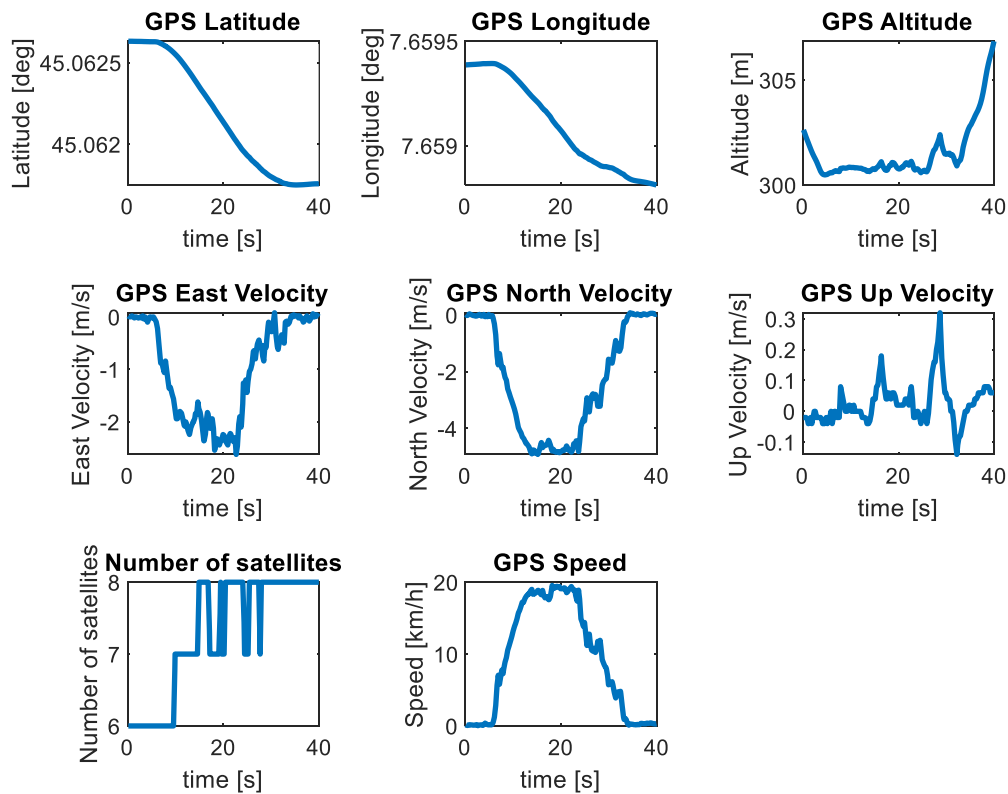


Figure 4.2.5.: Signals measured by the GPS

In the figure 4.2.5. it can be seen all these signals, that will be studied in the posterior points, for this preliminary analysis the signal in which the attention is focused is on the GPS speed. As it can be seen, there is a part where the speed is 0, that corresponds to the interval of time from the moment the record button of SCADA has been pressed, to the moment that the user starts to drive. Then another interval where the speed increases until the desired speed that is 19 km/h, after this interval it can be seen another one with constant speed that corresponds to the moment from the control cruise is achieved until a position after the bumps, and then another interval where the speed decreases to stop the scooter and then stopped the recording. With this first look it can be assumed as

with the accelerometers that the results are coherent. Then the measure is considered valid.

This procedure will be different for each type of experiment, but the procedure has been similar, comparing the results with how the measurements are taken, the obstacles or the type of experiments.

By doing this preliminary analysis, during the firsts experiments it has been able to detect a problem coming from one of the accelerometers. As all the other measures were coherent, the first thought was to change either the accelerometer or the cable. By doing this, and then performing other measures it was possible to identify the cable as the problem and then solve it by replacing it.

5. Data post processing

Each experiment has been studied in a different way, focusing in the information that it can offers. However, a treatment of the variables has been used in common for all the experiments.

First of all, it has been determined the time of study. In the experiments there is a large number of values that are not of interest. When the recordings of the SCADA were made, the user had to press the record button, then close the box that contained the SCADA system and start the procedure, that also needed a time to reach the speed, then perform the part that was of interest and finally some time to stop the recording manually. This procedure created a great amount of data that was not of interest. Is for that reason that it will be necessary to detect the interval of time of interest, and focus only on that part. For each experiment it will be explained which has been considered the part of interest and how has been isolated.

Another procedure that has been made in common for all the types of experiments is to filter the signal that came from the accelerometers. These signals had a lot of noise that was not produced by the physical vibration of the scooter. Applying a filter made the signals smoother, but is important that the filter do not modifies the signal, so the filter band has to be taken in a way that improves the signal but do not modify it. For each experiment it will show on the next points the difference between the signal without modify and the signal filtered with a frequency that has been considered.

5.1 Bike path bumps

For these experiments, the setup with all the accelerometers has been used.

As it has been explained before, the experiment was performed in the bike path of the Corso Castelfidardo. In the figure 5.1.1 it is shown the route taken by the scooter, recorded by the GPS.

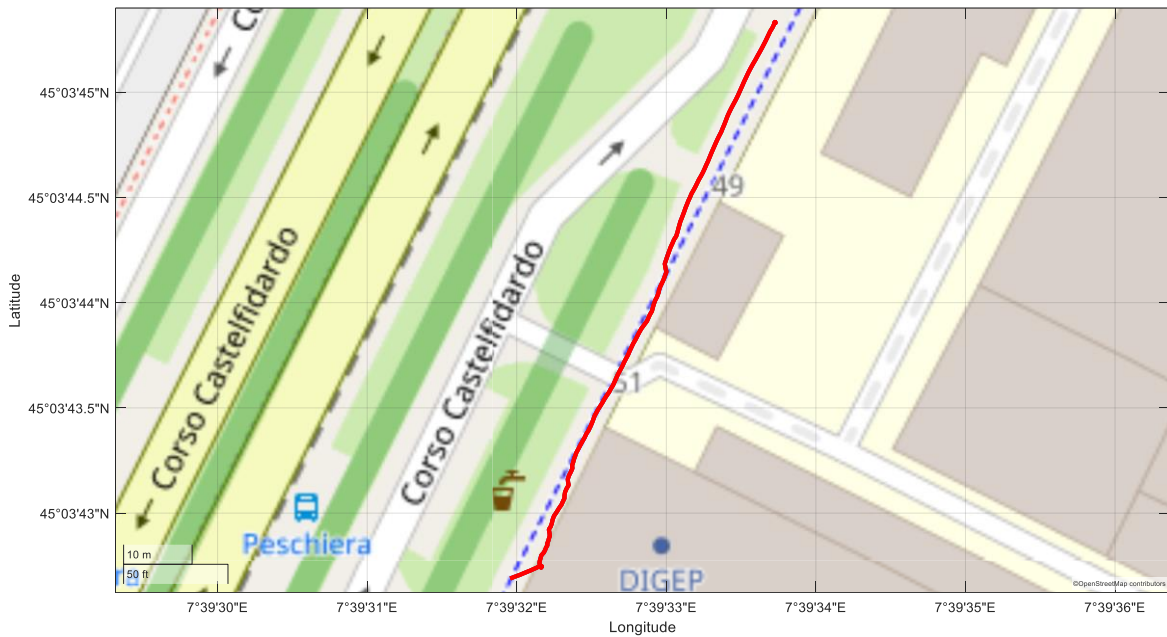


Figure 5.1.1: Route followed by the driver for the bike path bumps experiment

The first step made, as explained before, has been to isolate the interval of interest. For this case, this interval has been considered as the crossing of one series of bumps. To proceed with this isolation, it has been chosen the Z axis acceleration of the steering accelerometer. Once the interval has been chosen for this accelerometer, it has been applied the same one to the other accelerometers. This procedure has been applied to all the experiments but it will be illustrated with one experiment, in this case with one experiment at the velocity of 19 km/h. In the figure below, it can be seen all the signal recorded by the SCADA system.

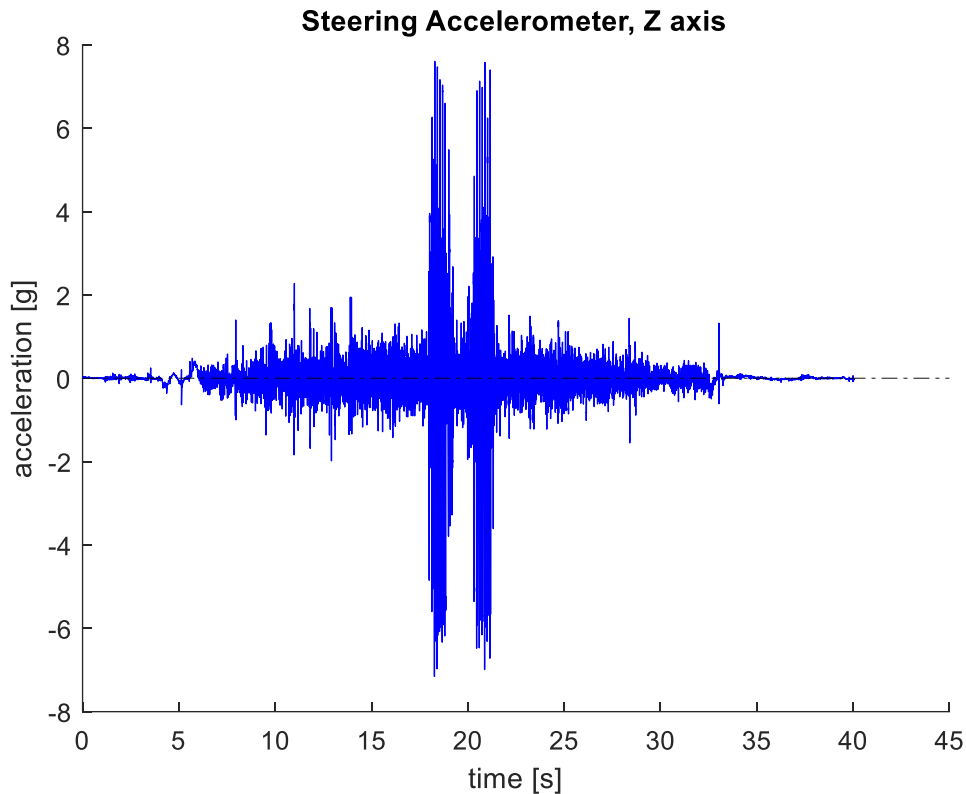


Figure 5.1.2.: Acceleration in Z axis of the Steering, for an experiment at 19 km/h

As it can be seen, there are the two expected intervals where the values of the acceleration are higher than the rest, each of these intervals correspond to two series of seven bumps. As explained before only one of these series will be considered, specifically, the first one. To isolate it, firstly it has been searched the peaks, and then an interval of time around the peak corresponding to the first peak has been imposed.

If the time at the mentioned peak is called tp , then the interval it has been generated as $t = [tp - C1 \quad tp + C2]$. Being $C1$ and $C2$ constants, that are equals for all the experiments at one speed. As it is logical, at higher speed, the smaller will be the time crossing the bumps, for this reason it is not the best solution to use one interval for all the speeds. These intervals have been chosen looking the plots of the bumps and deciding it in a way that the interval compresses all the bumps and a bit more before and after to appreciate better the phenomenon. In the figure 5.1.3 it can be seen the interval that will be isolated that is between the two red lines.

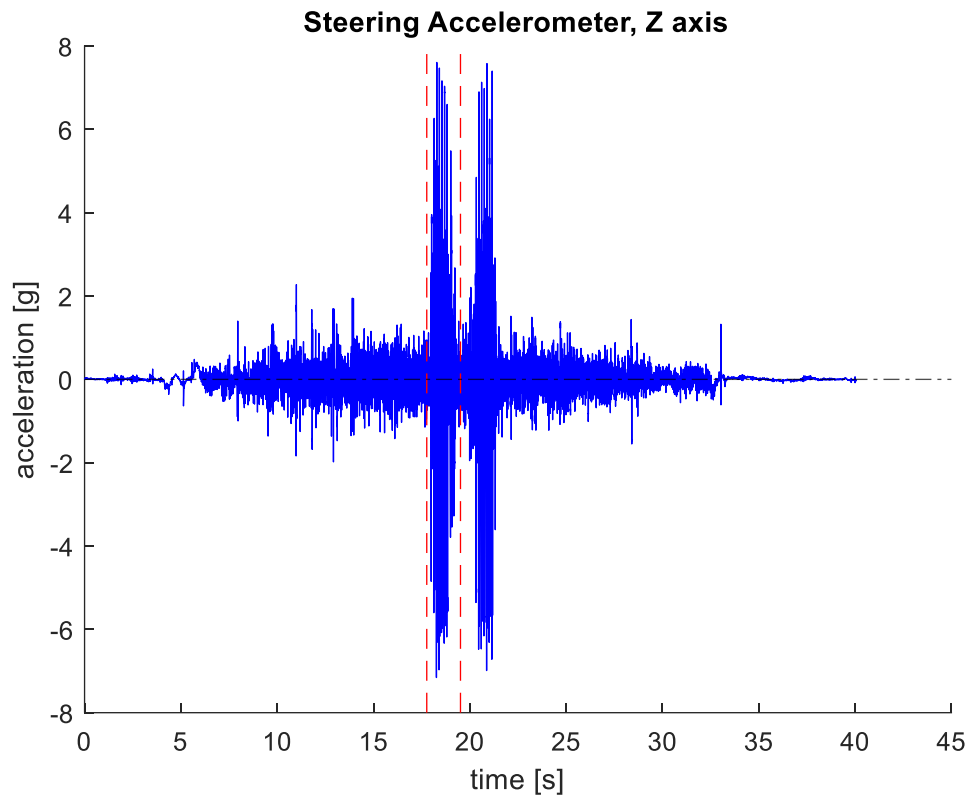


Figure 5.1.3: Isolation of the interval of interest

For each of the three velocities the interval has been set to:

$$9 \text{ km/h} \rightarrow t = [t_p - 0,5 \quad t_p + 3]$$

$$14 \text{ km/h} \rightarrow t = [t_p - 0,375 \quad t_p + 2,25]$$

$$19 \text{ km/h} \rightarrow t = [t_p - 0,25 \quad t_p + 1,5]$$

And then another extra step has been set in order to facilitate the next calculations. The instant of time $t=0$ has been assigned to the first peak of the bumps $t_p=0$. It is mandatory to not modify the increment of time between each measure, so the operation to modify the vector time it will consist on subtracting to each value of the vector, the original value of time of the first peak. In this way it is easier to compare between the different measurements. On the figures below it has been plotted for the 3 velocities, the intervals explained and with the variable time modified as explained.

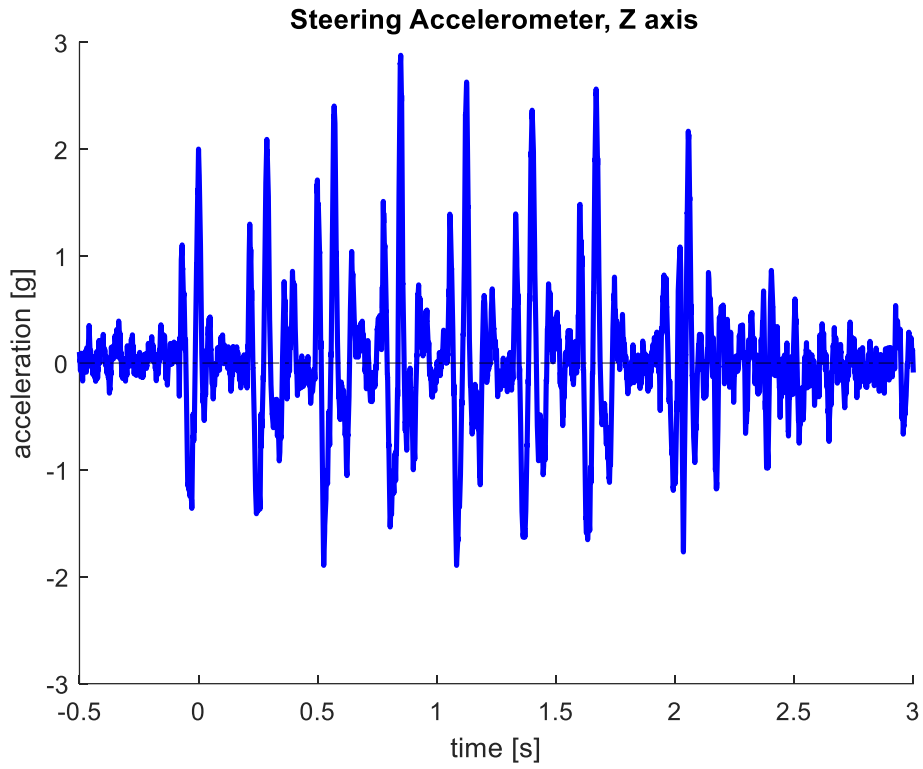


Figure 5.1.4. Time isolation for the 9 km/h experiment

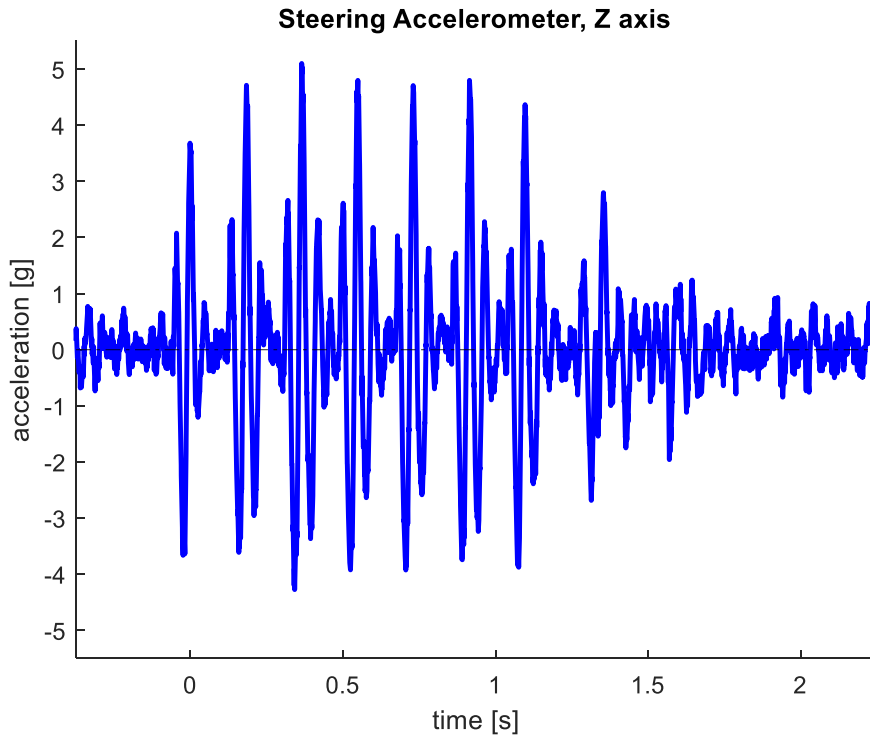


Figure 5.1.5: Time isolation for the 14 km/h experiment

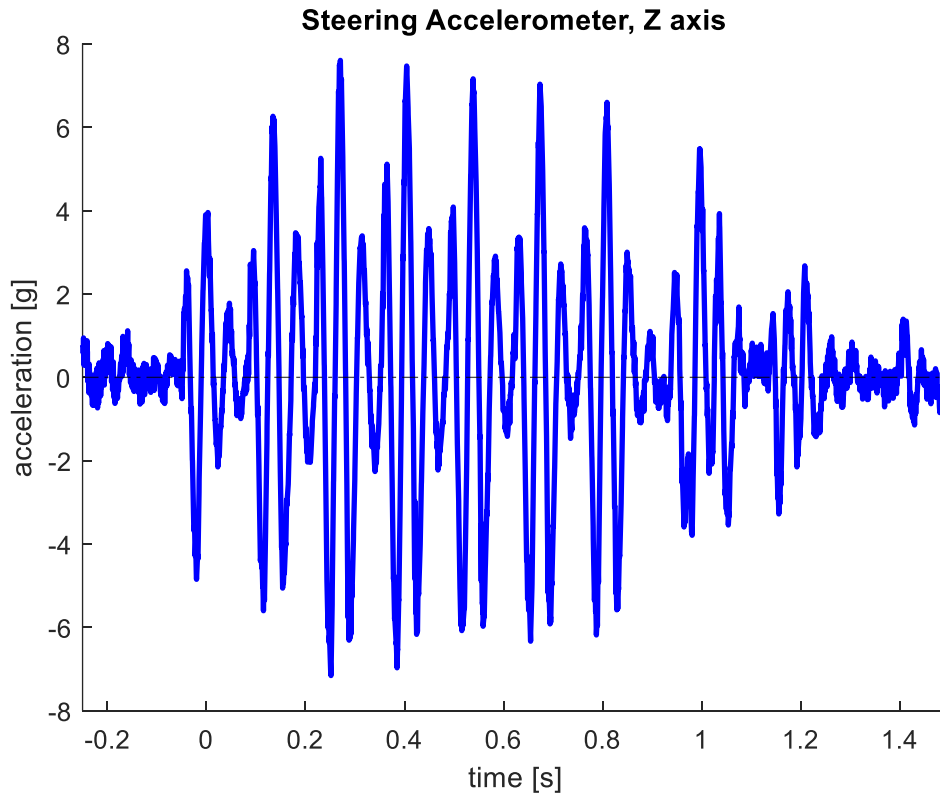


Figure 5.1.6: Time isolation for the 19 km/h experiment

The next step is to filter the signal. The selected band pass filter, it has been chosen by comparing directly by looking the signal filtered and the original. On the figure 5.1.7 it is represented this comparison for the X and Z axes of the 4 accelerometers, using a band pass filter of [1Hz 100Hz].

However, these comparisons cannot be appreciated in this figure, the figure is on order to expose how the procedure was made. In order to show how these differences are, it has been plotted for only one of the 8 signals, and limiting the time to the crossing of two bumps. This it can be seen in the figure 5.1.8, and as it can be observed, the signal is not modified and only the noise is eliminated.

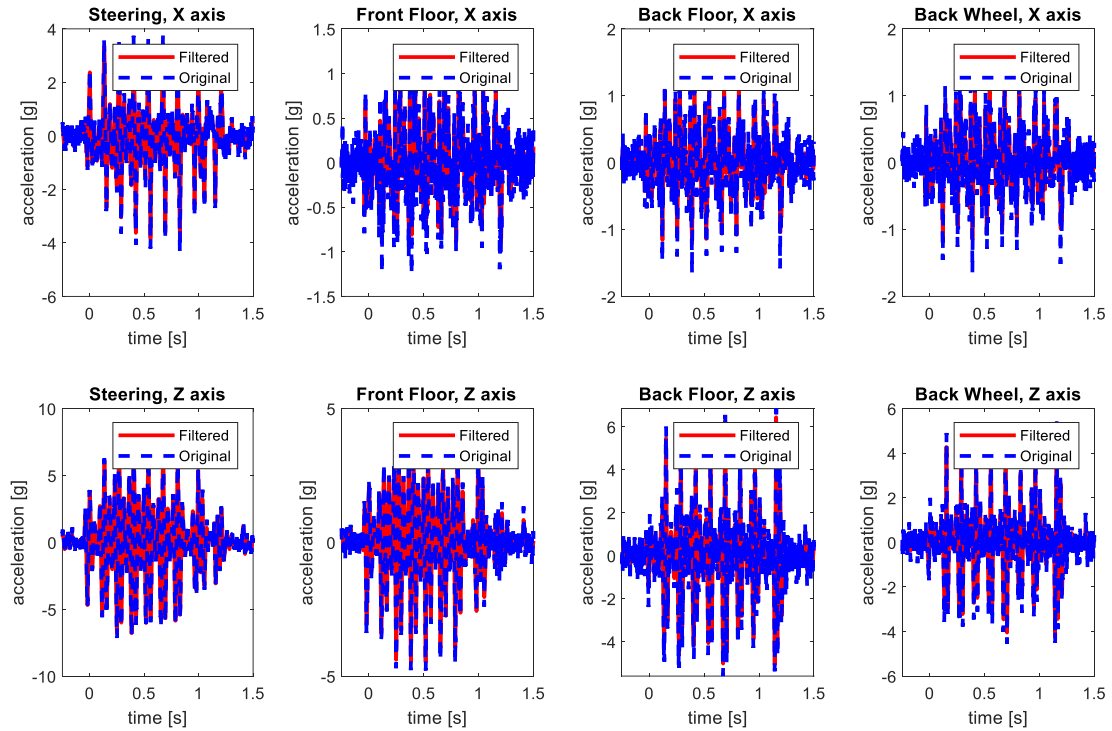


Figure 5.1.7 Comparison of filtered and original accelerations for X and Z axes for the 4 accelerometers

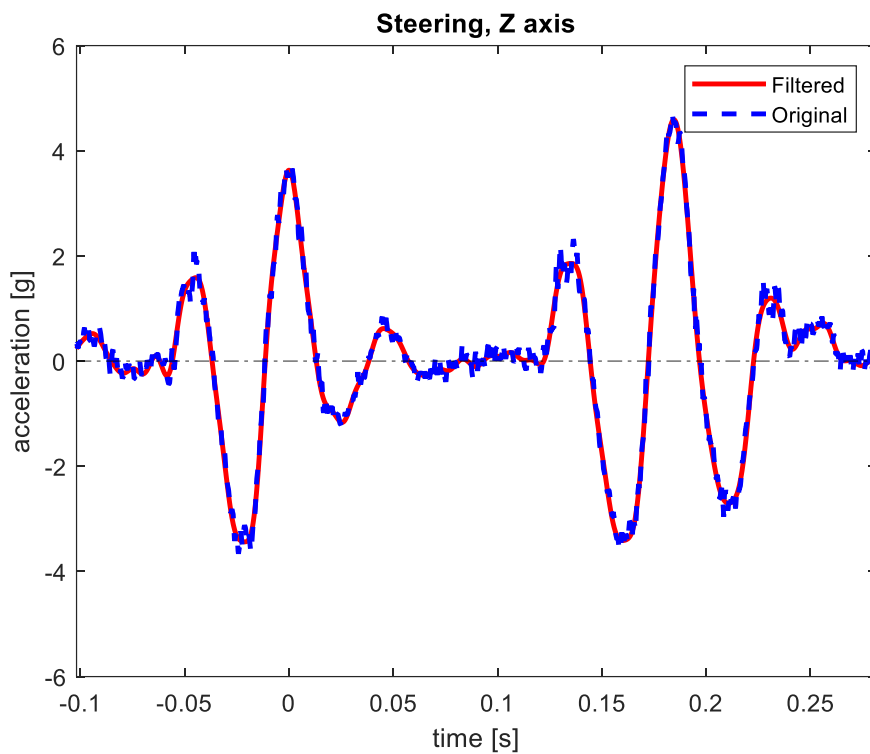


Figure 5.1.8: Comparison of filtered and original Acceleration, Steering Z axis

The next step it has been to compare the axial accelerations in order to understand which ones are of interest. To illustrate these differences, it has been studied one experiment at the speed of 19 km/h, because the higher the speed was the higher these differences were visible. In the figure 5.1.9 in can be seen the 3 axial accelerations of the steering accelerometer.

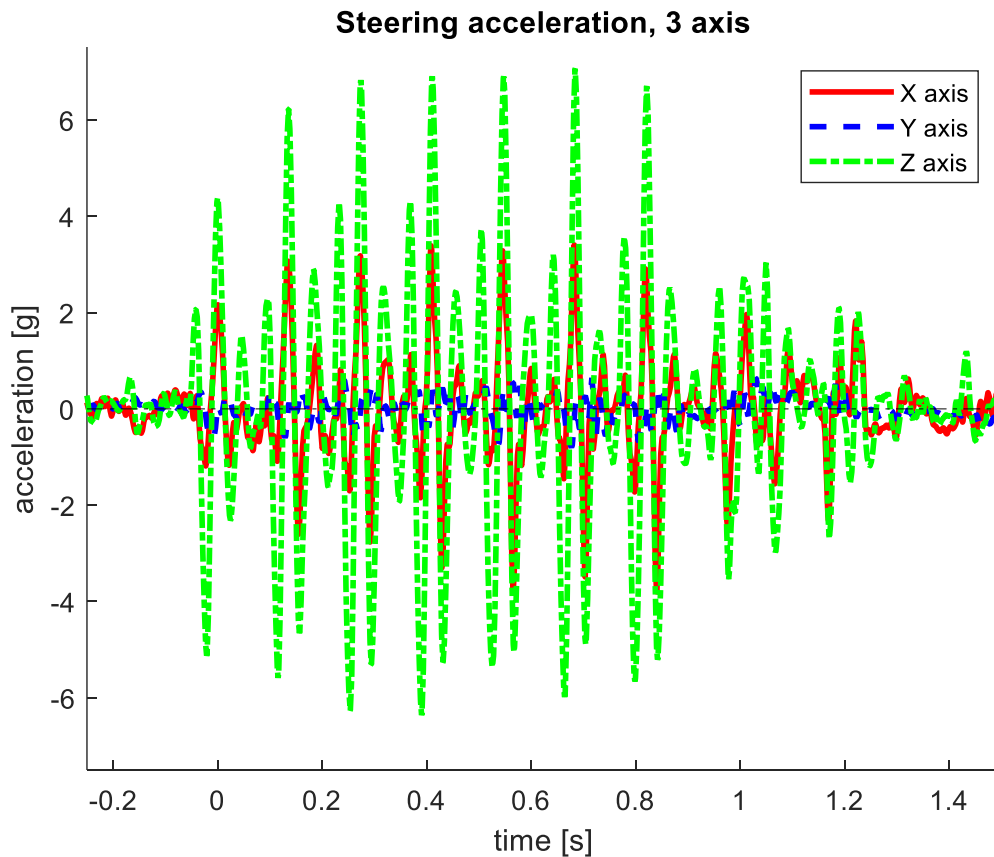


Figure 5.1.9: 3 Axial accelerations of the Steering accelerometer at 19 km/h

As it can be appreciated, the values of the accelerations on the X and Z axes, have higher peaks compared to the Y axis, and they have a remarkable difference between crossing the bumps or not crossing them, while the acceleration in the Y axis do not has a remarkable variation respect crossing or not the bumps. Then as it could be expected before performing the analysis, the acceleration signals of interest are the ones from X axis and Z axis.

5.1.1 Comparison of Back wheel accelerometer and Back floor accelerometer

When making the set-up of the accelerometers, it has been decided to put 2 accelerometers to record the vibrations of the back side of the scooter. The first one was connected to the back side of the scooter but on the platform where the user stands, and the other was putted very close to the back wheel. It was uncertain if the measures would be almost equal or very different, with these experiments it has been checked if there are differences or it can be assumed to have the same value.

To perform this comparison, it has been chose one of the measures at the speed of 19 km/h, and it has been made a 3 graphics corresponding to each of the 3 axes. In each graph there is the signals coming from the Back Floor accelerometer and the Back Wheel accelerometer. In the figure 5.1.1.1 it can be seen these graphics.

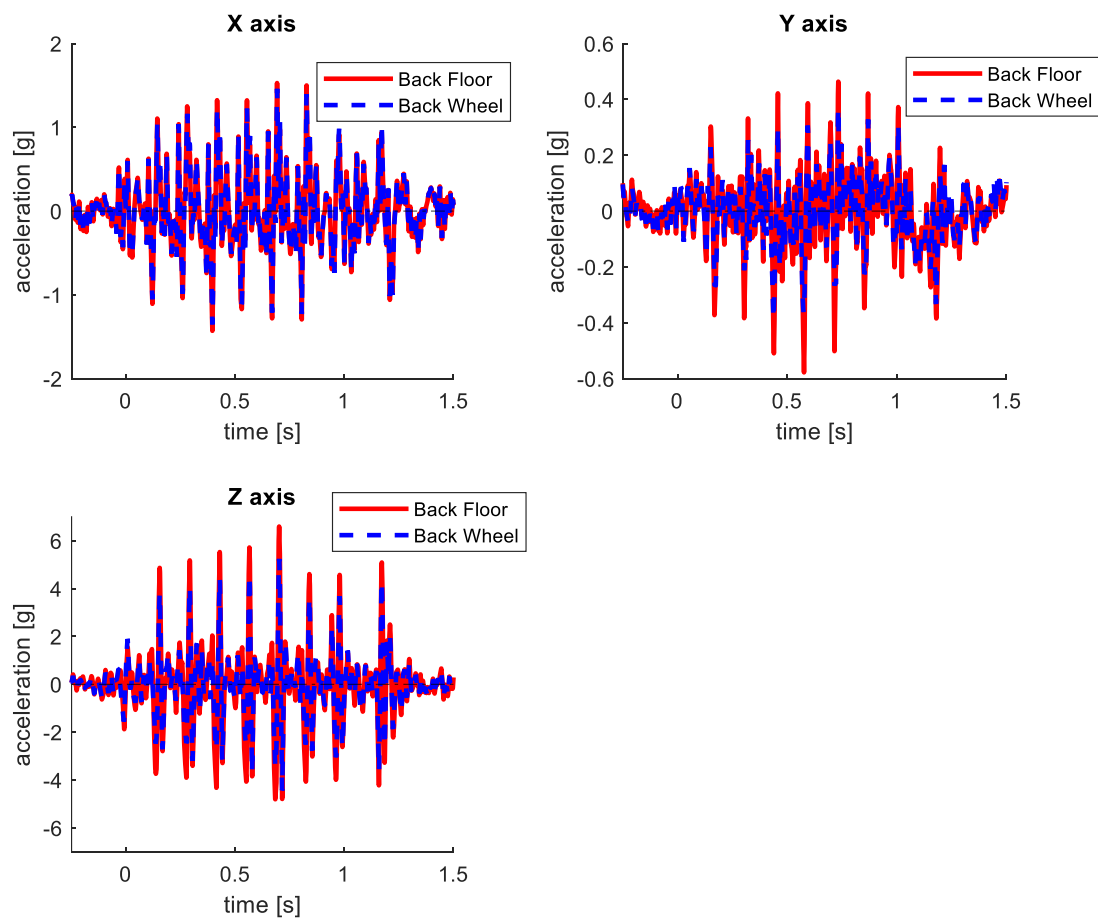


Figure 5.1.1.1: Back Floor accelerometer vs Back Wheel accelerometer

With these figures it can be seen that there is not a remarkable difference between these two sensors. The differences are very small and only present in the amplitude of the signals but not in a remarkable way. Thanks to this it has been possible to see that the system could be modelled directly with the vibration provoked by the pneumatic. This is important for the creation of the mathematical model of the e-scooter.

As it will be explained in more depth in the correspondent chapter, the system can be modelled as a mass-spring-damper system. However, knowing that the vibration of the wheel is the same that the floor of the scooter simplifies the model.

5.1.2 Repeatability of the experiments

The intention with this type of experiment is to understand how the scooter vibrates in reaction to obstacles that are known, this way it will be possible to create a model that represents the scooter. Then it is important to check the repeatability of these experiments. In other words, to see if the vibration of the scooter at a specific speed will be always the same.

To perform this study it will be compared the signals of the accelerometers of the different experiments.

To illustrate this procedure, it will be used an example. The accelerometer showed in the next figures it is the Front floor accelerometer. Then it will be showed for the velocity of 19 km/h. Then it has been plotted the acceleration in the X and Z axes for three different measurements.

In the figure 5.1.2.1 it has been plotted the time isolation for the three experiments, with the procedure explained before.

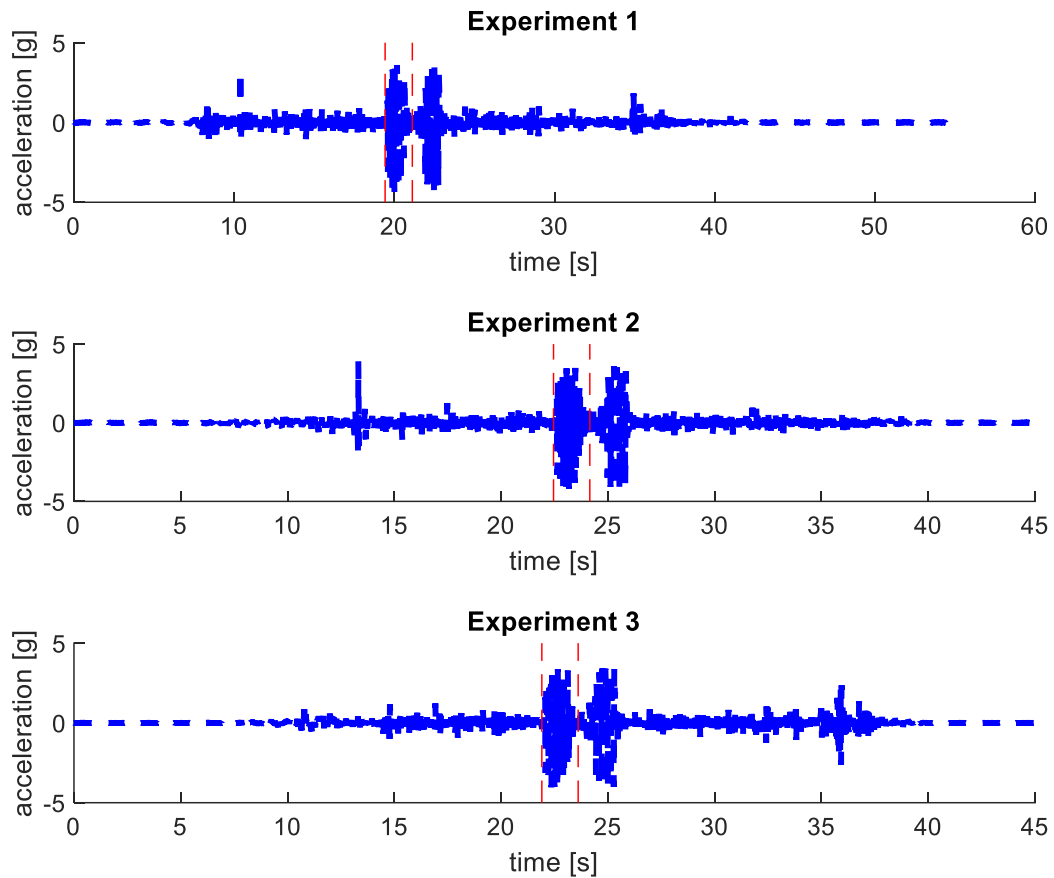


Figure5.1.2.1: Time isolation for the 3 experiments

This step allows to plot the three experiments on the same graph. In the figure 5.1.2.2 it is shown this representation. To sum up, this figure contains three experiments at 19 km/h. Specifically, the accelerations in the X and Z axes of the Front Floor accelerometer.

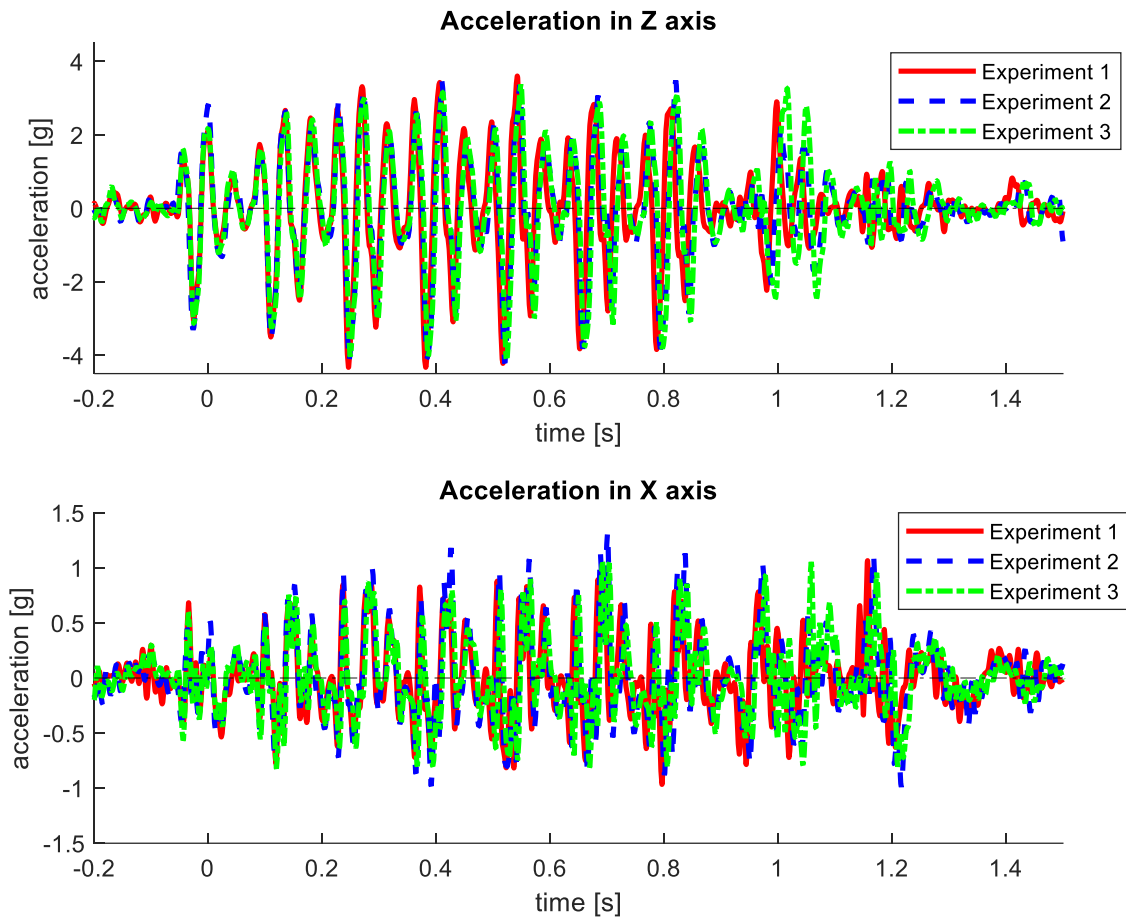


Figure 5.1.2.2: X and Z axes accelerations for three experiments at 19 km/h

Looking at this figure it can be seen that for the Z axis is practically identical the shape of these signals. For the X axis the signals are not so identical as in the other axis but they are still very similar, varying in the amplitude in some cases but almost identical on the shape. With this analysis made, it can be confirmed that the experiment has the same response in the different experiments, so it is repeatable. With this information the analysis of the behaviour of the acceleration in X and Z axes can be studied with one experiment for each velocity.

5.1.3 Bumps crossing at 19 km/h

For each speed it has been studied the values of the speed during the crossing of the bumps, measured by the GPS, and the values of the X and Z axes accelerations from 2 accelerometers: Front floor accelerometer and Back floor accelerometer.

For the values of accelerations, it is important to find the values of interest that will help to create a mathematical model. The values chosen to describe the shape of the function are the values of the peaks and their time instant. These peaks are the ones that occur during the cross of the 7 bumps. However, it seems unnecessary to focus on all the

bumps, as the response seems to repeat over the crossing of the bumps in some parts. Specifically, it has been divided in three parts of study. Then comparing these values it will be determined if it can be simplified as expected.

1. The first one during the time in which the front wheel crosses the 2 first bumps.
2. The second one will be during the time in which the front wheel crosses the second and the third bump.
3. The third zone will be during the time in which the front wheel crosses the third and the fourth bump.

As it has been explained before, during the cross of the first 2 bumps by the front wheel, the back wheel does not cross any bump. After the crossing of the second bump by the front wheel, the back wheel starts to cross the first bump. And after this situation, it has been observed that the function of the accelerometers seems periodical. These three zones are represented in the figure 5.1.3.1, with the points of interest.

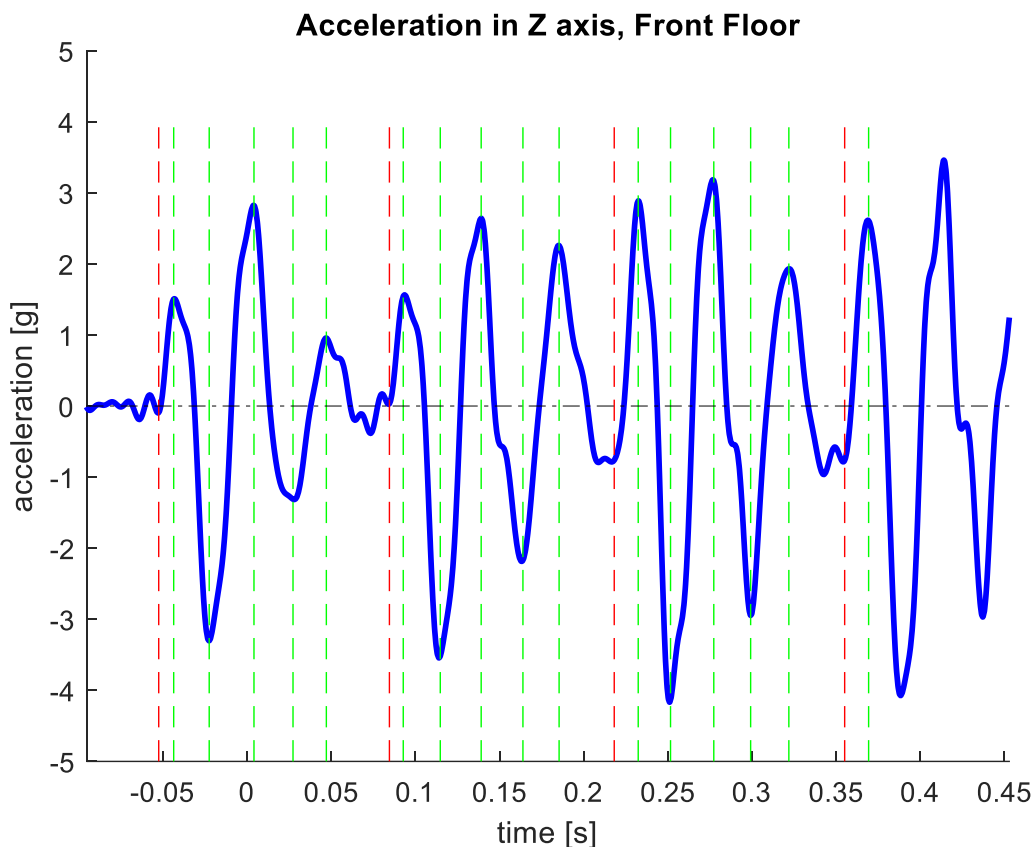


Figure 5.1.3.1: Z axis acceleration for the Front Floor. Three zones of study with peaks of interest

In the figure 5.1.3.1, there are red lines and green lines:

- The red lines refer to the start of the crossing of one bump by the front wheel. And between each consecutive red line it can be seen the response after crossing the bump. Between the firsts two red lines the e-scooter only crosses one bump

with the front wheel, but after the second red line, there is also the crossing of a bump by the back wheel.

- The green line marks the place where the different peaks can be found, specifically there are 5 green lines in each zone delimited by the red lines.

In the table 5.1.3.1 there is the values of these points. The numeration of these points has been made in ascending order of time, i.e., the red lines have been numbered as P1, P7, P13, P19.

Table 5.1.3.1: Acceleration and time instant of the Peaks

Number of peak	time (s)	acceleration (g)
P1	-0,0512	0,0135
P2	-0,0436	1,5061
P3	-0,0225	-3,3022
P4	0,0041	2,8221
P5	0,0273	-1,3116
P6	0,0471	0,9570
P7	0,0729	-0,3787
P8	0,0928	1,5418
P9	0,1148	-3,5150
P10	0,1391	2,6411
P11	0,1639	-2,1708
P12	0,1854	2,2583
P13	0,2129	-0,7389
P14	0,2324	2,8871
P15	0,2516	-4,1452
P16	0,2773	3,1661
P17	0,2992	-2,9462
P18	0,3219	1,9315
P19	0,3529	-0,7490

To check that there is periodicity, it has been calculated the relative error between the equivalent points, corresponding to the green lines, i.e., the firsts peaks after each red line: P2, P8, P14.

In the table 5.1.3.2 there is the values of the accelerations that has been compared and, in each row, there is the equivalent peaks. And in addition to the three zones of study, it has been added the values of the fourth zone.

Table 5.1.3.2: Acceleration values for the equivalent peaks

	Acceleration (g)		Acceleration (g)		Acceleration (g)		Acceleration (g)
P2	1,5061	P8	1,5418	P14	2,8871	P20	2,6075
P3	-3,3022	P9	-3,5150	P15	-4,1452	P21	-4,0740
P4	2,8221	P10	2,6411	P16	3,1661	P22	3,4603
P5	-1,3116	P11	-2,1708	P17	-2,9462	P23	-2,9689
P6	0,9570	P12	2,2583	P18	1,9315	P24	1,8024

In the table 5.1.3.3 it has been calculated the relative error between consecutive equivalent points.

Table 5.1.3.3: Relative errors between equivalent peaks

	Relative error		Relative error		Relative error
P2-P8	0,0237	P8-P14	0,8725	P14-P20	0,0968
P3-P9	0,0644	P9-P15	0,1793	P15-P21	0,0172
P4-P10	0,0642	P10-P16	0,1988	P16-P22	0,0929
P5-P11	0,6551	P11-P17	0,3572	P17-P23	0,0077
P6-P12	1,3599	P12-P18	0,1447	P18-P24	0,0668

Looking at these results, some conclusion can be made. First of all, as expected, the first zone that includes the time between the crossing of the first two bumps by the front wheel, is different from the others, because it does not include the crossing of any bump by the back wheel. In the second place, the second and third zone they are not as similar as expected, although the crossing of the bumps is equal, the response of the acceleration is quite different.

However, the third and the fourth ones are very similar, with a difference lesser than 10% for all the equivalent peaks

With this information, it has been considered the zone of study starting from the crossing by the front wheel of the first bump, until the crossing of the fourth one.

In the figures 5.1.3.2 it has been added the X axis acceleration, and maintaining the red and green lines to appreciate better the behaviour.

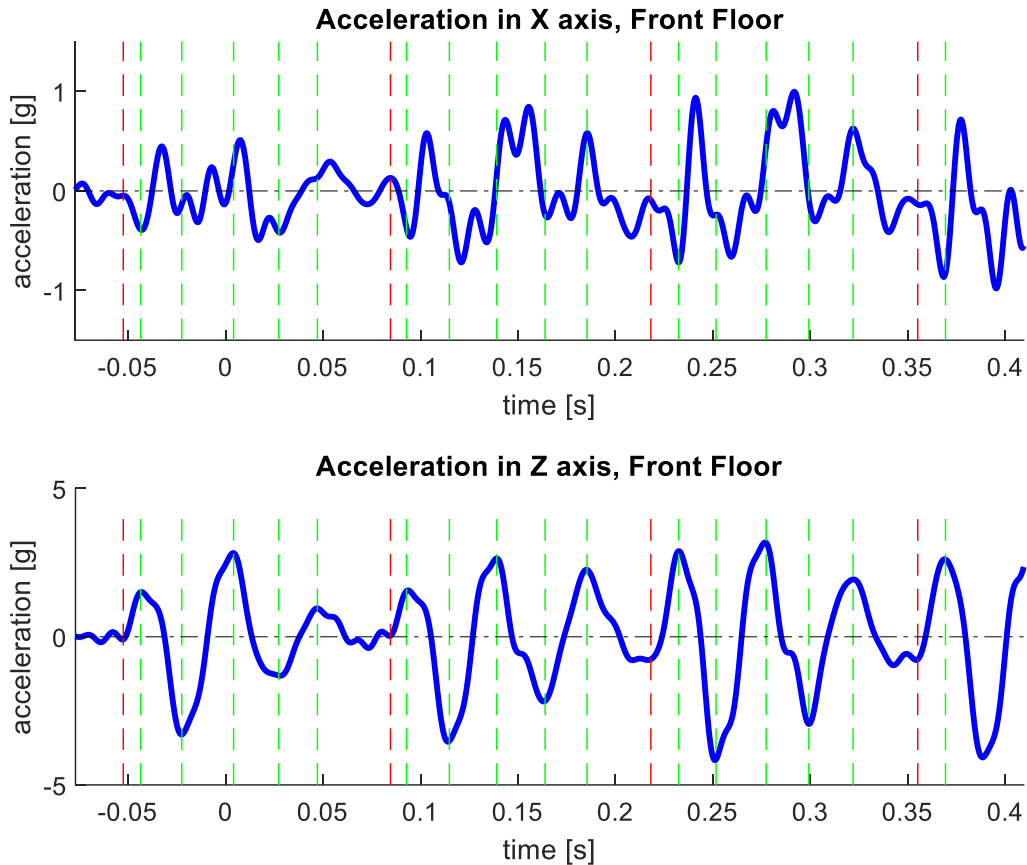


Figure 5.1.3.2: Zone of study, Front Floor Accelerometer, X and Z axes accelerations

Looking at the acceleration in the X axis, it can be observed as in the Z axis, that the shape of the response is different in the first zone. And then the second and third zones, are very similar in the shape but different in values.

This procedure of finding the peaks of interest, it has been repeated for the Back floor accelerometer. In the figure 5.1.3.3 there is the acceleration of the Back Floor accelerometer. The red lines are the same than the Front floor accelerometer to have a reference. And the green lines are the ones that indicates the peaks of interest.

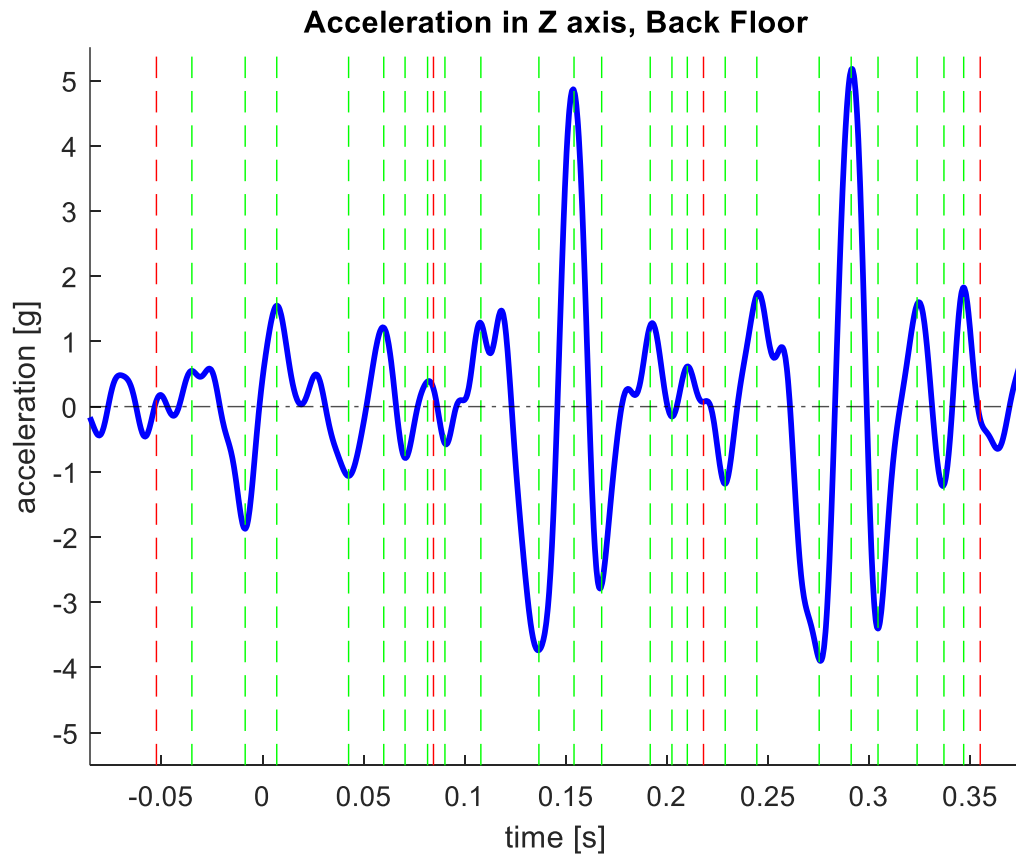


Figure 5.1.3.3 Zone of study, Back Floor Accelerometer, Z axis acceleration

As it can be observed, in the first zone that corresponds to the time between the front wheel crosses the 2 first bumps, the values of acceleration are not so big. However, the next zones that correspond to the moment that the front wheel has already crossed the second bump, and the back wheel starts to cross the bumps, the values of acceleration are bigger. As it could be expected, the accelerometer that is closer to the back wheel, has a higher acceleration due to the crossing of the bumps by the back wheel, that is why the values are lower before the back wheel starts to cross the bumps.

In the table 5.1.3.4 there are the values of the peaks of interest that are indicated in the figure 5.1.3.3.

Table 5.1.3.4: Acceleration and time instant of the Peaks

Number of peak	time (s)	acceleration (g)
P1	-0,0350	0,5482
P2	-0,0086	-1,8748
P3	0,0070	1,5496

Data post processing

P4	0,0426	-1,0646
P5	0,0600	1,2114
P6	0,0705	-0,7886
P7	0,0816	0,3852
P8	0,0902	-0,5682
P9	0,1080	1,2815
P10	0,1367	-3,7352
P11	0,1541	4,8454
P12	0,1678	-2,7366
P13	0,1918	1,2429
P14	0,2025	-0,1541
P15	0,2102	0,6155
P16	0,2289	-1,1844
P17	0,2445	1,7161
P18	0,2754	-3,8789
P19	0,2912	5,1644
P20	0,3045	-3,4050
P21	0,3238	1,5681
P22	0,3371	-1,2002
P23	0,3469	1,8271

Note that some of the values of time are negative as the time $t=0$ has been set to the first big peak.

In the figures 5.1.3.4 it has been added the X axis acceleration, and maintaining the red and green lines to appreciate better the behaviour.

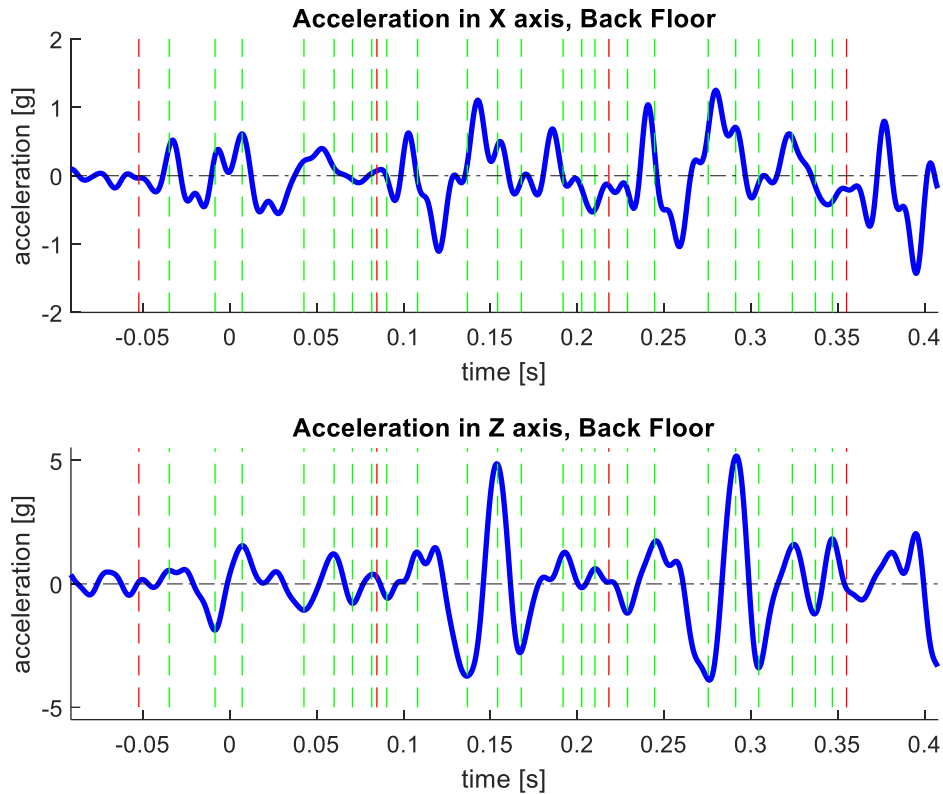


Figure 5.1.3.4: Zone of study, Back Floor Accelerometer, X and Z axes accelerations

Looking at the acceleration in the X axis, it can be observed as in the Z axis, that the shape of the response is different in the first zone. And then the second and third zones, are very similar in the shape but different in values.

5.1.4 Bumps crossing at 14 km/h

For this speed, it has been studied directly the first 3 zones. The procedure followed it has been to find the peaks of interest of the Z axis and store these values. In the figure 5.1.4.1 it can be seen the peaks of interest of the Z axis acceleration of one experiment at 14 km/h. And the table with these values can be found in the annex.

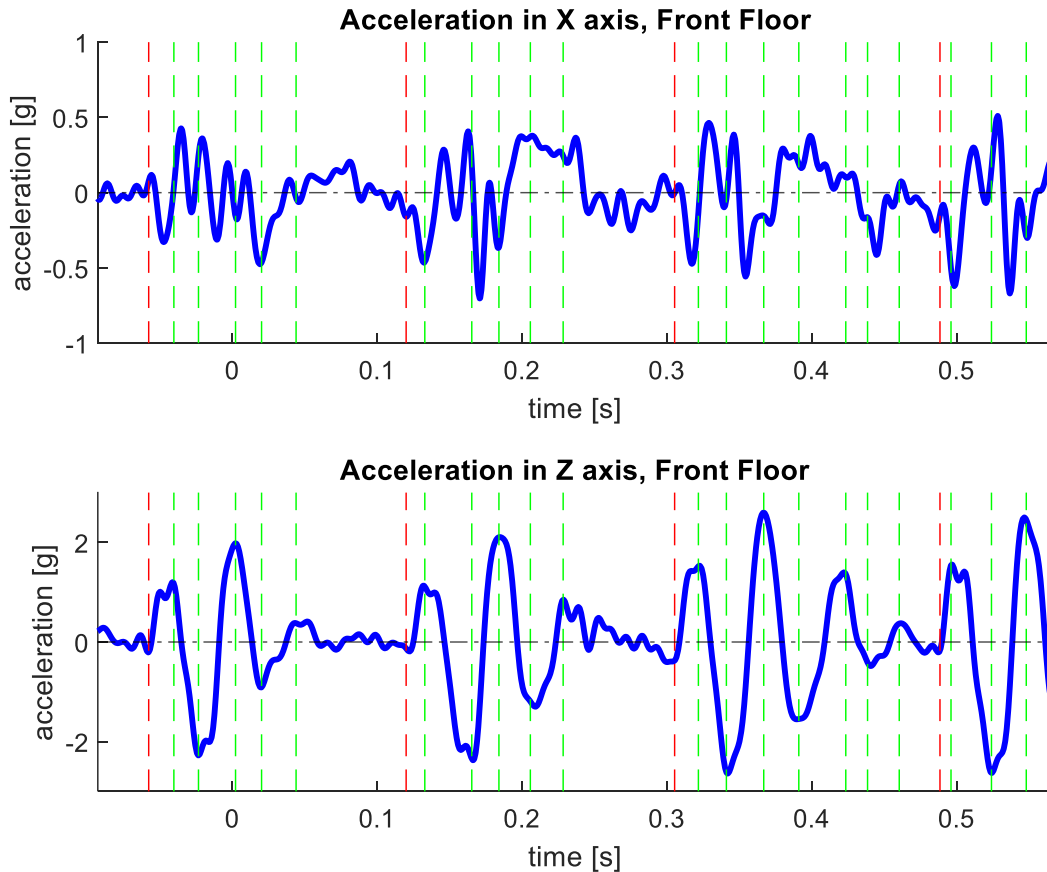


Figure 5.1.4.1: Zone of study, Front Floor Accelerometer, X and Z axes accelerations

Looking at the figure 5.1.4.1 it can be observed that in the first two zones, the values of acceleration seem to stabilize before reaching the next bump. This means that there is no superposition and the response of the bump can be clearly isolated. This can be helpful when creating the mathematical model.

For what concerns to the shape, if each zone it is compared to the correspondent zone of the experiment at 19 km/h, it can be observed that:

1. The first and second zone have the same shape, but as the time between bumps is bigger, the stabilization of the acceleration is present in the experiment of 14 km/h, with this information it can be seen that in the 19 km/h, only a small part of stabilization is missing.
2. The third zone in the 14 km/h has the same shape for their 5 first peaks than the 20km/h. But it has two more peaks of interest. With this information it can be seen that at 19 km/h before the acceleration is stabilized to zero, the front wheel crosses another wheel.

This procedure has been repeated for the back floor accelerometer, that can be seen in the figure 5.1.4.2. The red lines are the same than the Front floor accelerometer to have a reference. And the green lines are the ones that indicates the peaks of interest.



Figure 5.1.4.2: Zone of study, Back Floor Accelerometer, X and Z axes accelerations

Comparing the Back floor acceleration with the Front floor, it can be seen that the values of accelerations are the same order, 2 [g] for the Z axes and 0,5 [g] for the X axes. However, the Back floor acceleration has more peaks for the same period of time. As in the Front floor accelerometer, in the first two zones the response seems to stabilize before reaching the next bump (red lines). But from the third zone, before it stabilizes, there is a crossing of another bump.

5.1.5 Bumps crossing at 9 km/h

As in the case of 14 km/h, it has been studied directly the first 3 zones. The procedure followed it has been to find the peaks of interest of the Z axis and store these values. In

the figure 5.1.5.1 it can be seen the peaks of interest of the Z axis acceleration of one experiment at 9 km/h. And the table with these values can be found in the annex.

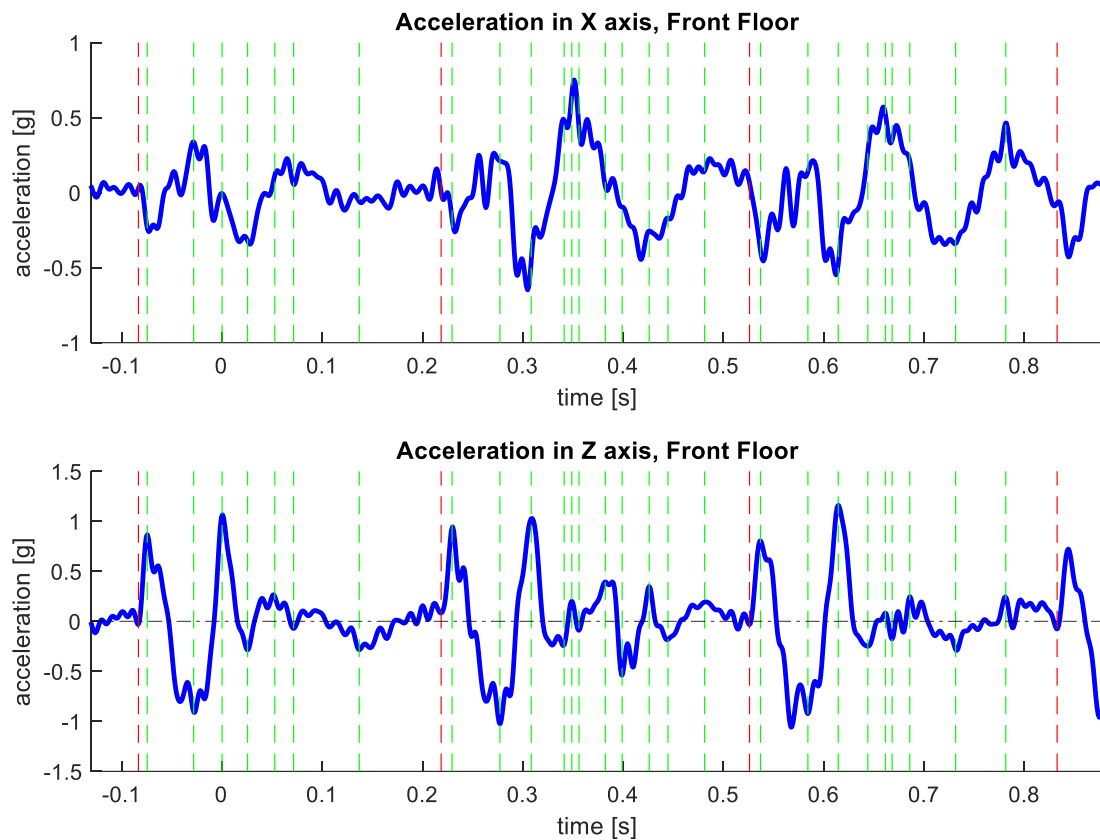


Figure 5.1.5.1: Zone of study, Front Floor Accelerometer, X and Z axes accelerations

Looking at the figure 5.1.5.1 it can be observed that, as in the case of 14 km/h, in the first two zones, the values of acceleration seem to stabilize before reaching the next bump. Moreover, looking at the third zone, it seems that it stabilizes too.

For what concerns to the shape, if each zone it is compared to the correspondent zone of the experiment at 14 km/h, it can be observed that:

1. The first and second zone have a similar shape, but as the time between bumps is bigger, the stabilization of the acceleration is more remarkable in the experiment of 9 km/h.
2. The third zone in the 14 km/h has the same shape for their 5 first peaks than the 20km/h, but the case of 9 km/h only the first three peaks are remarkable, making the shape more similar to between the zones 1,2 and 3.

This procedure has been repeated for the back floor accelerometer, that can be seen in the figure 5.1.5.2. The red lines are the same than the Front floor accelerometer to have a reference. And the green lines are the ones that indicates the peaks of interest.



Figure 5.1.5.2: Zone of study, Back Floor Accelerometer, X and Z axes accelerations

Comparing the Back floor acceleration with the Front floor of 9 km/h, it can be seen that the values of accelerations are the same order, 1 [g] for the Z axes and 0,5 [g] for the X axes. However, the Back floor acceleration has more peaks for the same period of time.

As in the Front floor accelerometer, in the first two zones the response seems to stabilize before reaching the next bump (red lines). But from the third zone, before it stabilizes, there is the crossing of the next bump.

5.2 Road bump

For these experiments, the setup with all the accelerometers has been used.

As it has been explained before, the experiment was performed on the road, in the via Paolo Braccini. In the figure 5.2.1 it is shown the route taken by the scooter, recorded by the GPS.

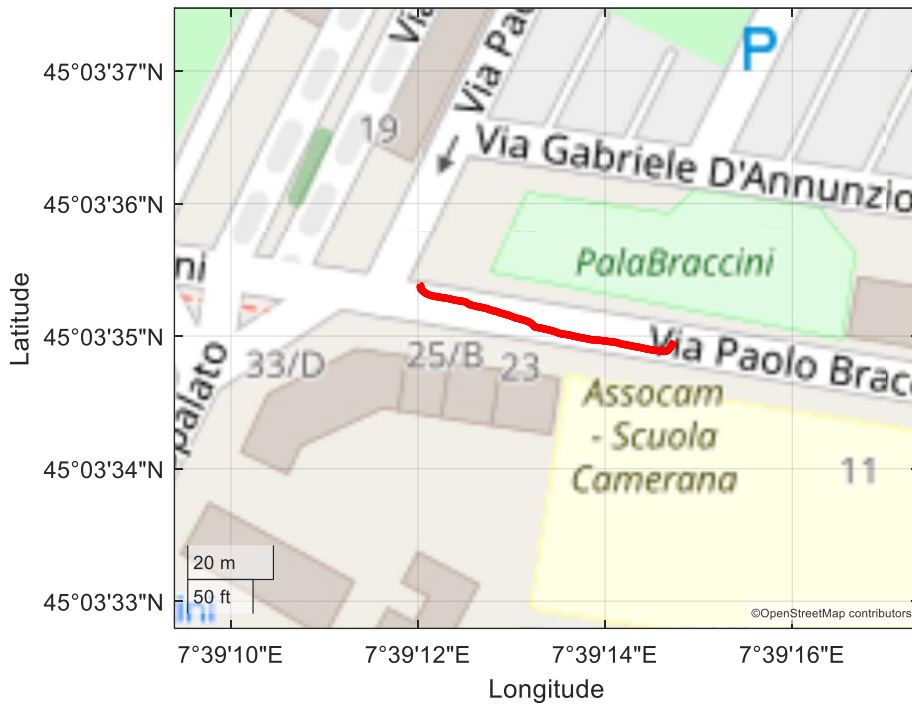


Figure 5.2.1: Route followed by the driver for the road bump experiment

The first step made, as with the bike bumps, has been to isolate the interval of interest. For this case, this interval has been considered as the crossing of the bump. To proceed with this isolation, it has been chosen the Z axis acceleration of the steering accelerometer. Once the interval has been chosen for this accelerometer, it has been applied the same one to the other accelerometers. This procedure has been applied to all the experiments but it will be illustrated with one experiment, in this case with one experiment at the velocity of 19 km/h. In the figure below, it can be seen all the signal recorded by the SCADA system, and the interval isolated compressed by the two red lines.

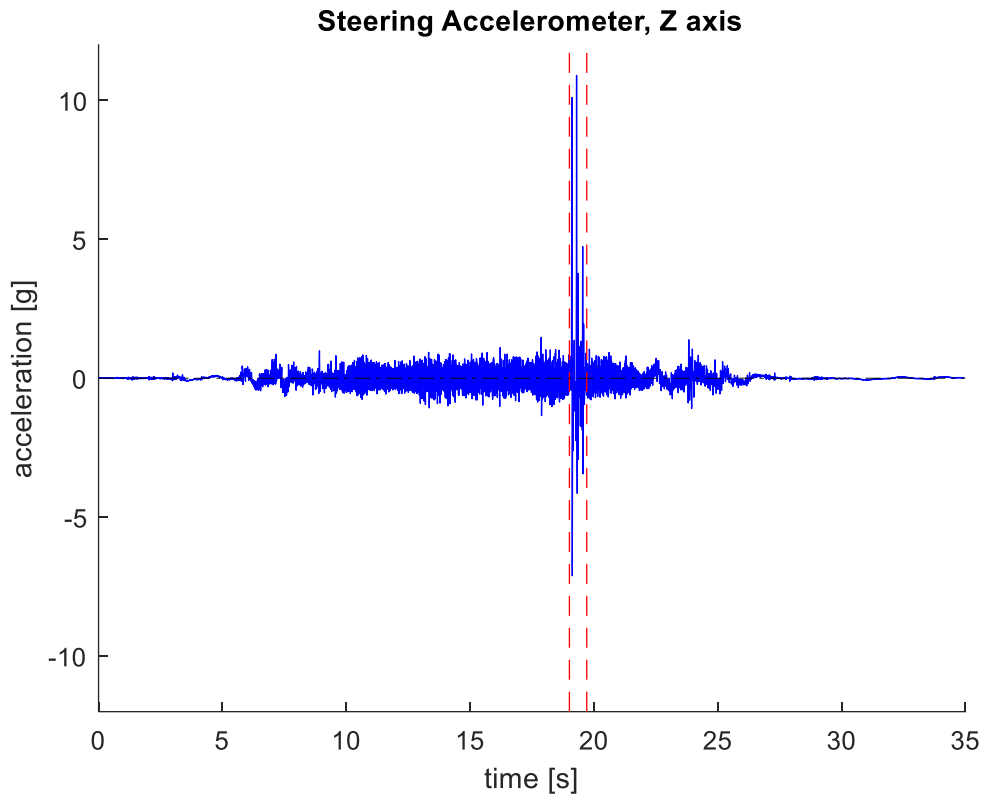


Figure 5.2.2: Isolation of the interval of interest

For each of the three velocities the interval has been set to:

$$9 \text{ km/h} \rightarrow t = [t_p - 0,2 \quad t_p + 0,9]$$

$$14 \text{ km/h} \rightarrow t = [t_p - 0,15 \quad t_p + 0,75]$$

$$19 \text{ km/h} \rightarrow t = [t_p - 0,1 \quad t_p + 0,6]$$

And then another extra step has been set in order to facilitate the next calculations. The instant of time $t=0$ has been assigned to the first peak of the bumps. On the figure below it has been plotted for the 19 km/h experiment, the interval explained and with the variable time modified as explained.

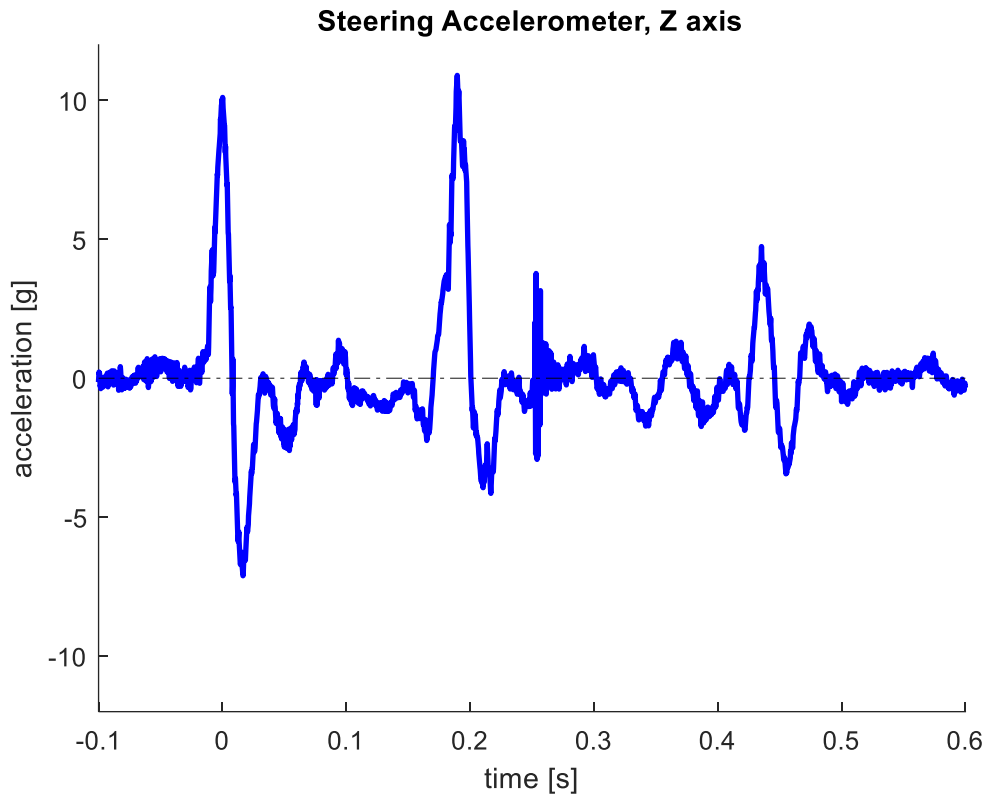


Figure 5.2.3: Time isolation for 19 km/h

The next step is to filter the signal. The selected band pass filter, is [1Hz 100Hz], as with the bike path bumps.

The procedure has been the same than in the bike path bumps, to simplify the explanation, it has been plotted directly a closer view to the signal so the difference between filtered and not filtered can be appreciated. This graph it can be seen on the figure 5.2.4.

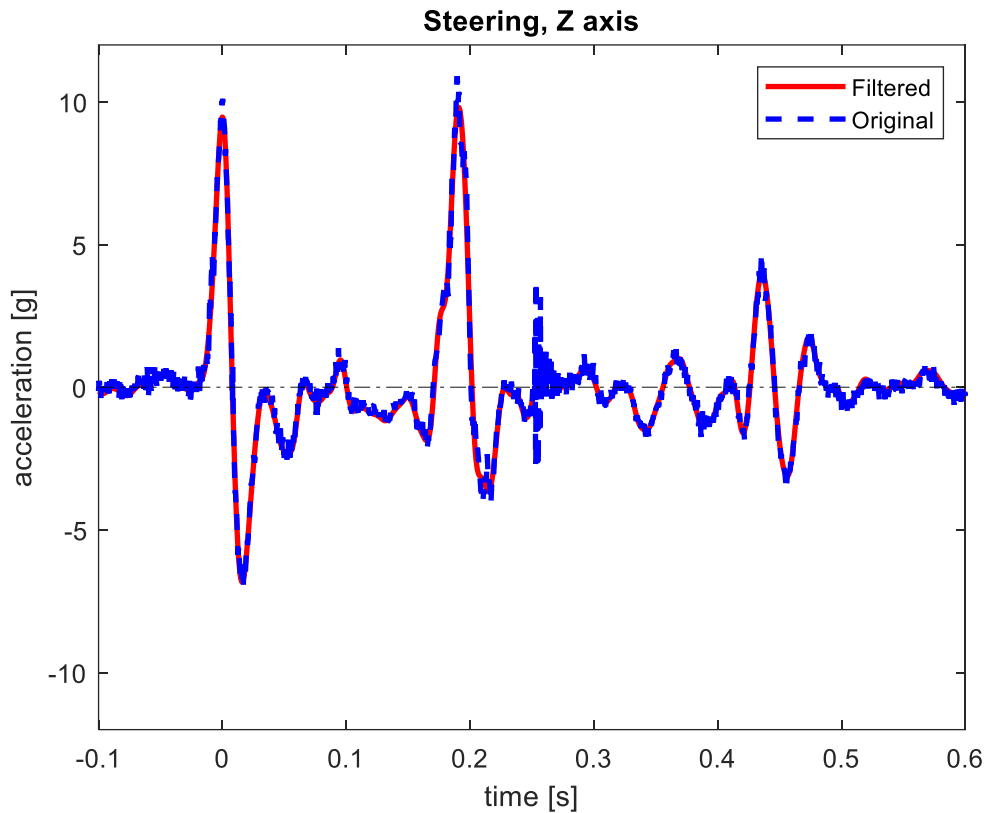


Figure 5.2.4: Comparison of filtered and original Acceleration, Steering Z axis

As it can be observed in the figure, the acceleration continues to have the same response, in this way it has been eliminated the noise without perturbing the signal. The next step it has been to compare the axials accelerations in order to understand which ones are of interest. As in the bike path bumps to illustrate these differences, it has been studied one experiment at the speed of 19 km/h. In the figure 5.2.5 it can be seen the three axial accelerations of the steering accelerometer.

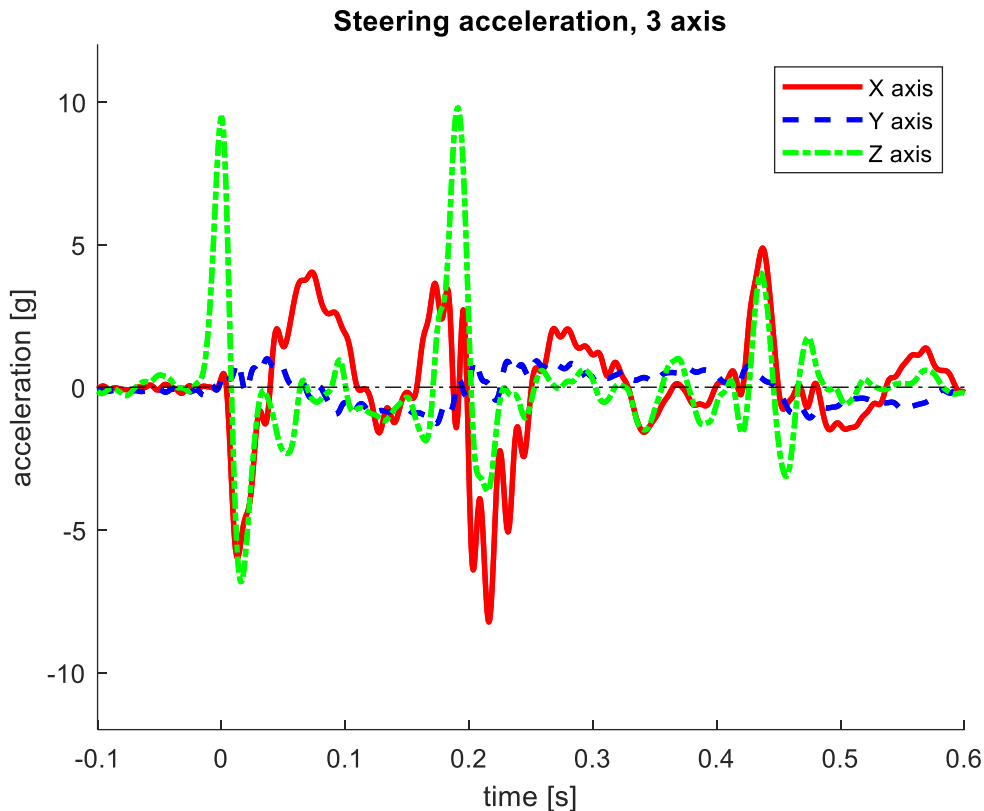


Figure 5.2.5: 3 axial accelerations of the Steering at 19 km/h

As in the bike path bumps, the values of the accelerations on the X and Z axes, have higher peaks compared to the Y axis, and they have a remarkable difference between crossing the bump or not crossing it, while the acceleration in the Y axis do not has a remarkable variation respect crossing or not the bump. Then as in the precedent experiment, the acceleration signals of interest are the ones from X axis and Z axis.

5.2.1 Repeatability

The intention with this type of experiment is the same that with the bike path bumps. For this reason and as explained before the repeatability of these experiments has been studied

To perform this study, it will be compared the signals of the accelerometers of the different experiments. To illustrate this procedure, it will be used an example. The accelerometer showed in the next figure it is the Front floor accelerometer from different experiments at the velocity of 19 km/h. The accelerations plotted are the ones in the X and Z axes (fig.5.2.1.1).

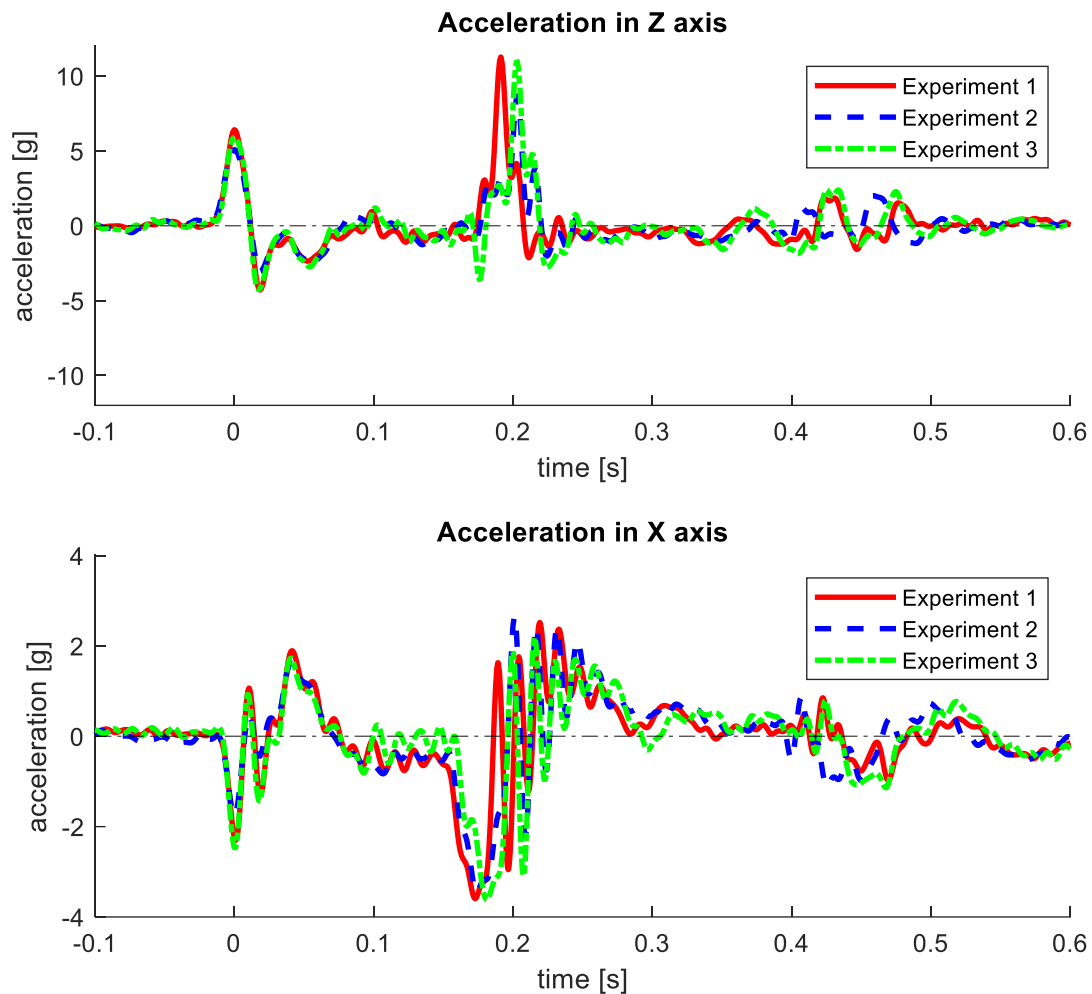


Figure 5.2.1.1: Front floor accelerometer, X and Z axes acceleration for three experiments

Looking at this figure it can be seen that for both axes is practically identical the shape of these signals, but with a small delay that is caused by the difference in velocity. With this analysis made, it can be confirmed that the experiment has the same response and then the measurements are reliable as to use them to create a model.

5.2.2 Bump crossing at 20 km/h

For each speed it has been checked that the values of the speed during the crossing of the bump, measured by the GPS are coherent to each experiment. And then it has been studied the values of the X and Z axes accelerations from 2 accelerometers: Front floor accelerometer and Back floor accelerometer.

For the values of acceleration, it is important to find the values of interest that will help to create a mathematical model. The values chosen to describe the shape of the function are the peaks. These peaks are the ones that occur during the cross of the bump. In the case of the big bump, as it does not repeat like the bike bumps, the studied zone it will be all the zone concerning the bump.

The procedure followed is similar to the bike bumps. In the figure 5.2.2.1 it can be observed. First a red line that indicates the point before the e-scooter crosses the bump, and then with green lines some peaks of interest are indicated.

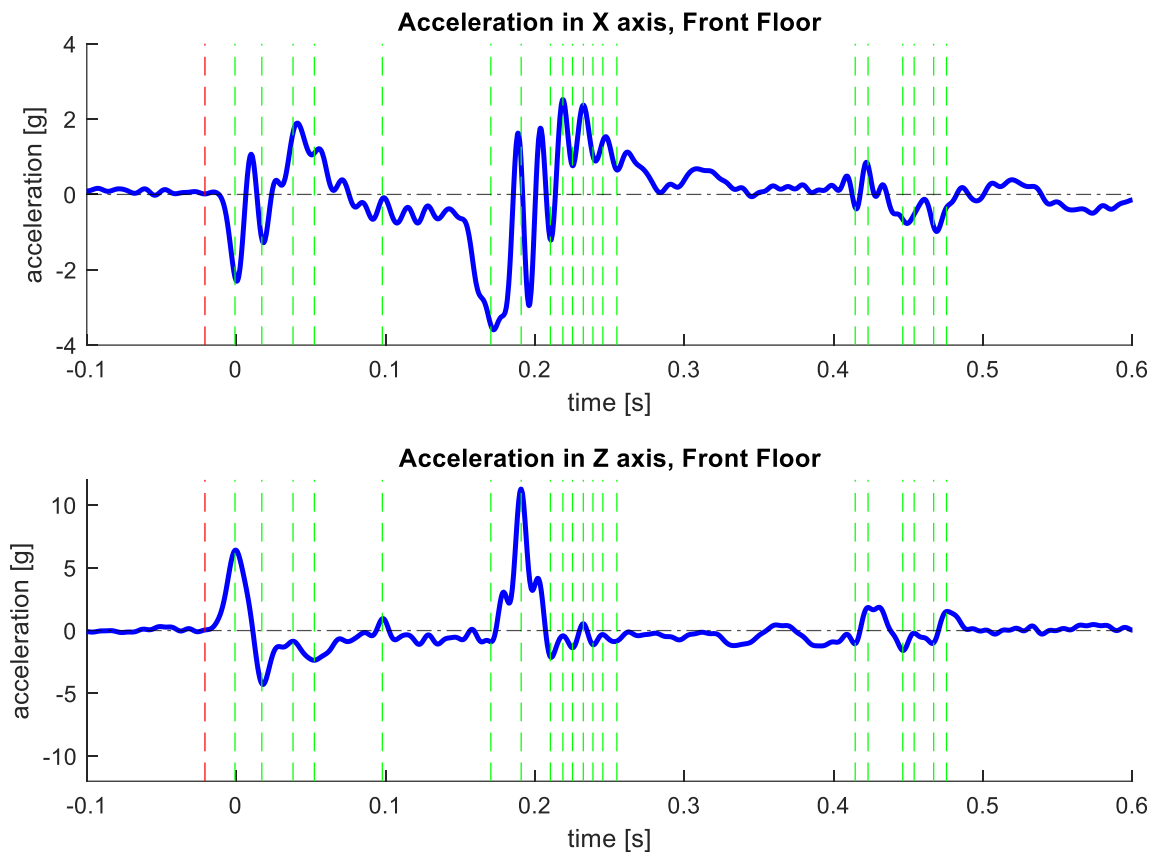


Figure 5.2.2.1: Front Floor Accelerometer, X and Z axes accelerations

The peaks of interest can be found in the annex.

Observing the figure 5.2.2.1 it can be denoted 3 zones where there is a concentration of the peaks that has been considered of interest. The first zone corresponds to the crossing of the bump as it is the first obstacle that makes an impact that it is transformed into a vibration.

To understand better the phenomenon that provokes the vibration in the next zones, it has been studied the time that the front wheel needs to cross all the bump. The longitude of the bump is 0,9 m, and the speed during this interval of time is approximately 18 km/h. Then it can be calculated that from the moment that the front wheel starts to cross

the bump to the moment that it impacts again to the road is approximately 1,8 s. The distance between wheels is 88,5 cm, that is almost 0,9 m.

With this information, and observing the figure 5.2.2.1 it is seen that the second zone correspond to the impact on the road of the second wheel and the start of the crossing of the bump by the back wheel, and then the third zone is probably related to the impact on the road by the back wheel.

The same procedure has been made for the Back floor accelerometer (fig. 5.2.2.2).

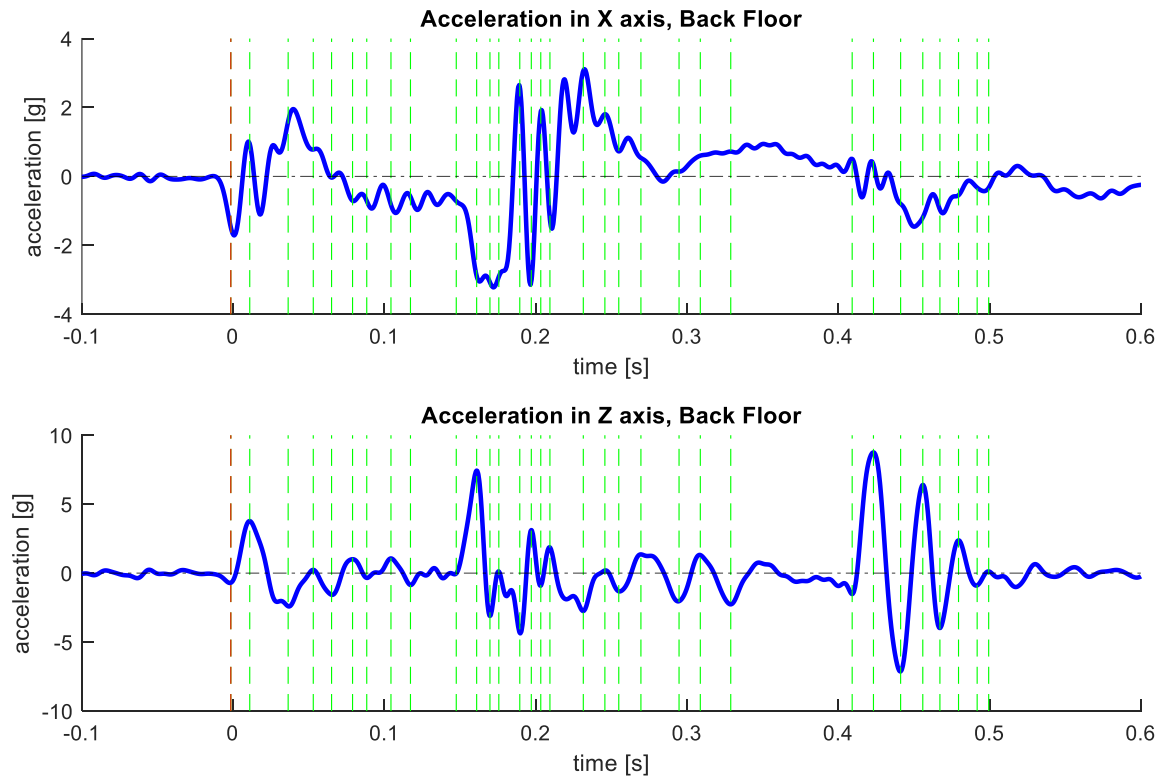


Figure 5.2.2.2: Back Floor Accelerometer, X and Z axes accelerations

Observing the figure 5.2.2.2 it can be denoted as the X axis acceleration is very similar to the front floor accelerometer. For what concerns to the Z axis, and looking the second zone, it can be seen that the first peak occurs slightly before in the back floor accelerometer. This has sense, as the crossing of the back wheel also starts slightly before that the impact of the front wheel to the ground. This corroborates, even more, the hypothesis made. And for what concerns the third zone, it can be seen as the values are higher than in the front floor, that has sense to the hypothesis that it corresponds to the impact of the back wheel after crossing the bump. Moreover, the response of this acceleration in the third zone has the typical second order system response to an impulse, that can be very helpful when creating a mathematical model.

5.2.3 Bump crossing at 14 km/h

The same procedure has been followed for the 14 km/h experiment (fig 5.2.3.1)

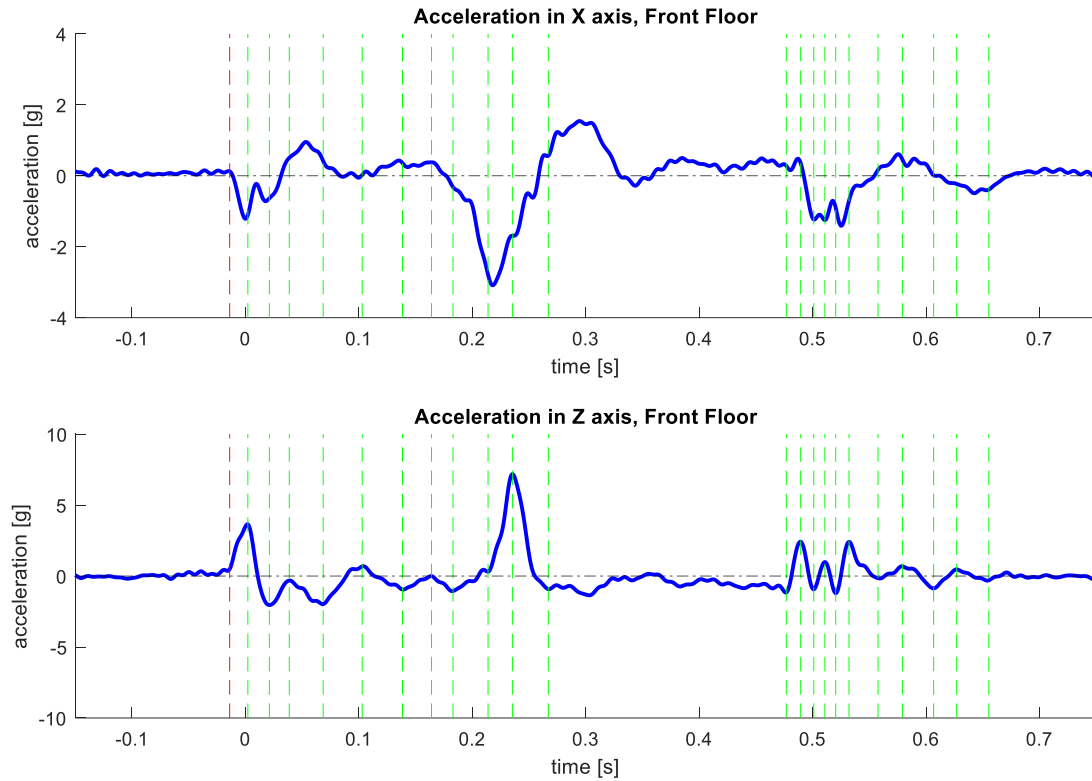


Figure 5.2.3.1: Front Floor Accelerometer, X and Z axes accelerations

Comparing this response to the 20 km/h, it can be seen as there are still three zones of peaks. The shape is similar, the main difference is the values of this acceleration, being in this case, as expected, lower than 20 km/h.

In the figure 5.2.3.2 there is the same response for the back accelerometer.

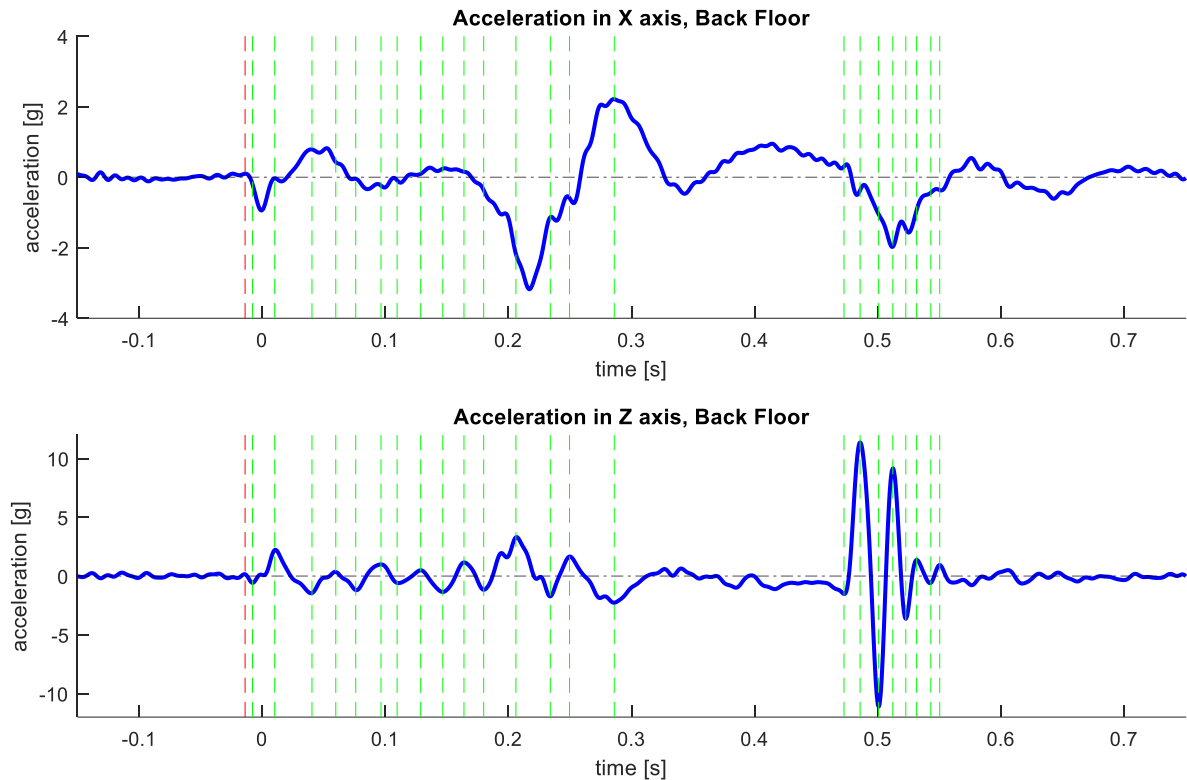


Figure 5.2.3.2: Back Floor Accelerometer, X and Z axes accelerations

Observing the figure 5.2.3.2, it can be denoted that the first two zones are not so clear, as it does not have a zone between them with stable (and close to zero) acceleration. However, comparing with the 20 km/h experiment, the X axis is more similar, then it can be made a connection. In the 20 km/h experiment, the second zone started when there was a high negative acceleration on X axis. Observing the case at 14 km/h this phenomenon would correspond to the instant of time $t=0,21$ s. That is coherent as it corresponds to the biggest peak in the Z axis of the first two zones.

It can be also observed as the third zone is maintained practically identical in shape, and amplitude.

5.2.4 Bump crossing at 9 km/h

The same procedure has been followed for the 14 km/h experiment (fig 5.2.4.1)

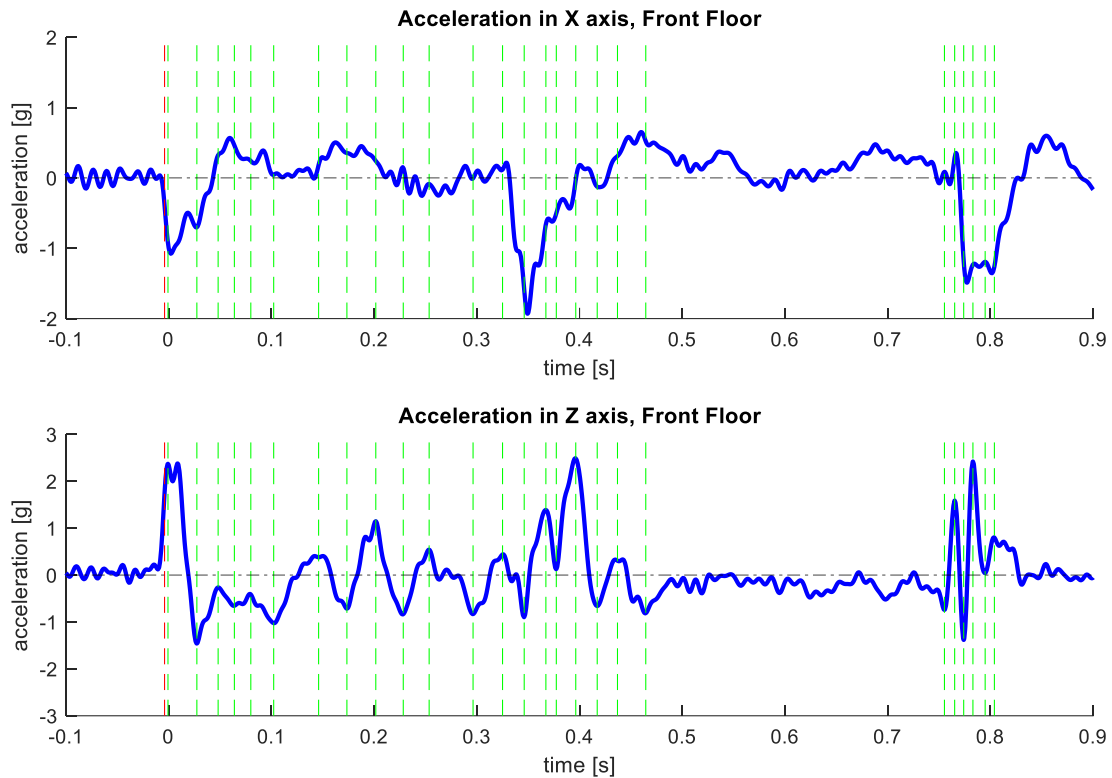


Figure 5.2.4.1: Front Floor Accelerometer, X and Z axes accelerations

Comparing this response to the precedent experiments, it can be seen that in this case, looking at the Z axis, the three zones are not so easily distinguished. However, comparing with the X axis, the response is very similar and then a connection to the other experiments can be made. The second zone then, it starts approximately at the time $t=0,35$.

The shape does not seem so similar, but it has to be taken into account that the scale of the acceleration axis is much lower. On the 20 km/h there are peaks between the two first zones of the same magnitude that in this case, but were neglected for being much smaller than the other ones.

In the figure 5.2.4.2 there is the same response for the back accelerometer.

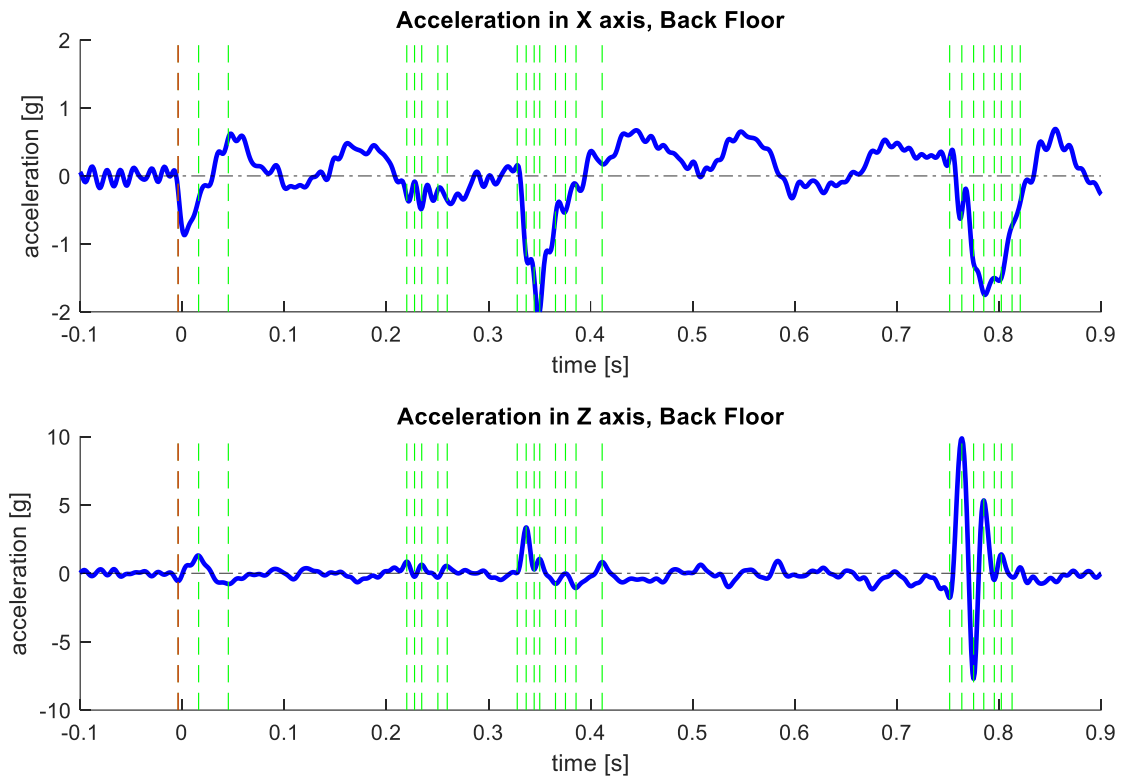


Figure 5.2.4.2: Back Floor Accelerometer, X and Z axes accelerations

Observing the figure 5.2.4.2, it can be denoted the same phenomenon that in the 14 km/h. The first two zones are not so clear, as it does not have a zone between them with stable (and close to zero) acceleration. However, comparing with the 20 km/h experiment, the X axis is more similar, then it can be made a connection. In the 20 km/h experiment, the second zone started when there was a high negative acceleration on X axis. Observing the case at 9 km/h this phenomenon would correspond to the instant of time $t=0,35$ s. That is coherent as it corresponds to the biggest peak in the Z axis of the first two zones.

It can be also observed as the third zone is maintained practically identical in shape, and amplitude.

5.3 Cobblestoned Road

For this experiment, a different approach has been taken to study the experiments. For the known obstacles, the objective was related to the understanding of the acceleration response in front of a known input. On the cobblestoned road experiments, it will be related to the study of the comfort of the user. This will modify some parts of the procedure.

This experiment as it was mentioned before, it was carried out in the Corso Sati Uniti. In the figure 5.3.1 it can be seen the route taken by the driver.



Figure 5.3.1: Route followed by the driver for the cobblestoned road experiment

The next step followed has been to isolate the interval of time that will be studied. With this type of experiment, it would be interesting to study all the interval of time in which the scooter has a constant speed. Unfortunately, it has not been possible to maintain the constant speed with a good accuracy, as the obstacles produced a strong variation. In the figure 5.3.2 it can be seen an example of the isolation of time considering the GPS speed, of an experiment of 10 km/h.

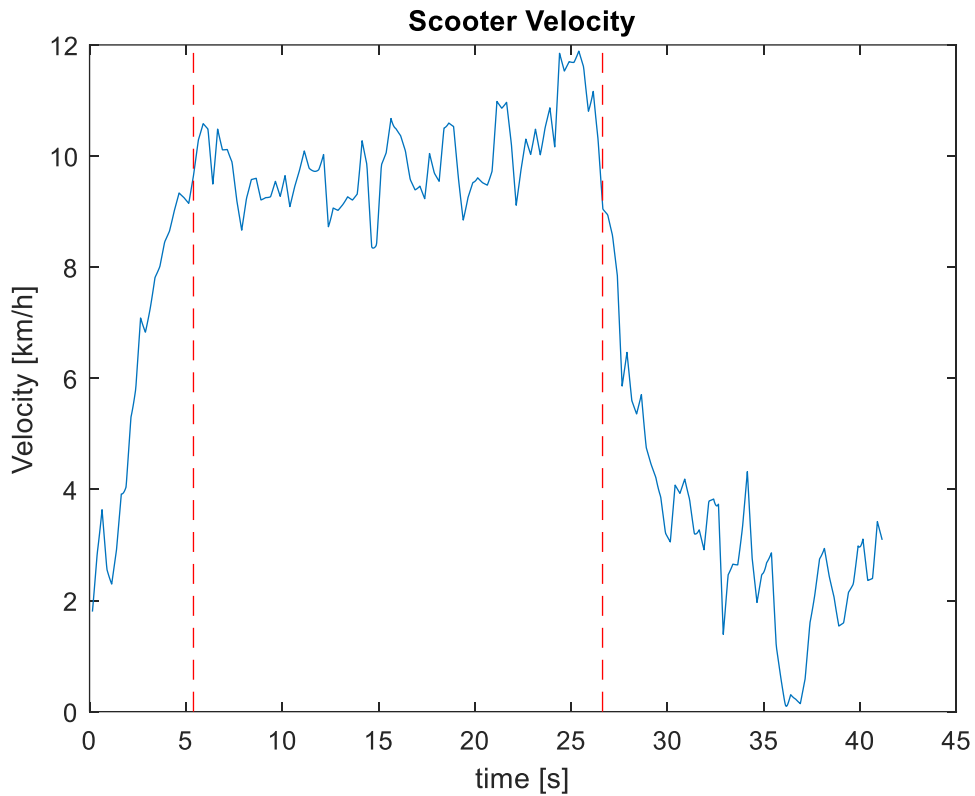


Figure 5.3.2: Time Isolation of the interval at constant speed

As it can be observed in the figure 5.3.2 the speed is not constant, the desired speed with this experiment was 10 km/h, and it variates from 8 to 12 km/h.

In the figure 5.3.3 it can be seen how this time isolation has been applied to the Z acceleration signal coming from the steering accelerometer.

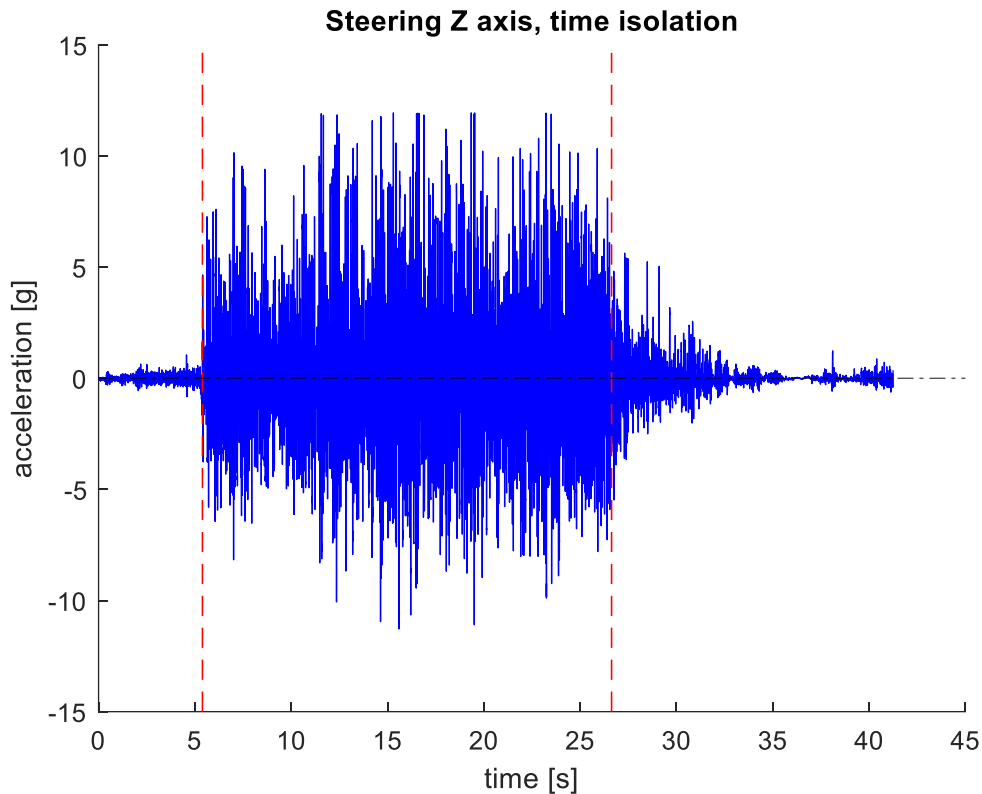


Figure 5.3.3: Isolation of the interval of interest applied to the Steering acceleration

As it can be observed in the figure 5.3.3, the amplitude of the acceleration it is also more uniform in the zone of speed selected.

The next step is to filter the signal. As in these experiments the main purpose is to study the comfort the filtering it has been different. The study zone is from 0,5 to 80 Hz. And as the procedure itself to calculate the weighted frequency r.m.s acceleration uses a filters, it has been only filtered above 100 Hz.

Apart from filtering only above 100 Hz the procedure has been the same than in the other experiments. To simplify the explanation, it has been plotted directly a closer view to the signal so the difference between filtered and not filtered can be appreciated. This graph it can be seen on the figure 5.3.4.

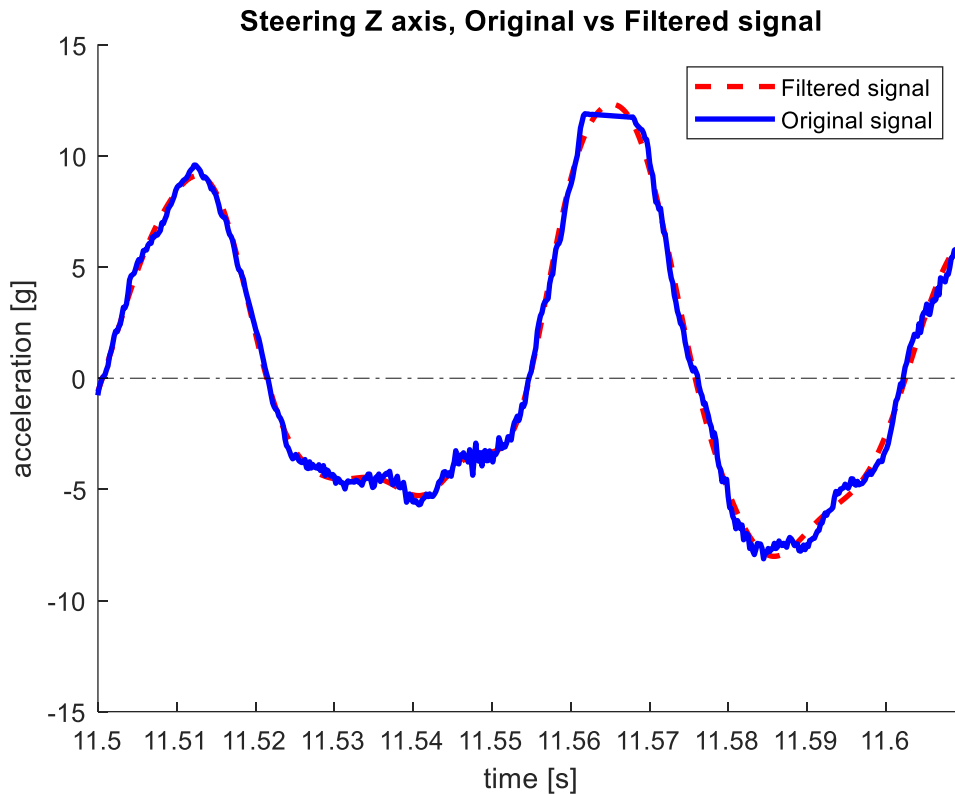


Figure 5.3.4: Comparison of filtered and original Acceleration, Steering Z axis

As mentioned before, the objective is to study the comfort and not to create a model. And as the obstacles are unknown, and different from each run, that would not have sense to study the repeatability.

As the point of interest is the part of the scooter where the user has the feet, but there is not any accelerometer on that zone. It has been studied for the front floor and the back floor accelerometers.

Then to calculate the value of the total weighted-frequency root mean square acceleration, for one experiment (for each accelerometer), it has been followed the next procedure:

Select the central frequencies in which a third-octave band calculation will be held. In the case of study are the ones on the figure 2.1.1.2. For each of these frequencies, with the MATLAB library: *Audio Toolbox*, it has been calculated the third-octave band. To calculate the r.m.s it has also used a function available in MATLAB. Then the rest of the procedure it has been explained on the point 2.1.1.

On the table 5.3.1 there are the results of these weighted frequencies r.m.s accelerations for the front floor and the back floor accelerometer, for the velocities of 10 km/h, 15 km/h and 19 km/h. Moreover, it has been added a column with the r.m.s accelerations of the front floor but without weighting the frequencies to see how it changes the result.

Table 5.3.1: weighted frequencies r.m.s accelerations

Velocity [km/h]	A_{rms} Front Floor [m/s^2]	A_{wrms} Front Floor [m/s^2]	A_{wrms} Back Floor [m/s^2]
10	2,5363	1,32	1,31
15	3,2426	1,44	1,49
19	3,2858	1,58	1,53

The first observable fact is that the weighting is lowering the value of the r.m.s acceleration, as not all the frequencies are perceived the same way.

The second one is that all the values are higher than 1,3. Looking at the table of guidelines of the ISO it is seen that the user experience in response to this vibration is very uncomfortable.

5.4 Braking test

For this experiment, as with the cobblestoned stoned one, a different approach has been taken to study the experiments.

This experiment as it was mentioned before, it was carried out in the parking located on Corso Castelfidardo 36. In the figure 5.4.1 it can be seen the route taken by the driver.

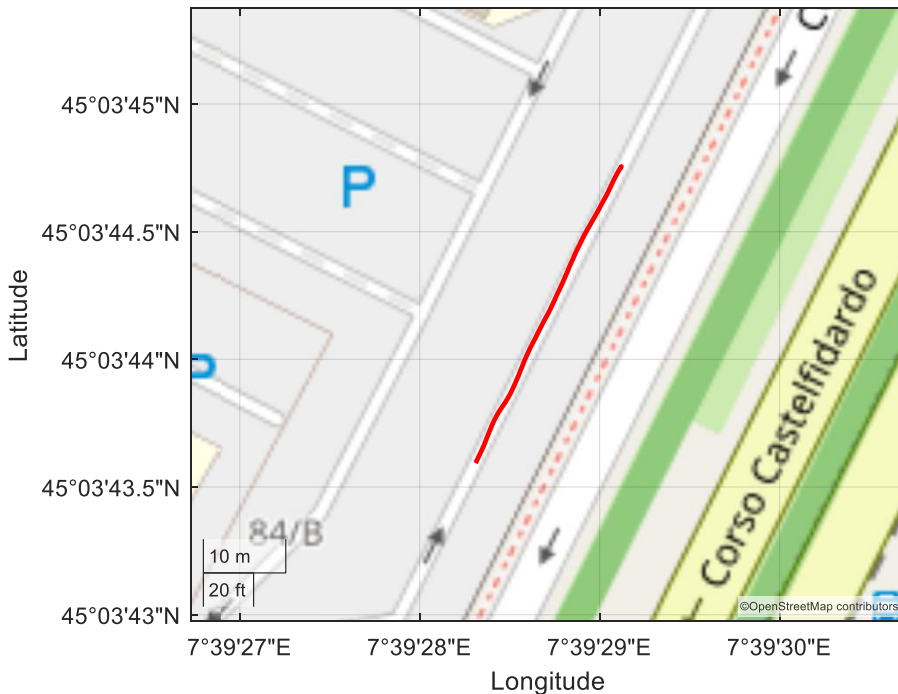


Figure 5.4.1: Route followed by the driver for the braking test experiment

The table 5.4.1 shows the measurements taken by hand. The speed corresponds to the one achieved by the control cruise before the braking was realised, and the braking distance is the one that has been measured with a meter as explained in the point 2.2.

Table 5.4.1: Measures taken by hand

Speed (km/h)	9	9	9	9.5	9	9	14	14.5
Braking Distance (m)	1.73	1.38	1.62	1.60	1.66	1.89	3.40	3.20
Speed (km/h)	13.5	14	14	20	20	20	20	20
Braking Distance (m)	3.02	2.77	3.14	5.30	5.19	5.15	6	5.42
Speed (km/h)	20	20	20	20	20	16.5	16	18
Braking Distance (m)	5.72	5.62	5.29	5.50	5.53	3.51	3.99	4.46
Speed (km/h)	11.5	11	12	12	8.5	9	9	9
Braking Distance (m)	2.43	2.15	2.18	2.44	1.3	1.67	1.65	1.63
Speed (km/h)	14	15	20	20	17	12		
Braking Distance (m)	3.27	3.45	4.99	5.28	4.17	2.02		

Before starting with the main analysis of this part, it has been compared the results taken by hand with the ones measured by the GPS. The main goal with this first analysis is to validate the results taken by hand, checking that they are similar to the ones measured with the GPS.

To compare these results, first of all is necessary to find the braking distance with the GPS data. It does not give the data directly but it can be found using the data of the speed.

The first step is to find for each experiment the evolution of the speed starting from the braking point until the e-scooter completely stops. To proceed with this step, it has been first plotted all the experiments speed in function of time to have a first view of these speeds. This speed has been calculated as a composition of the east speed with the north speed that are the values measured by the GPS. In the figure 5.4.2 it has been plotted the first 15 experiments.

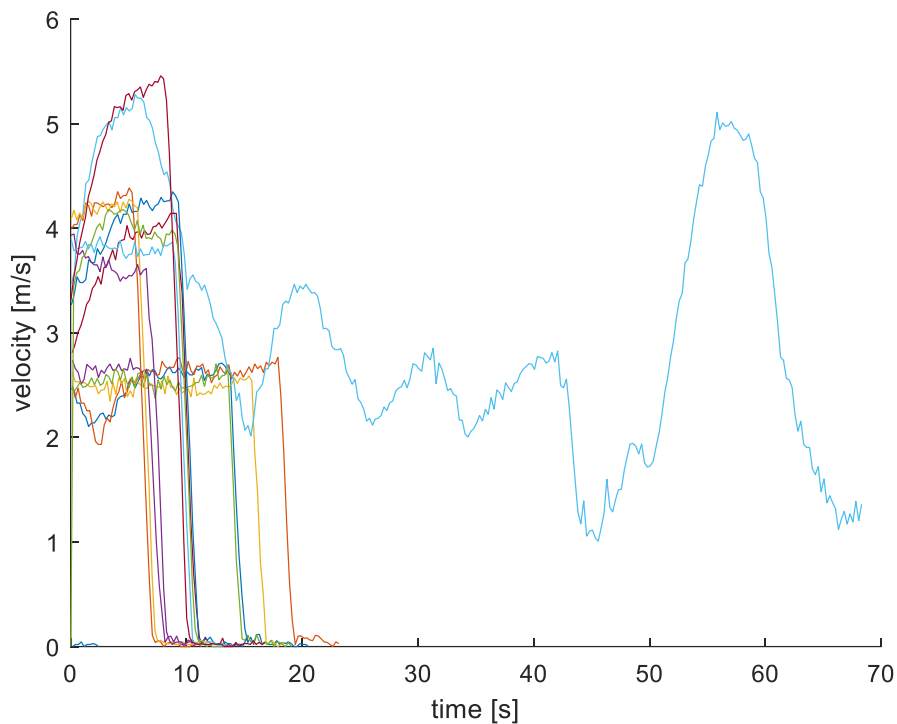


Figure 5.4.2: GPS signals of the speed during all the experiment

In the figure 5.4.2, it can be seen in different colours the first 15 experiments. First of all, it has been seen that in some experiments the data given by the GPS was clearly wrong as it did not have sense. Specifically for a total of 8 experiments (in the table 5.4.1 the ones corresponding to the 6,15,27,30,31,36,37). For these experiments it has not taken into account to compare the GPS data to the measurements taken by hand. Secondly it has been possible to see that in all the other cases the velocity had always the same shape. A shape that was the expected, having a first part of high speed and more or less constant, then a great descent until a speed close to zero, and then a last part with a speed almost null.

Then, the part of interest to study, is this descent for each experiment. The next step has been to isolate this part, and setting for each experiment, the time $t=0$ to the moment when it starts to brake (fig. 5.4.3)

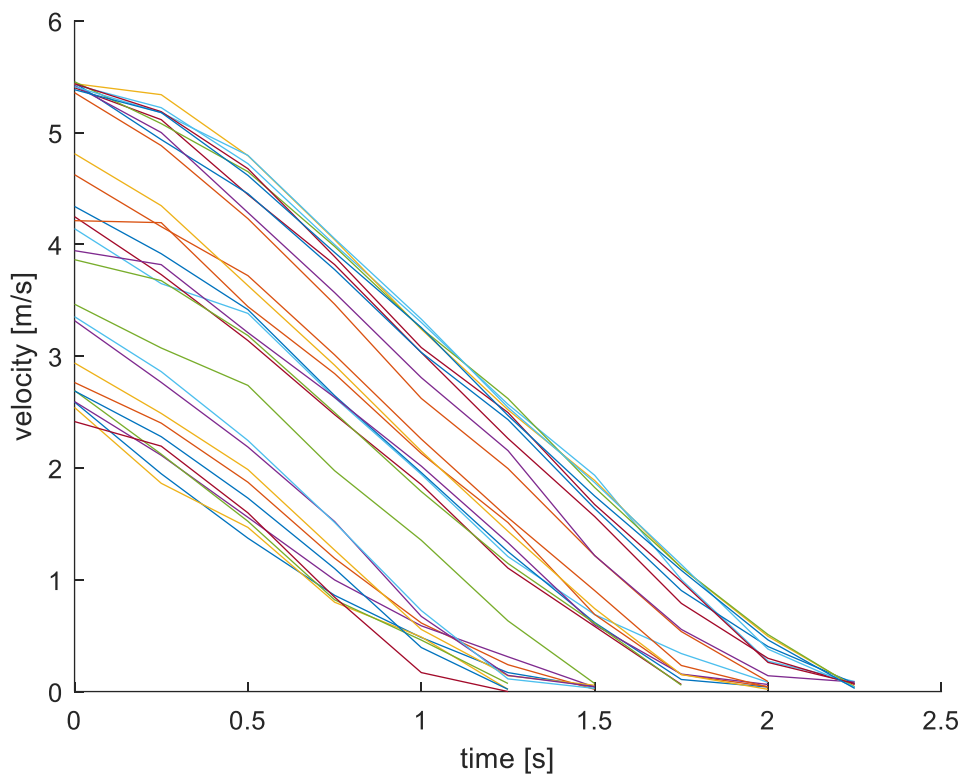


Figure 5.4.3: GPS signals of the speed during the braking

In the figure 5.4.3 it can be seen different lines each one corresponding to the experiments from which the GPS data had sense. It can be appreciated 3 main zones, that correspond to the three velocities chosen to perform the experiment. These trends have sense, as the higher is the speed the higher is the time to completely stop, but the slope seems to be very similar in all the cases.

The next step is to find the braking distance from these velocities. To perform this calculation, it has been integrated the speed for each experiment (fig. 5.4.4).

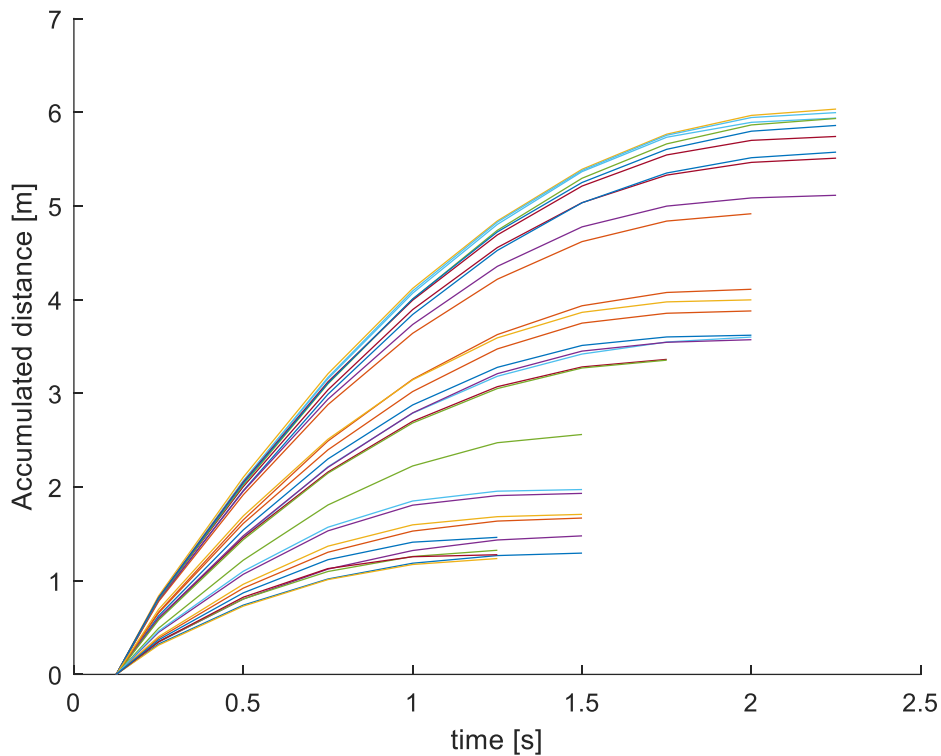


Figure 5.4.4: Accumulated distance over time.

In the figure 5.4.4 it can be seen for each experiment the accumulated distance travelled during the braking. Each line represents one experiment. As it can be observed, the slope starts very high and goes down during the process. Fact that was expected as the speed goes down over the time.

For each experiment, the final value of the accumulated distance has been considered as an indirect measurement of the GPS of the braking distance.

With these values it has been compared the braking distance measured by hand to the ones resulting of the GPS data (fig 5.4.5).

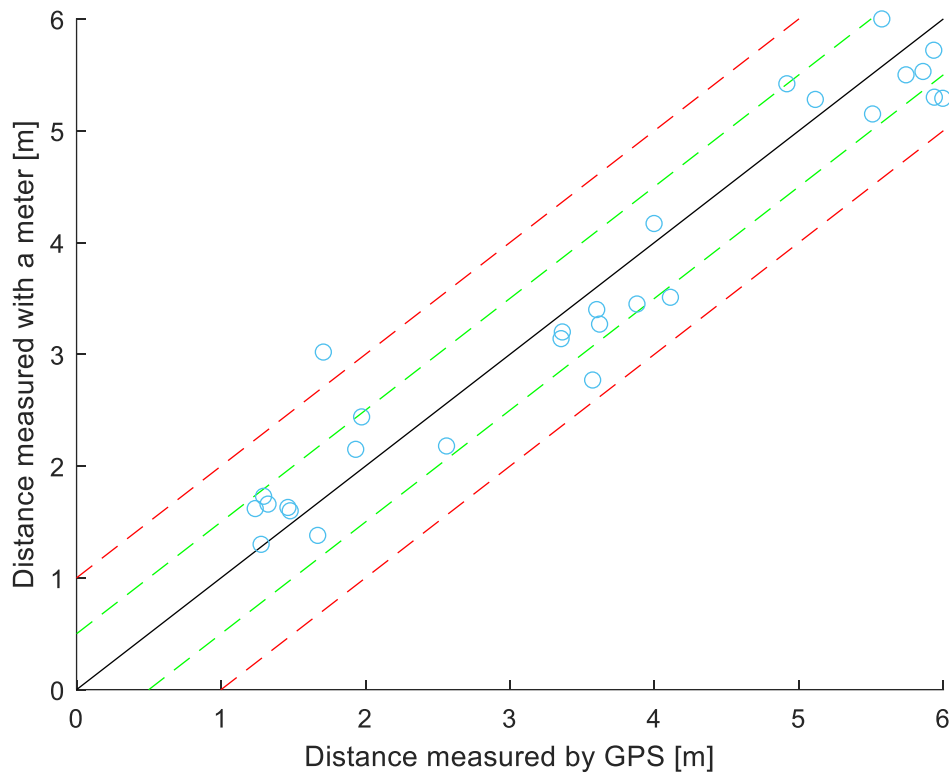


Figure 5.4.5: GPS vs By hand measurements of braking distance

In the figure 5.4.5 it has been plotted 5 lines to follow the relation between each pair of results. The black line has a slope of 1 and starts at the origin. It marks the perfect relation 1 to 1. Then two green lines with the same slope but with a distance of half a meter on both sides of the black line have been plotted, and then 2 other red lines at a distance of 1 meter. It was expected that not all the experiments had a perfect relation of 1 to 1, meaning that both measurements were equal. As both measurements are not 100% reliable, it was expected. However, having the most part of the values between the green lines, and almost all the others between the red lines, gives more reliability to the measurements taken by hand.

Once it has been validated the measurements, it has been started the analysis explained in the point 2.2. The first objective has been to study the relation between the speed of the e-scooter and the braking distance. The speed has to be converted in m/s in order to match the units. In the figure 5.4.6 it has been plotted the speed and the distance of these experiments to have a first view.

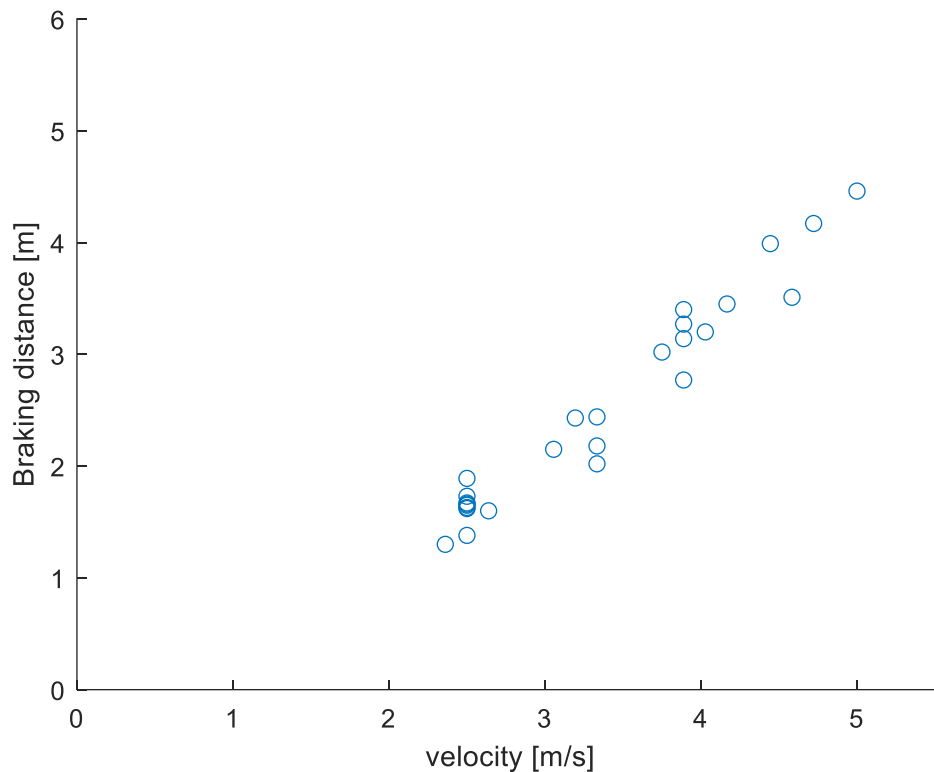


Figure 5.4.6: Braking distance over speed of the measurements by hand...

Looking at the figure 5.4.6, it could seem that the relation is either a first order or a second order one. To find the coefficients of this relation with the software MATLAB is easy if the relation is known. For this reason, it has been studied the theoretical braking distance in order to understand how these variables are related.

The theoretical braking distance can be found determining the work W , required to dissipate the vehicle's kinetic energy E [16].

To calculate the work W done by the braking the formula 5.4.1 has to be applied:

$$W = \mu mgd \quad (5.4.1)$$

Where μ is the friction coefficient, m is the total mass of the e-scooter and user system, g is the gravity of the earth and d is the braking distance.

Then, the kinetic energy it has to be calculated with the following formula:

$$E = \frac{1}{2} mv^2 \quad (5.4.2)$$

Where v is the speed at the start of the braking.

Applying $W=E$ the braking distance can be found as follows:

$$d = \frac{v^2}{2\mu g} \quad (5.4.3)$$

Then the formula that describes the relation between the braking distance and the speed is given by a formula of the type:

$$y = ax^2 \tag{5.4.4}$$

Where y is the braking distance, x is the speed at the moment of the braking, and a is the constant coefficient that has been calculated with MATLAB, with the curve fitting tool.

In the figure 5.4.7 it can be seen how this tool has been used to find the coefficient a :

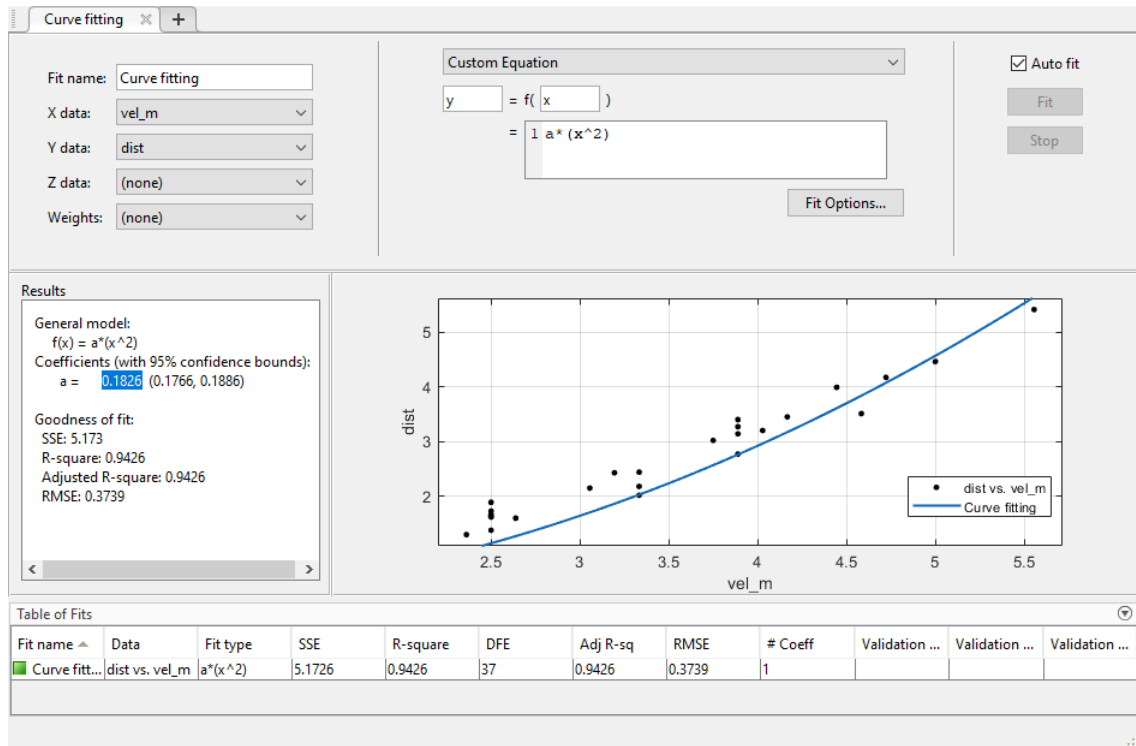


Figure 5.4.7: Calculation of the coefficient a with the Curve Fitting Tool

With this procedure it has been found the coefficient $a=0,1826$. As a result, the curve can be written as:

$$d = 0,1826v^2 \tag{5.4.5}$$

Using this coefficient, it has been plotted the function of the braking distance in function of velocity and compared with the experimental results (fig. 5.4.8).

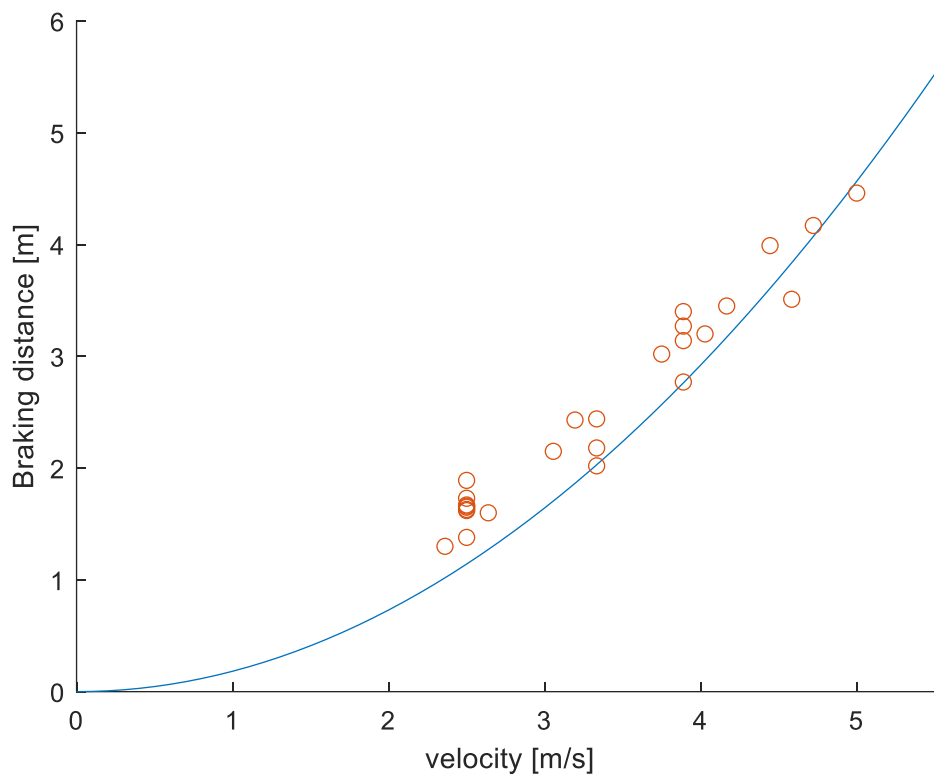


Figure 5.4.8: Braking distance as a function of velocity

In the figure 5.4.8 it can be seen the curve of the Braking distance in function of velocity, with this function it is possible to estimate the Braking distance at any speed when driving in an asphalt road.

To finish with the braking distance analysis, it has been made a calculation of the friction coefficient and a comparison with other electrical two-wheeled vehicles.

As it has been explained before, the braking distance is calculated with the following equation:

$$s_b = \frac{v^2}{2g\mu}, \quad (5.4.6)$$

In the previous steps it has been found following relation:

$$d = 0,1826v^2 \quad (5.4.5)$$

Combining the equations 5.4.5 and 5.4.6, the friction coefficient can be calculated as:

$$\mu = \frac{1}{2g \cdot 0,1826} = 0,2791 \quad (5.4.7)$$

To have an overview of the performance of the e-scooter braking response, it has been compared with two other two-wheeled vehicles, a bicycle [17] and a motorcycle. [18] (table 5.4.2).

Table 5.4.2: Friction coefficient of different vehicles

	e-scooter	Bycicles	Motorcycles
Friction coefficient (μ)	0,28	0,4	0,4-0,9

The e-scooter has the lower coefficient of the three types of vehicle. Comparing this value with the bycicle it can be seen that although not very different it is lower, and the speed that reach a regular person on the city has an average of 15 km/h [19]. Having a worse response to a bracking and reaching similar or even higher speeds with the scooter means that it is less safe for the scooter users and in consequence for the pedestrians. This can be a point to start to improve the performance of the scooter and the safety of the persons.

6. Numerical model of the e-scooter

To modelate the behaviour of the scooter it has been used the mass-spring-damper model. This model is one of the most common models used.

This model it can be expressed as a second-order differential equation:

$$m\ddot{x} + c\dot{x} + kx = g(x, \dot{x}, t) \tag{6.1}$$

Where m is the mass (kg), c is the damper coefficient (Ns/m), k is the spring coefficient (N/m), x is the displacement of the mass in reference to the resting position (m), \dot{x} the speed (m/s) and \ddot{x} the acceleration (m/s²). g is the external force [20]., in the case of study it will refer to the variation of the road

The spring carries the body mass by storing energy and helps to isolate the body from road disturbances, while damper dissipates this energy and helps to damp the oscillations [21].

The typical 2-wheeled vehicle or half of the 4-wheeled vehicle can be modelled as follows (fig. 6.1.1):

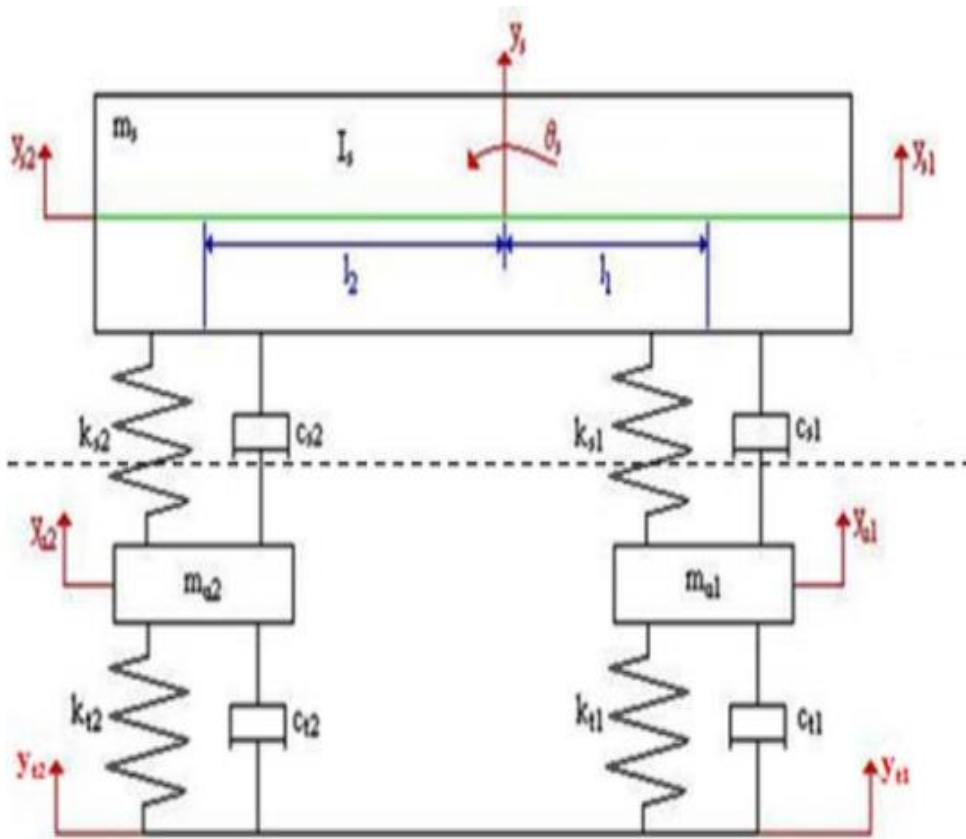


Figure 6.1.1: Mass-spring-damper model for 2-wheeled vehicle [21]

However, this model does not fit the scooter. This is a typical model in which the vehicle has an internal suspension. The springs and dampers of the bottom part represent the tyres, the small mass represents the mass of the suspended elements (in this case the wheels) and the springs and dampers of the top part represent the internal suspension. The model of the studied scooter does not have an internal suspension; therefore the model can be simplified (fig 6.1.2).

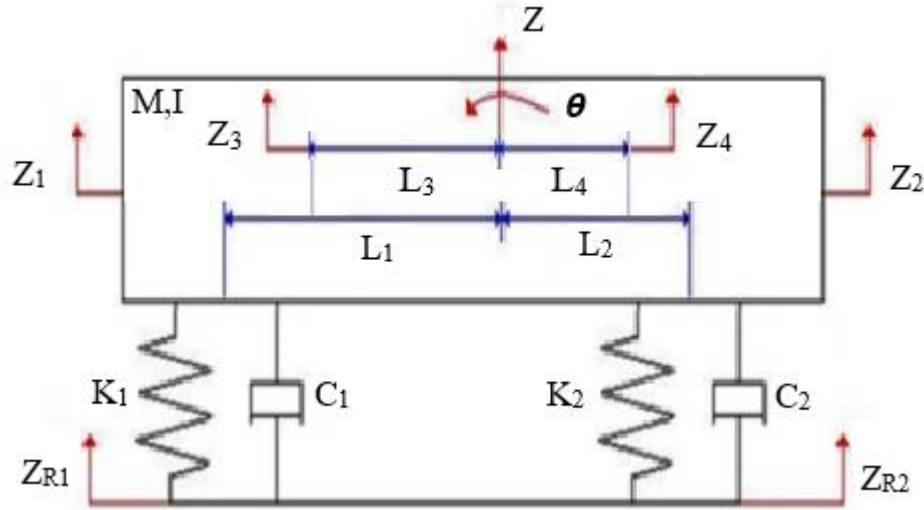


Figure 6.1.2: Mass-spring-damper model for the e-scooter

Where:

- Z_{R1} and Z_{R2} are the vertical travel of the tyre due to road disturbance.
- Z_1 and Z_2 are the body vertical displacements at the front and back wheels.
- Z_3 and Z_4 are body vertical displacements at the points where there are the front and back accelerometers.
- Z is the centre of gravity vertical displacement.
- θ is the angular displacement
- K_1 and C_1 are the spring and damper coefficients that model the front wheel.
- K_2 and C_2 are the spring and damper coefficients that model the back wheel.
- L_1 and L_2 are the distances from the centre of gravity, to the front and back wheel.
- L_3 and L_4 are the distances from the centre of gravity, to the front and back accelerometers.
- M is the mass and I the moment of inertia of the scooter and user.

M , I , L_1 , L_2 , L_3 and L_4 are calculable and the calculation with the results are showed on the next point. The displacements Z_{R1} and Z_{R2} are also calculable as they depend on the road disturbance.

Z and θ are the variables that are used to create the two second-order differential equations. Z_1 and Z_2 are used to create the model but they are a function of Z , θ and the

geometry. Z_3 and Z_4 are not necessary to create the model, but they will be used to compare with the experimental data, in order to find the parameters K_1 , C_1 , K_2 and C_2 .

6.1 Mathematical equations

Once all the geometry, the parameters and variables has been described, it can be written the two differential equations of second order. One referring to the vertical motion (eq. 6.1.1) and the other to the rotation (6.1.2):

$$M\ddot{Z} = -\left(K_1(Z_1 - Z_{R1}) + C_1(\dot{Z}_1 - \dot{Z}_{R1}) + K_2(Z_2 - Z_{R2}) + C_2(\dot{Z}_2 - \dot{Z}_{R2})\right) \quad (6.1.1)$$

$$I\ddot{\theta} = L_1[K_1(Z_1 - Z_{R1}) + C_1(\dot{Z}_1 - \dot{Z}_{R1})] - L_2[K_2(Z_2 - Z_{R2}) + C_2(\dot{Z}_2 - \dot{Z}_{R2})] \quad (6.1.2)$$

Where Z_1 and Z_2 can be expressed as follows:

$$Z_1 = Z - \theta L_1 \quad (6.1.3)$$

$$Z_2 = Z + \theta L_2 \quad (6.1.4)$$

And as it has been explained, although Z_3 and Z_4 are not used directly in the equations, they have been used for the comparison with the experimental data, specifically the value of the acceleration of these variables, then it is necessary to find their equations (eq 6.1.5 and 6.1.6)

$$\ddot{Z}_3 = \ddot{Z} - \ddot{\theta} L_3 \quad (6.1.5)$$

$$\ddot{Z}_4 = \ddot{Z} + \ddot{\theta} L_4 \quad (6.1.6)$$

The next step is to find all the calculable values of these expressions.

6.2 Calculations of the parameters

To calculate the parameters, it has been started with the mass, and then the centre of gravity. Once this values are found, all the other parameters can be calculated.

As explained before, the only parameters that have not been found are K_1 , C_1 , K_2 and C_2 . However is interesting to mention the order of magnitude of these parameters. For the tyres of a scooter, the values are approximately between $1,3 \cdot 10^5$ and $3,6 \cdot 10^5$ N/m for the damper coefficient the values are much lower in this case it will be used a range

between 100 and 5000 Ns/m [22]. These values will be used in the simulation in order to establish boundaries.

6.2.1 Mass and centre of gravity

The value of the mass of the system is the result of three values. The one referring to the scooter, the user mass and the SCADA set-up (eq. 6.2.1.1).

$$M = m_{scooter} + m_{driver} + m_{SCADA} = 101,26 \text{ kg} \quad (6.2.1.1)$$

To calculate the centre of gravity is necessary to impose a reference coordinate system, find the centre of gravity of each body and finally find the centre of gravity of the whole system.

The origin of the coordinate system it has been set in the centre of the front wheel. The centre of gravity of the driver it is located at the 56% of it's height [23]. To calculate it for the scooter, it has been calculated dividing the scooter in steering, front and back wheel and steering, as they are quite regular shapes and the mass of each element are known [22], the centre of gravity of each element has been considered as their barycentre. To calculate the resultant centre of gravity of the system can be calculated as follows [24]:

$$C.G. = (X, Z) = \left(\frac{\sum m_i x_i}{\sum m_i}, \frac{\sum m_i z_i}{\sum m_i} \right) \quad (6.2.1.2)$$

In the table 6.2.1.1 there are the values that has been used to find the C.G of the whole system.

Table 6.2.1.1: Centre of gravity and mass of the different elements

		F.Wheel	B.Wheel	Base	Steering	Scada	Driver
Centre mass [cm]	xg	0	-88,5	-45	-12	-7	-54,4
	zg	0	0	1,2	54,6	105	106,06
Mass [kg]		1,5	0,65	9,5	2,5	2,11	85

The C.G is on (-50,9 92,7) cm

With this value it is found the lengths L₁, L₂, L₃ and L₄.

$$L_1 = 50,9 \text{ cm} = 0,509 \text{ m}$$

$$L_2 = 37,6 \text{ cm} = 0,376 \text{ m}$$

$$L_3 = 25,9 \text{ cm} = 0,259 \text{ m}$$

$$L_4 = 16,6 \text{ cm} = 0,166 \text{ m}$$

6.2.2 Moment of inertia

To calculate the moment of inertia of the whole system it is necessary to sum the inertias of each element plus the value found by the Steiner's theorem, that depends on the mass of the element and the distance between local and global centre of gravity. Therefore, the moment of inertia can be calculated as follows [24]:

$$I = (I_{scooter} + m_{scooter} \cdot d_{scooter-C.G}^2) + (I_{driver} + m_{driver} \cdot d_{driver-C.G}^2) \quad (6.2.1.1)$$

The moment of inertia of a human in this axis is $11,64 \text{ kg}\cdot\text{m}^2$ [24] and the inertia of the scooter is $2,672 \text{ kg}\cdot\text{m}^2$ [22]. And the distance between the scooter and C.G. and the distance between driver and the C.G are calculable as the C.G of the system has been already calculated.

$$I = 24,43 \text{ kg}\cdot\text{m}^2$$

With all the equations that model the system and the parameters found, the next step is to create the *SIMULINK* model with all this information.

6.3 Simulink Model

To apply all the equation in order to perform a simulation it has been used *SIMULINK* from the software *MATLAB*. In the figure 6.3.1 it is showed the model created with *SIMULINK*.

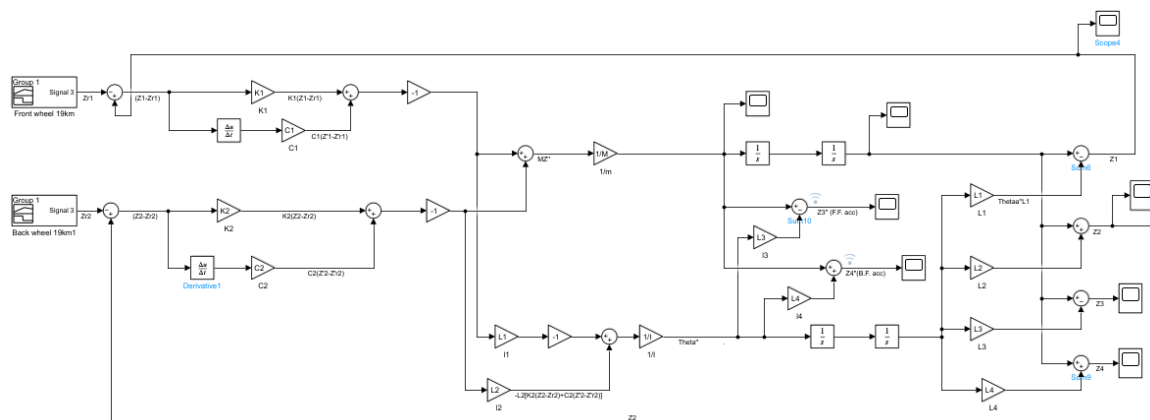


Figure 6.3.1 Numerical model of the scooter with SIMULINK

As it is difficult to see it on this figure, it has been divided in two (fig. 6.3.2 and 6.3.3), focusing first in the left half part and then to the right one.

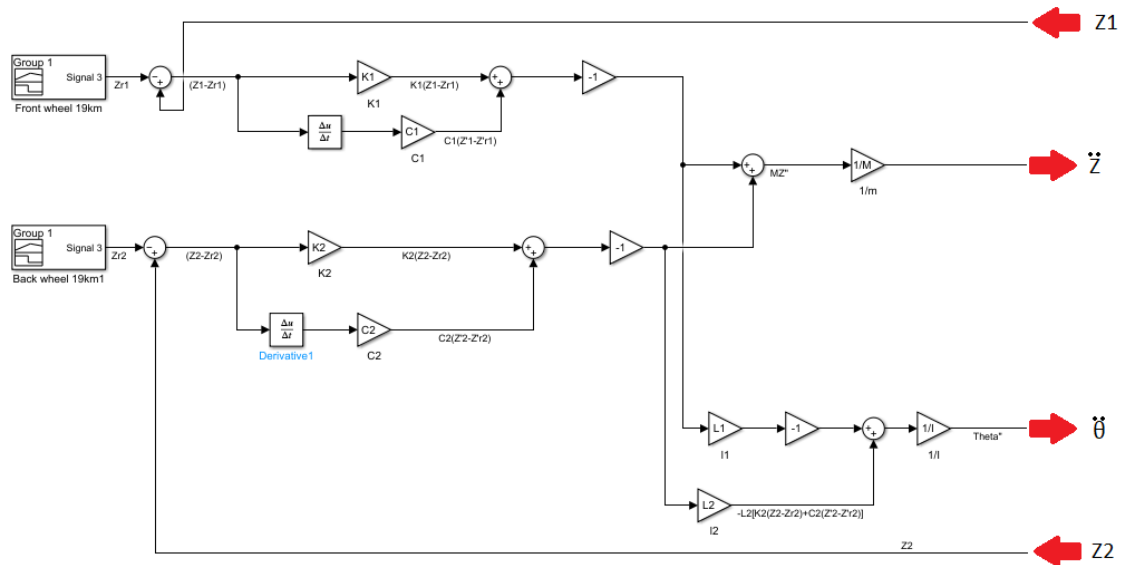


Figure 6.3.2: Left side of the SIMULINK model

As it can be observed in the figure 6.3.2, there is the left part of the model, and with red arrows it has been indicated how it is connected to the figure 6.3.3.

On the left of the figure there are two blocks that represent the input of the system. These signals are waves that represent the variation of the vertical displacements of the tyre due to the road variation (Z_{R1} and Z_{R2}). These signals will be discussed later.

Then there are some blocks representing the different operations of the equations 6.1.1 and 6.1.2. First of all, the values of the input signals are subtracted to Z_1 and Z_2 , and then performing the operations as multiplying by the parameters, deriving or subtracting, it results into 2 values, the vertical acceleration of the centre of gravity and its rotational acceleration.

In the figure 6.3.3 it is showed the right side of the model.

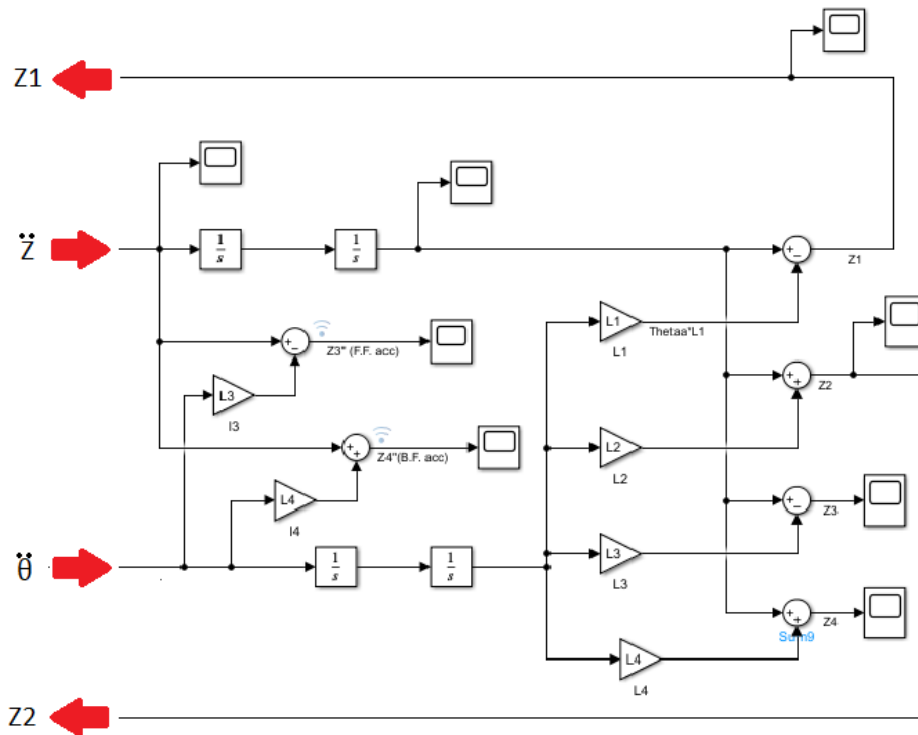


Figure 6.3.3: Right side of the SIMULINK model

In this part of the model, the values that have been calculated in the left side (vertical acceleration and rotational acceleration) are used to calculate its derivatives and consequent operations, to find the vertical positions Z_1 and Z_2 that are needed for the feedback of the system. Moreover in the centre part of the figure it can be seen the calculation of the vertical accelerations of the points where there are the accelerometers: Z_3 and Z_4 . These values are the ones used to optimize the system with the parameters. Finally, some other values are calculated in order to monitor their values as the vertical displacement of the accelerometer's points.

The last step before starting with the simulation, it is to create an input signal that models the road shape.

For the simulation it has been used the bike bumps. To create a signal, these shape it has to be converted in a function that depends on the time. This it will be achieved by using the distances (fig.2.1.2.4) and the speed of the different experiments. For the first simulations it has been used the different speeds of 9, 14 and 19km/h. But comparing with the experimental data, the periods were not equal, then it has been calculated the local speed for each bump, and seen that the speed was not exactly 9, 14 or 19 km/h. And this small variation, had a great impact. Having a speed of 13,8 instead of 14 had enough impact to consider the local speed for each bump. For the signal of the back wheel the shape will be the same but with a delay corresponding to the distance between the wheels. For the amplitude of this signal, it has been used directly the height of the bumps.

In the figure 6.3.4 it can be seen an example of the creation of this signal, for an experiment at 14 km/h for the front wheel input displacement.

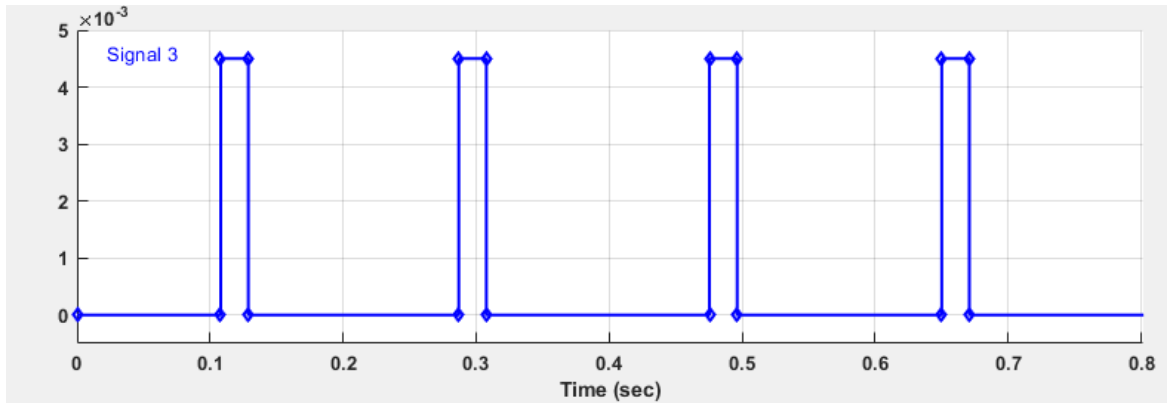


Figure 6.3.4: Input signal, front wheel

With these signals, when performing the simulations that will be discussed later, it has been seen that the positions of the peaks were much more coherent, than using a global mean speed. However, the model still had problems to find a solution similar to the experimentation. For that reason it has been tried to improve the model, by improving the input signal, as the variation of the Z_1 and Z_2 were not exactly as represented. To understand better this displacement and to model a better signal, it has been used the trigonometry (fig. 6.3.5).

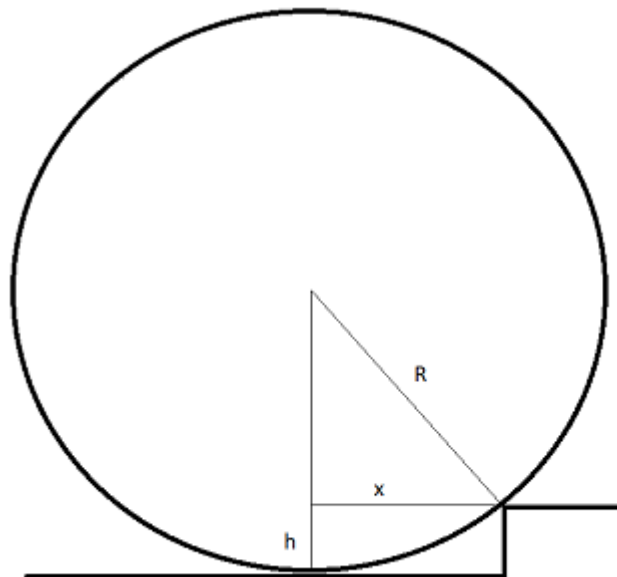


Figure 6.3.5: Geometry of the wheel and a bike bump

understand better this displacement and to model a better signal, it has been used the trigonometry (fig. 6.3.5).

First it has been calculated the value of the distance x , and then converted with the speed of each experiment into a time. To model better the input signal, it has been considered that the variation of amplitude will be uniform during the time that the x distance is crossed. In the figure 6.3.6 it can be observed this modification of the signal.

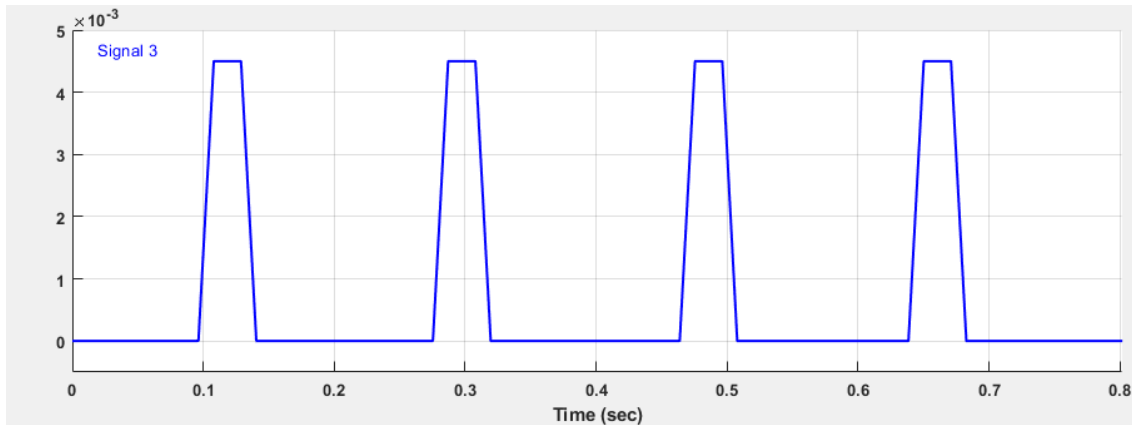


Figure 6.3.6: Modification of the input signal

Now the final step is to use the created model to find the parameters K_1 , C_1 , K_2 and C_2 .

6.4 Results and parameter optimization

To find the values of the parameters K_1 , C_1 , K_2 and C_2 it has been used the application *Parameter Estimator* in the *SIMULINK*. However, at the beginning of the simulation it has been made the simulation without this tool as it was not known, doing it by hand, changing the parameters on each run. As it can be expected, using the tool was much better as the option of doing it manually did not converge into a good solution. However, some interesting observations have been made doing it manually that helped in the usage of the *Parameter Estimator* application.

In the table 4 runs of the experiment at 9 km/h. On the first column there is the experimental values of the first three positive peaks that occurs after the crossing of the first bump by the front wheel. In the next columns there is the values of the simulation with different values for the parameters.

Table 6.4.1: Simulations changing parameters manually

		Sim.1	Sim.2	Sim.3	Sim.4	
	Experimental	K1=K2 [N/m]	200000	200000	220000	220000
		C1=C2 [Ns/m]	1300	1500	1500	1700
1st peak Acceleration [m/s ²]	8,5		10,94	10,98	10,56	11,59
2nd peak Acceleration [m/s ²]	10,5		13,76	12,42	13,64	12,77
3rd peak Acceleration [m/s ²]	2,5		3,09	2,5	2,93	2,2

Observing this values it can be noted that increasing the values of K's had the opposite effect of decreasing the C's. With these and other simulations, it has been seen that if from the first simulation, two other simulations are performed, one with an increase ok K and a decrease of C, and the other simulation with a decrease of K and an increase of C, the two simulations seemed to improve the parameters.

This could mean that by doing the simulation there is not a unique solution. This fact helped a lot in the optimization of the parameters with the *Estimator Parameter* app. As the first simulations of some experiments converged into a values as negative C's or K's outside the range. This problem was solved by doing the optimization with a different initial value of the parameters and applying limits for the parameters.

6.4.1 Estimator parameter

The *Estimator parameter* tool allows to iterate the model with different values of the parameters until it converges. For this is necessary an experimental signal, in this case the signal of the accelerometers, an output signal that corresponds to the acceleration of these points, and the parameters that can be modified in order to match the output model signal to the experimental one.

The output signals of the model will be the ones corresponding to the acceleration of the front floor and de back floor points. Then the experimental data of the front and back floor accelerators will be the ones used as a base to optimize. And the parameters that can be modified in order to achieve a convergence will be the K's and C's.

For what concerns to the experimental data of the accelerations, the first thought was to use directly the one that measured the accelerometers. However, the first simulations gave a result of the simulated signal that were not similar to the experimental data. Then it has been thought that the high frequency values could be a problem. In order to solve it, it has been tried to filter the experimental accelerations. With this modification the experimental and the simulated data were much more similar, but there was a derivated

problem. The modification of the values of the peaks after applying a more restrictive filter were not neglectable.

To find a solution to this problem it has been used the values of the important peaks stored on the point 5.1. of this thesis. With this solution it has ben removed the high frequency content but without modifying the values of the peaks. Although it is an approximation and not a perfect way, with this solution it has ben found a much better result for the optimization and values for the parameters that were in the range that they are supposed to be. In the figure 6.4.1.1 how the experimental data has been modified for the front floor at 9 km/h.

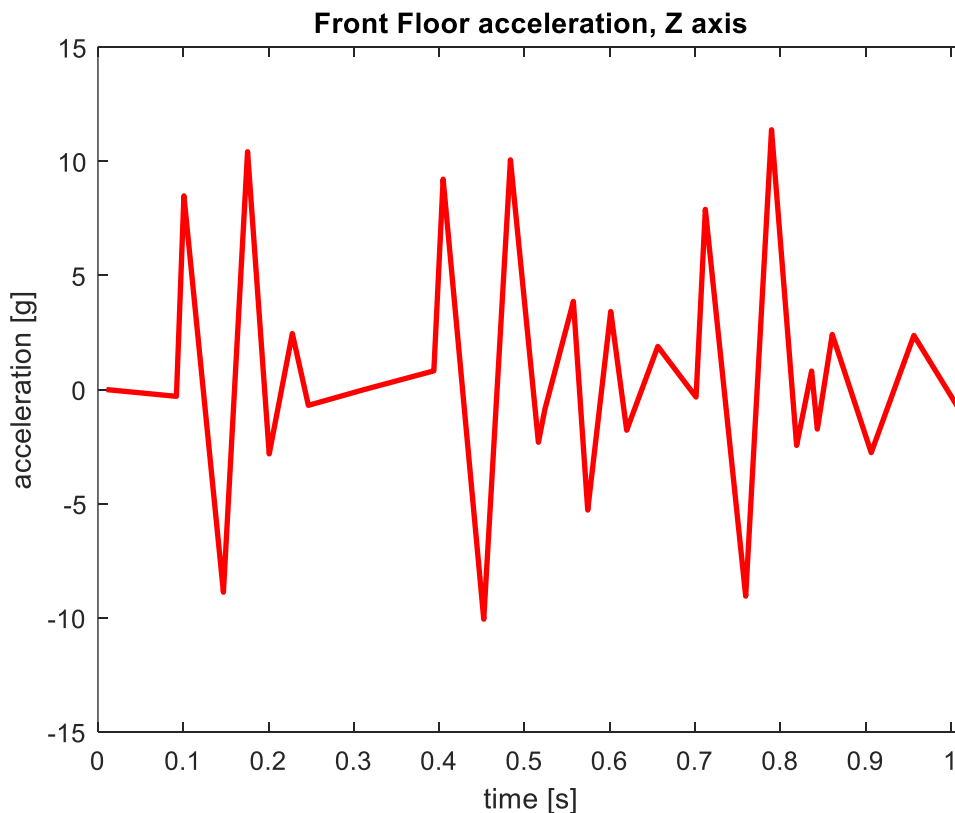


Figure6.4.1.1: Modified experimental acceleration

The procedure to optimize the parameters have been made by first finding a first convergence for the front accelerometer of the 3 different speeds. In the figure 6.4.1.2 it can be seen this run for the case of 9 km/h.

The initial values of the parameters have been set to $K_1=K_2=200000$ N/m and $C_1=C_2=1000$ Ns/m.

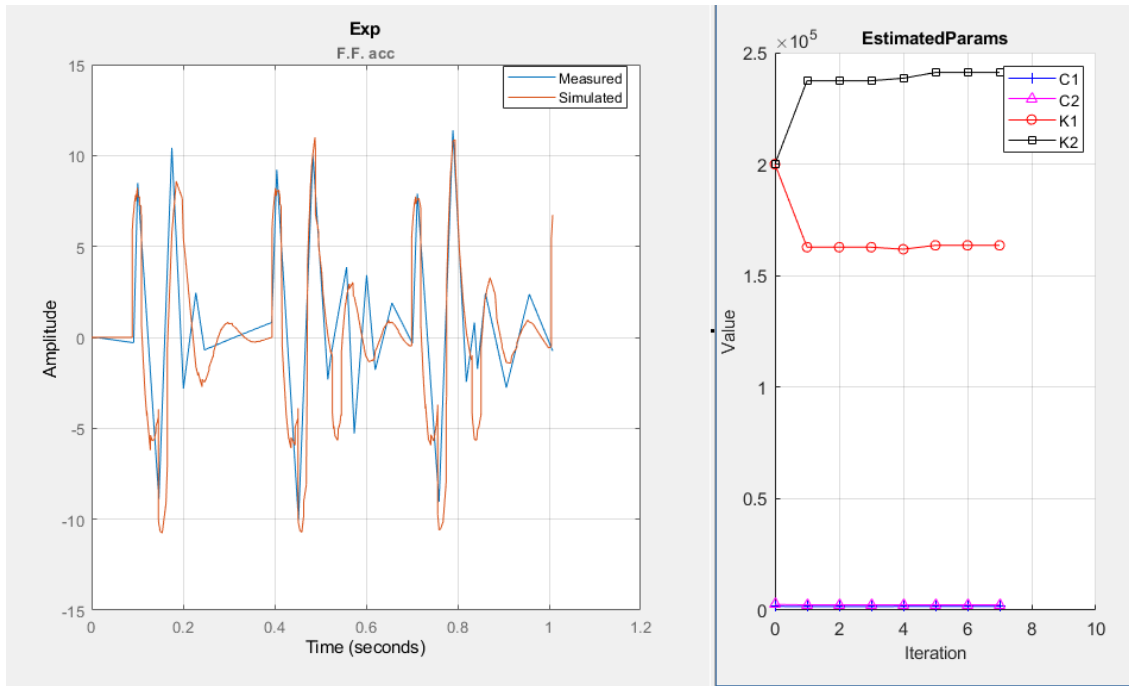


Figure 6.4.1.2.: Parameter optimization for the experiment of 9 km/h

In the figure 6.4.1.2 it is showed a graph on the left that includes the measured data and the simulated one, and on the right side the evolution of the parameters during the iterations.

As it can be observed, it is a really good approximation. However it is not perfect as not all the peaks occurs on the same instant of time nor have the same value of amplitude.

As it is a good approximation it has been considered now as the new initial values of the parameters, the ones resulting from this run.

This process has been made for the three speeds and the values are shown in the table 6.4.1.1.

Table 6.4.1.1: Parameter's values for the three speeds

	9 km/h	14 km/h	19 km/h
C1 [Ns/m]	1710	3683	3516
C2 [Ns/m]	2397	3047	1571
K1 [N/m]	163600	153700	133000
K2 [Nsm]	241200	290900	331000

The values are quite similar but in order to find a solution for all the three experiments, it has been calculated the mean of the parameters and then reduced the boundary range in order to decrease the difference between these values on each iteration.

The final values after performing some iterations are:

$$C_1=2856 \text{ Ns/m}$$

$$C_2=2375 \text{ Ns/m}$$

$$K_1=1,48 \cdot 10^5 \text{ N/m}$$

$$K_2=2,83 \cdot 10^5 \text{ N/m}$$

And in the figures below it is showed the final comparison between the experimental accelerations (front floor and back floor) and the simulated acceleration with these parameters, for the three speeds.

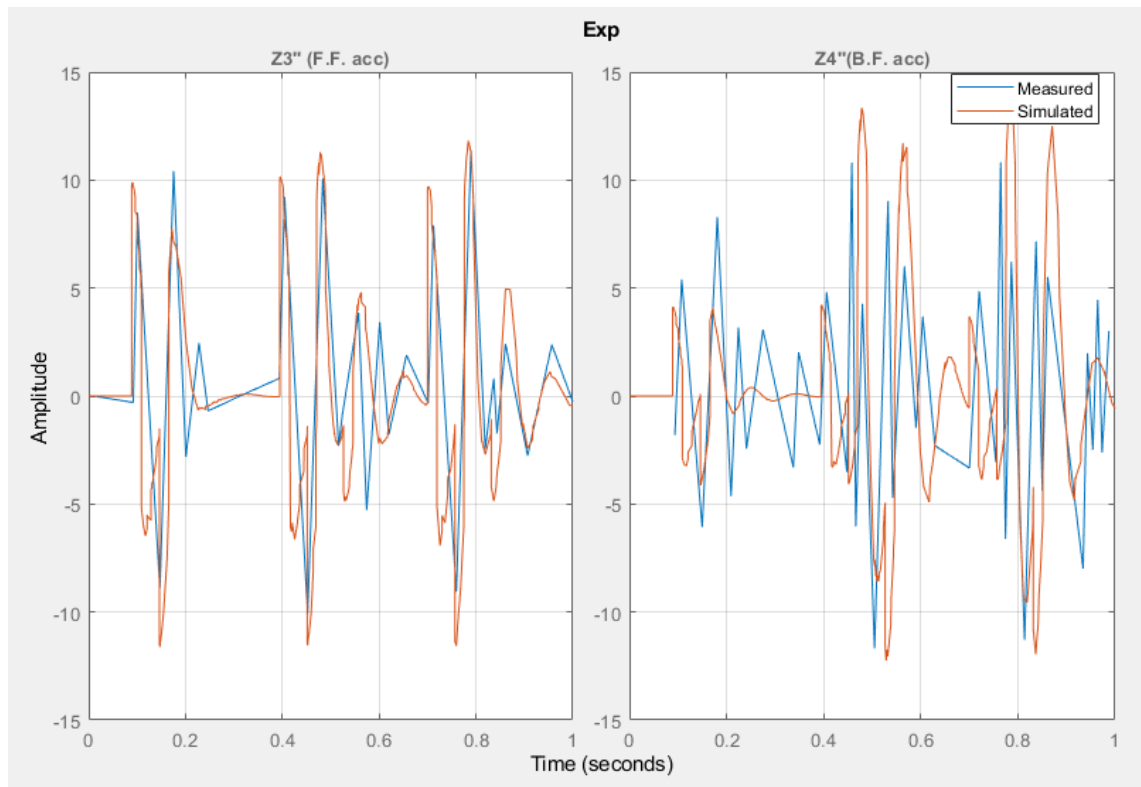


Figure 6.4.1.3 Experimental vs. Simulated. 9 km/h

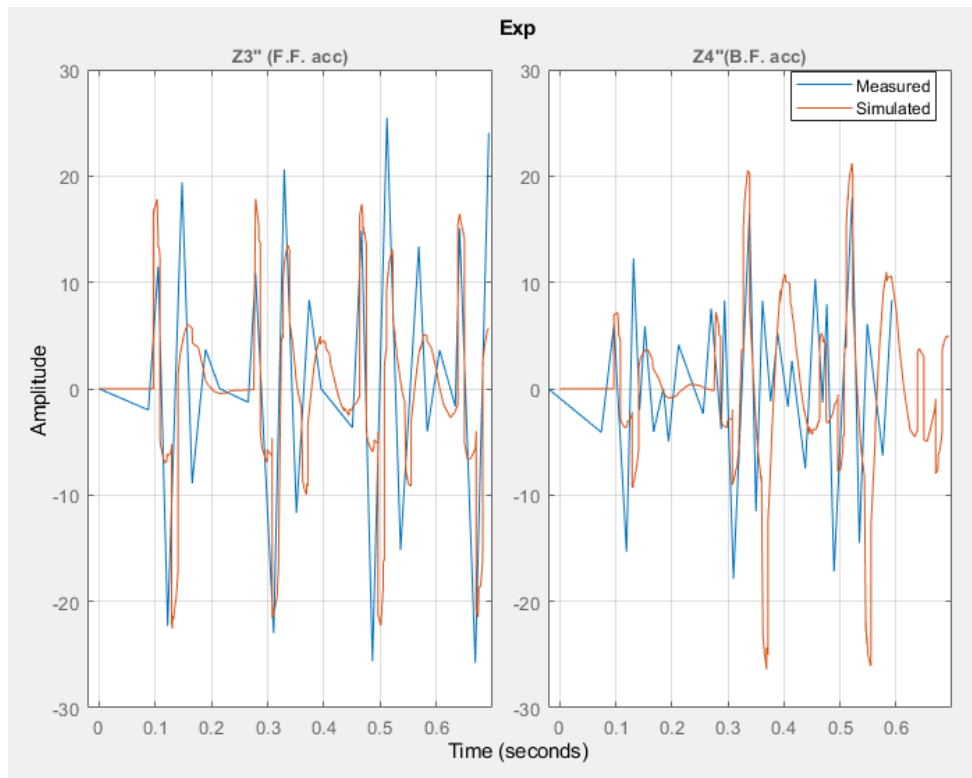


Figure 6.4.1.4: Experimental vs. Simulated. 14 km/h

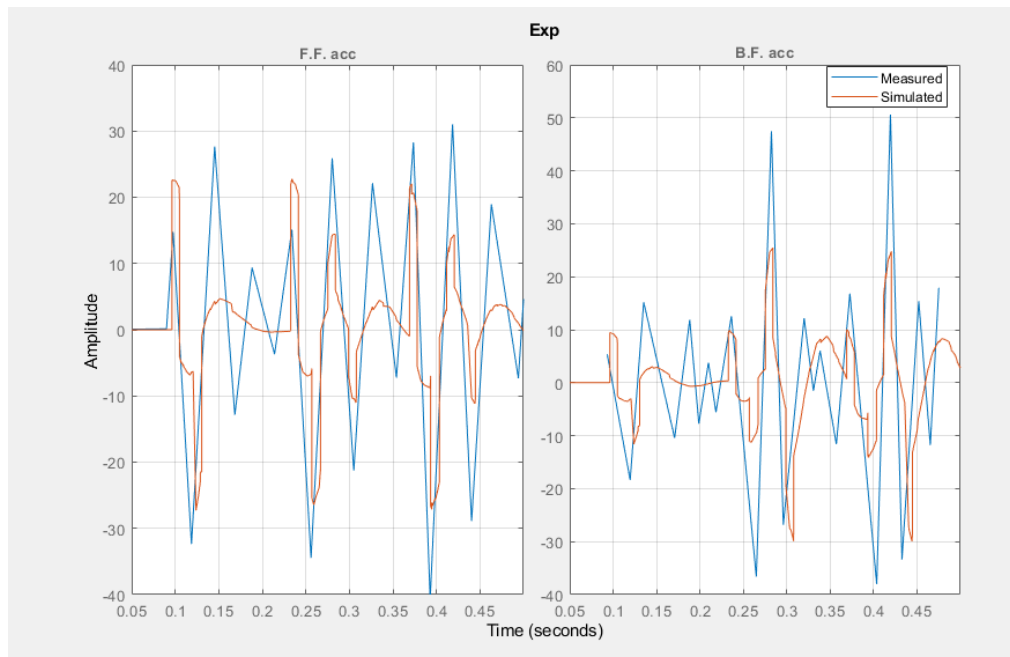


Figure 6.4.1.5: Experimental vs. Simulated. 19 km/h

Observing the figures for the experiments at the different speeds it can be observed as not all the simulations seems to be equally accurate. The higher is the speed used during the experiment, the higher seems to be the error. But in general, the simulated data reflect a very similar behaviour in comparison to the measured data.

Conclusions

The work on this thesis allowed to perform many experiments and measure different parameters that allowed to study different aspects concerning the e-scooter.

First of all it allowed to study the comfort of the driver, in an existent road of Torino, similar to many others, in which the road has not the better conditions. And observe the need of an improvement in this field, as in the road of study the vibrations occasionated in all the range of speed were considered by the ISO 2631-1:1997 as “very uncomfortable”.

Secondly it has allowed to measure the braking distance and compare it with other vehicles, observing as the performance it is not as good as other two-wheeled vehicles, and specifically, having a lower performance than a bicycle while the speed is usually higher.

Thirdly with the measurement of experiments where the road shape was known, it has allowed to create an initial approximation of a numerical model of the e-scooter, by knowing the inputs that the scooter received.

Finally, this work it can be used as a base for next works, as a prediction of the behaviour of the scooter in different situations or to try to find how to improve

Reference

- [1] <https://environmental-conscience.com/electric-scooters-pros-cons/>
- [2] <https://unagiscooters.com/articles/who-invented-the-scooter/>
- [3] PikeResearch. “Electric two-wheel vehicles: Electric bicycles, mopeds, scooters and motorcycles market analysis and forecast”. www.pikeresearch.com
- [4] <https://vpe.es/noticias/el-patinete-un-futuro-imparable-e-imbatible/>
- [5] <https://www.scooterred.co.uk/xiaomi-pro-2-electric-scooter-full-specification.html>
- [6] Mechanical vibration and shock - Evaluation of human exposure to whole-body vibration - Part 1: General requirements. International Standard ISO 2631-1; ISO: Geneva, Switzerland, 1997.
- [7] <https://electric-scooter.guide/guides/electric-scooter-regenerative-brakes/>
- [8] J.M. Piéplu, “*GPS et Galileo, Systèmes de navigation par satellites*”, Groupe EYROLLES, 2006.
- [9] <https://www.pcb.com/products?m=356A15>
- [10] <https://www.pcb.com/products?m=356A24>
- [11] Simcenter SCADAS XS User Manual, 2019.
- [12] D. Hermógenes Gil Martínez, “*Manual del automovil,.Suspension, dirección, frenos, neumáticos y airbag*”, CULTURAL, S.A., Madrid, 2002.
- [13] P. Davidovits, “*Physics in Biology and Medicine*” Elsevier Inc. Amsterdam, 2019
- [14] W.S. Erdmann, “*Acta of bioengineering and biomechanics, Vol 1, No 1, Geometry and inertia of the human body*”, University School of Physical Education, Gdańsk, Poland, 1999
- [15] W.F. Riley, L.D. Sturges, D.H. Morris, “*Statics and Mechanics of Materials: An Integrated Approach*”, John Wiley & Sons, 1996
- [16] E. Aycock, “*Traffic Accident Reconstruction*”, Investigative Engineers Association, 2010
- [17] R. Redfield, “*Bike Braking Vibration Modelling and Measurement, Procedia Engineering, Volume 72*”, 2014, Pages 471-476

- [18] D.Barta, “*Experimental investigation of the motorcycle braking properties riding on different road surfaces*”, 2020
- [19] https://en.wikipedia.org/wiki/Bicycle_performance#cite_note-10
- [20] ESMI department of Applied Math. “*The Mass-Spring-Damper Model*”, 25 Jun 2019
- [21] M. Avesh, R. Srivastava. “*Modeling Simulation and Control of active suspension system in Matlab Simulink environment*”, 2015
- [22] J.D. Cano-Moreno, M.E. Islán, F. Blaya, R. D’Amato, J.A. Juanes, E. Soriano. “E-scooter Vibration Impact on Driver Comfort and Health.”, 2021.
- [23] P. Davidovits, “*Physics in Biology and Medicine*”, 2019.
- [24] W. S. Erdmann. “*Geometry and inertia of the human body*”, 1999